Search for Higgs Bosons at LEP2 and Hadron Colliders

T. Trefzger
LMU Munich, Sektion Physik, Am Coulombwall 1, 85748 Garching, Germany

24th September 2001

Abstract

The search for the Higgs boson was one of the most relevant issues of the final years of LEP running at high energies. An excess of 3 σ beyond the background expectation has been found, consistent with the production of the Higgs boson with a mass near 115 GeV/c^2. At the upgraded TeVatron and at LHC the search for the Higgs boson will continue. At TeVatron Higgs bosons can be detected with masses up to 180 GeV with an assumed total integrated luminosity of 20 fb^{-1}. LHC has the potential to discover the Higgs boson in many different decay channels for Higgs masses up to 1 TeV. It will be possible to measure Higgs boson parameters, such as mass, width, and couplings to fermions and bosons. The results from Higgs searches at LEP2 and the possibilities for searches at hadron colliders will be reviewed.

Contents

1 Introduction

The Standard Model is extremely well described by experimental data: leptons and quarks were discovered as the fundamental constituents of matter. The photon, the W and Z bosons, and the gluons were identified as the carriers of the electromagnetic, weak and strong forces. Measurements of the lineshape and couplings of the Z boson with the e^+e^- data at LEP1 and SLC and the precision measurements of the properties of the W boson at TeVatron and LEP2 confirmed that the experimental analysis is in excellent agreement with the Standard Model.
In the Standard Model the generation of the masses of gauge bosons and fermions is described by the Higgs mechanism. Associated with this mechanism is the existence of massive scalar particles called Higgs bosons. The proof for the Higgs mechanism would be the direct observation of this particle.
This is after the discovery of the top quark the only particle missing which has been predicted in the framework of the Standard Model. The mass of the Higgs boson is a free parameter in this model.
After a short phenomenological introduction on the Higgs mechanism and theoretical constraints on the Higgs boson mass and the possible decay modes the results of searches for the Higgs boson in the Standard Model and its extensions will be described in three parts: past, present and near future.

Past:
In the first part of this review the LEP results are given. During the final years of LEP - the Large Electron Positron collider at CERN - the search for the Higgs boson was one of the most relevant issues. Since 1995 LEP has increased the centre-of-mass energy up to $\sqrt{s}$ =209 GeV/c^2 in the year 2000. LEP is sensitive for Higgs boson masses up to $\sqrt{s} - m_Z$. Some emphasis will be given to the latest LEP results where an excess of $\sim$2.9 σ beyond the background expectation was found, consistent with the production of the Higgs boson with a mass near 115 GeV/c^2. Shortly after this exciting result LEP has been shut down to make place for a new generation of colliders: the LHC.

Present:
The second part is dedicated to the results and prospects of Higgs searches at TeVatron. Before LHC will start data-taking in the year 2006 TeVatron at Fermilab has the amazing chance to search for the Higgs boson and to verify the excess seen at LEP. At TeVatron a Higgs boson with a mass around 115 GeV/c^2 could be excluded at 95% confidence level with 2 fb^{-1} per experiment. To make a 5 σ discovery a luminosity of 15 fb^{-1} per experiment is required. To collect 15 fb^{-1} of data an upgrade of the two detectors DØ and CDF is needed. The aim is to collect this amount of data until the year 2006. Such data samples will extend the combined sensitivity of CDF and DØ well beyond the LEP reach and allow large domains in the Minimal Supersymmetric Standard Model parameter space to be investigated.

Near Future:
Finally the possibilities at the next hadron collider LHC are given in the third part. At LHC - the Large Hadron Collider - with a centre-of-mass energy of $\sqrt{s}$=14 TeV - it will be possible

to search for Higgs bosons in a much broader mass range. The ATLAS and CMS detectors have been optimized for Higgs boson searches. In 2006 first physics collisions at LHC will take place. 1 fb^{-1} luminosity is foreseen in the first year of running. In 2007 10 fb^{-1} of data will be taken. With this data a Higgs boson with a mass near 115 GeV/c^2 can be found in the $H \to \gamma\gamma$ and $b\bar{b}$ decay channel. If the Higgs boson mass is above 135 GeV/c^2 other decay channels like $H \to ZZ^* \to 4$ leptons or $H \to WW^* \to l\nu l\nu$ will be used to search for the Higgs boson. The possibility at LHC to search for Higgs bosons in the mass range between $\sim$100 and $\sim$1000 GeV/c^2 will help to solve the question about the origin of the Higgs boson. At TeVatron it will be very difficult to distinguish between a Standard Model and a MSSM Higgs boson because there is only a marginal chance to detect more than one Higgs boson. At LHC it will be possible to search for supersymmetric particles and additional Higgs bosons in a much broader range than in the final years of LEP running or at TeVatron. With the huge amount of data taken at LHC parameters of the Higgs bosons can be measured, such as mass, width and couplings to fermions and bosons.

Next Future:
This report covers Higgs boson searches at LEP and present and near future hadron colliders. e^+e^- linear colliders with a centre-of-mass energy around 500 GeV are ideal machines to search for the Higgs boson and to measure the mass and the couplings. At many different laboratories e^+e^- linear colliders are planned but the machine wherever it will be built can not be ready before the year 2012.
Until then most probably results from TeVatron and LHC will be found to decide whether one or more Higgs bosons exist. Furthermore the properties like the mass or the width might have been measured with a precision of a few percent.

2 Overview

In the Standard Model fermions, of which there are quarks and leptons, form the elementary constituents of matter. All interactions are mediated by so-called gauge bosons. The photon, the exchange particle of the electromagnetic interaction is massless, likewise massless are the gluons as carriers of the strong interaction, which forces quarks at low energies to form hadrons, as for example protons or neutrons. In the case of the weak interaction the exchange particles, the Z^0, W^+ and W^- bosons, are almost 100 times heavier than a proton.
Predictions of the Standard Model have been verified with extremely high precision in modern experiments. The key making this theory so successful is its building principle: invariance of the fundamental equations under local symmetry transformations, referred to as gauge invariance. The proof that gauge invariant theories are renormalizable [1, 2] received the nobel prize in 1999. Gauge invariance would be violated if gauge bosons were a priori massive. The Standard Model [3–5] therefore proposes a dynamical mechanism to generate particle masses. Despite the fact that all experimental results support the gauge symmetry of the Standard Model, no direct observation can be linked to the mechanism of mass generation, which predicts at least one elementary scalar particle, the so-called Higgs boson. In the Standard Model most of the free parameters are linked to the mechanism of mass generation. It is therefore not surprising

that the mass of the Higgs boson itself is a free parameter of the theory. As yet the Higgs boson withdraw from detection.
The discovery of a Higgs boson or maybe the exclusion of its existence in a wide range of masses is therefore at present one of the most important topics of the experimental particle physics, which brings extensive consequences for our understanding of the smallest components of matter.

2.1 The Higgs Boson in the Standard Model

2.1.1 Higgs Mechanism

The Higgs mechanism allows to introduce masses to gauge bosons and fermions in the framework of the Standard Model. The masses of the fundamental particles are generated through the interaction with the scalar background field [6–8].
To accommodate all observed phenomena a complex isodoublet scalar field is introduced. The Lagrangian for this field respects a global SU(2)-symmetry. Through self-interactions the field acquires a non-vanishing vacuum expectation value. The ground state of the field therefore does not reflect the global SU(2)-symmetry of the Lagrangian. This phenomena is referred to as spontaneous symmetry breaking. It gives rise to massless scalar bosons, so called Goldstone bosons. If then the global symmetry of the Lagrangian is transformed into a local symmetry by coupling the scalar field to a priori massless gauge boson these Goldstone bosons can be absorbed as longitudinal degrees of freedom of the gauge bosons, thus generating their masses. Also fermions acquire their masses by interaction with the scalar background field.
Of the four degrees of freedom of the scalar background field one degree is not absorbed by the gauge bosons, manifesting itself as a massive particle which should be observable: the Higgs boson. Once the Higgs mass will be known, all decay widths and production processes of the Higgs particle will be uniquely determined [9].
While the electroweak theory is usually associated with spontaneous symmetry breaking via the Higgs mechanism, the Higgs boson does not *have* to exist. It could be replaced by some other dynamical mechanism, e.g. W substructure. A common feature of many alternative scenarios are yet undiscovered particles or processes which should become visible at centre-of-mass energies $\mathcal{O}(1\ \text{TeV})$.

2.1.2 Mass of the Higgs Boson

Although the mass of the Higgs boson cannot be predicted within the Standard Model, the permitted region for its mass can be limited due to the demand for self consistency of the theory and extrapolations of the model to high energies. Several theoretical upper and lower bounds on the mass can e derived from the hypothesis that the Standard Model remains valid up to an energy scale without the influence of new physical phenomena. The high energy behavior of the scattering of longitudinal polarized W bosons is one of the reasons to introduce the Higgs boson. Under consideration of the Higgs boson exchange the s-wave amplitude of the W boson scattering at very high energies is:

$$A = \frac{G_F M_H^2}{4\sqrt{2}\pi}.$$

With the requirement that the amplitude has to be compatible with unitarity, follows [10]:

$$M_H^2 \leq \frac{2\sqrt{2}\pi}{G_F} \approx (850)\ GeV^2.$$

Quite restrictive bounds on the value of the Standard Model Higgs mass follow from hypotheses on the energy scale Λ up to which the Standard Model can be extended before new physical phenomena emerge, which would be associated with new strong interactions between the fundamental particles. The key to these bounds is the evolution of the quartic Higgs coupling λ with the energy (i.e. the field strength) due to quantum fluctuations [11–15].
A lower bound on the Higgs mass can be derived from the requirement of vacuum stability [11–17]. By considering that the Higgs potential has been stable over a time long enough to allow the present universe to have formed, quantitative statements can be made about its shape. There is full vacuum stability if the present Higgs minimum is an absolute one. Even if this is not the case, then estimates of its value can be made which depend on the observed age of the universe. This constraint leads to a lower bound that is well below the present experimental predictions. The lower bound depends on the cut-off value Λ. For any given Λ the allowed value of the Higgs boson mass m_H is shown in Figure 1. For a cut-off value of 10^{19} GeV the Higgs mass is restricted to a window between 130 and 190 GeV/c^2 [18]. A top mass of $m_t = 175$ GeV/c^2 is assumed. The observation of a Higgs mass above or below this window would demand a new physics scale below the GUT scale. For new physics interactions with a scale of the order of one TeV, the Higgs boson mass is much less constrained, lying between 50 to 800 GeV/c^2.
The mass of the Higgs boson can be measured by collecting the decay products of the particle. Moreover, in e^+e^- collisions m_H can be measured best by exploiting the kinematical characteristics of the Higgs-strahlung production process $e^+e^- \to Z^* \to ZH$, where the Z boson can be reconstructed in both its hadronic and leptonic decay modes. The Higgs boson mass determination relies on a kinematical 5C fit imposing energy and momentum conservation and requiring the mass of the jet pair closest to the Z mass to correspond to m_Z. This procedure gives a mass resolution of approximately 2 GeV for individual events. A fit to the resulting mass distribution gives an expected accuracy of $\delta m_H \sim 100$ MeV/c^2.
In pp or $p\bar{p}$ collisions the Higgs boson mass reconstructed from the decay products is broader then the decay width for Higgs boson masses up to 300 GeV/c^2. For higher masses the expected precision at LHC is 5% to 6%.

2.1.3 Decay of the Higgs Boson

The properties of the Higgs particle is uniquely determined if the Higgs mass is fixed. The strength of the Yukawa couplings of the Higgs boson to fermions is set by the fermion masses m_j, and the couplings to the electroweak gauge bosons $V = W, Z$ by their masses M_V:

$$g_{ffH} = [\sqrt{2}G_F]^{1/2} m_f$$

$$G_{VVH} = 2[\sqrt{2}G_F]^{1/2} M_V^2.$$

Because of the proportionality of the coupling to fermion mass, the Higgs boson will decay preferentially to the heaviest available quark or lepton pair. The total decay and lifetime, as well

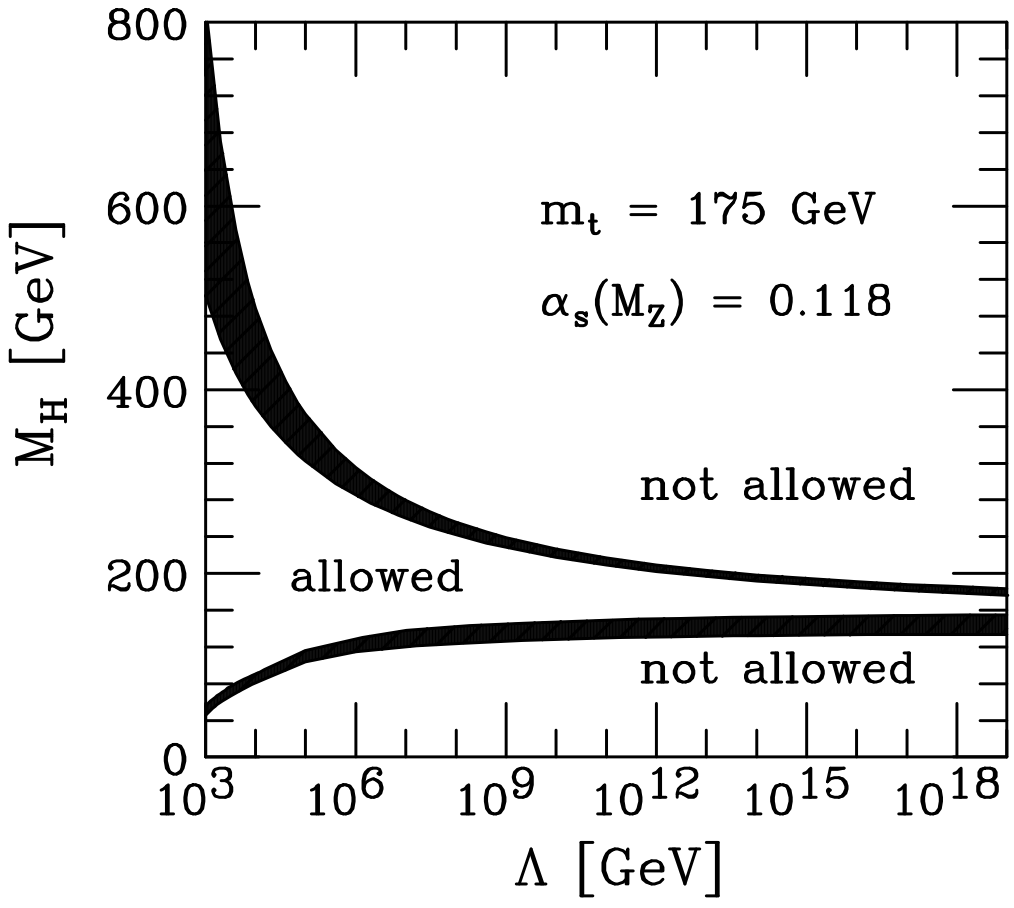

Figure 1: Bounds on the mass of the Higgs boson in the Standard Model. Here Λ denotes the energy scale at which the Higgs boson system of the Standard Model would become strongly interacting (upper bound). The lower bound follows from the requirement of vacuum stability. A top mass of $m_t = 175$ GeV/c^2 is assumed.

as the branching ratios for specific decay channels, are determined by these parameters. For Higgs particles in the intermediate mass range $\mathcal{O}(M_Z) \leq M_H \leq 2M_Z$, the main decay modes are decays into $b\bar{b}$ pairs and WW, ZZ pairs, one of the gauge bosons being virtual below the respective threshold. Above the WW, ZZ pair thresholds, the Higgs particles decay almost exclusively into these two channels at a ratio of 2:1, with a small admixture of top decays near the $t\bar{t}$ threshold. Below 140 GeV/c^2, the decays $H \rightarrow \tau^+\tau^-, c\bar{c}$ and gg are also important besides the dominating $b\bar{b}$ channel; $\gamma\gamma$ decays, though suppressed in rate, nevertheless provide a clear 2-body signature for the formation of Higgs particles in this mass range.
The branching ratios of the main decay modes are displayed in Figure 2. For Higgs boson masses

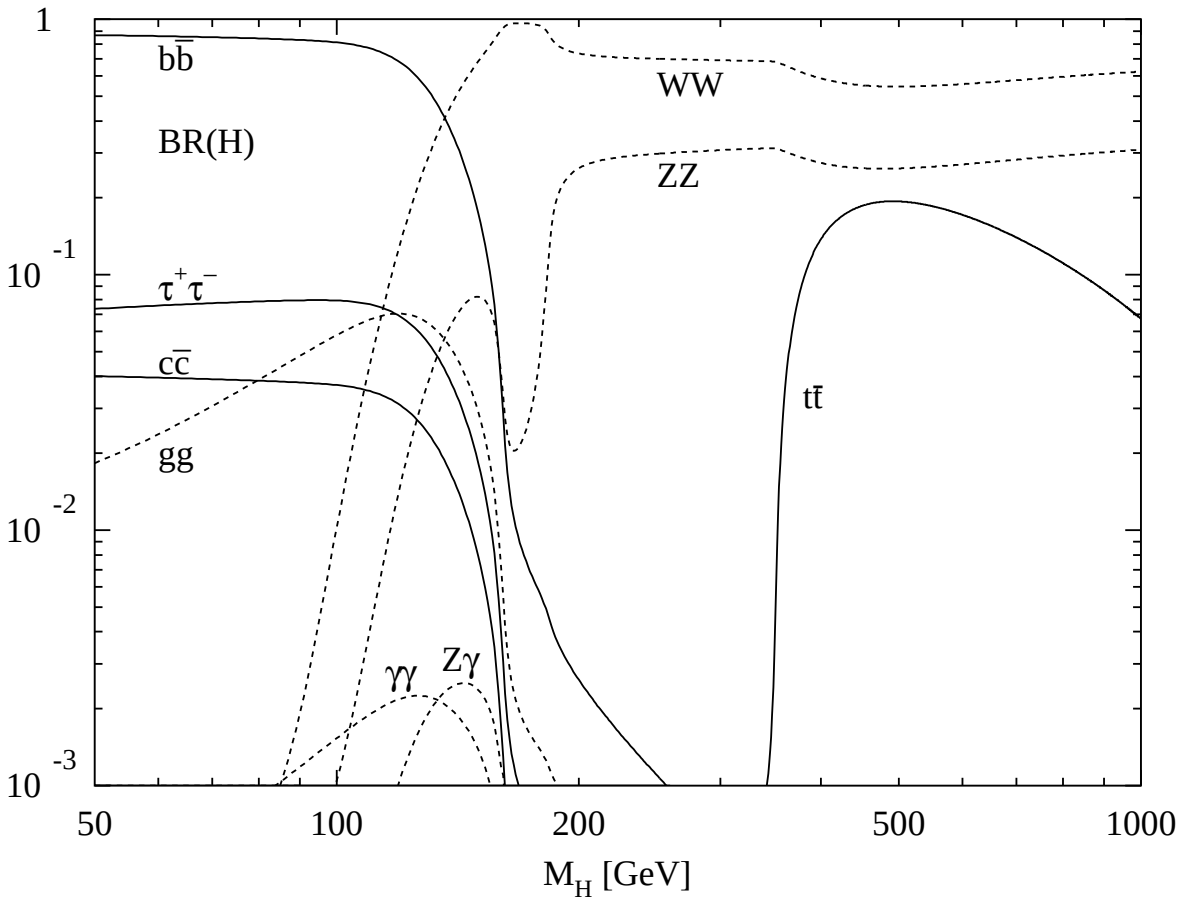

Figure 2: Branching ratios of the dominant decay modes of the Standard Model Higgs particles. All relevant higher-order corrections are taken into account [19].

accessible at LEP energies ($m_H < 115$ GeV/c^2) the Higgs boson decays dominantly in $b\bar{b}$ pairs ($\sim 80\%$). At TeVatron searches for the Higgs boson will be possible in the mass range between 110 GeV/c^2 and 180 GeV/c^2. Here the dominant decay modes are $b\bar{b}$ (up to 135 GeV/c^2) and W^+W^- (above 135 GeV/c^2). At LHC the whole mass range up to 1 TeV/c^2 will be accessible

allowing to search for Higgs bosons in many different decay channels.
By adding up all possible decay channels the total width as shown in Figure 3 is obtained. Up to masses of 140 GeV/c^2 the Higgs decay width is very narrow (<10 MeV). After opening the mixed real/virtual gauge boson channels, the state becomes rapidly wider, reaching a width of $\sim$ 1 GeV at the ZZ threshold. Since the width grows with the third power of the mass, the Higgs boson becomes very wide, $\Gamma(H) \sim \frac{1}{2} M_H^3 [TeV]$. Whether the Higgs boson is searched for at

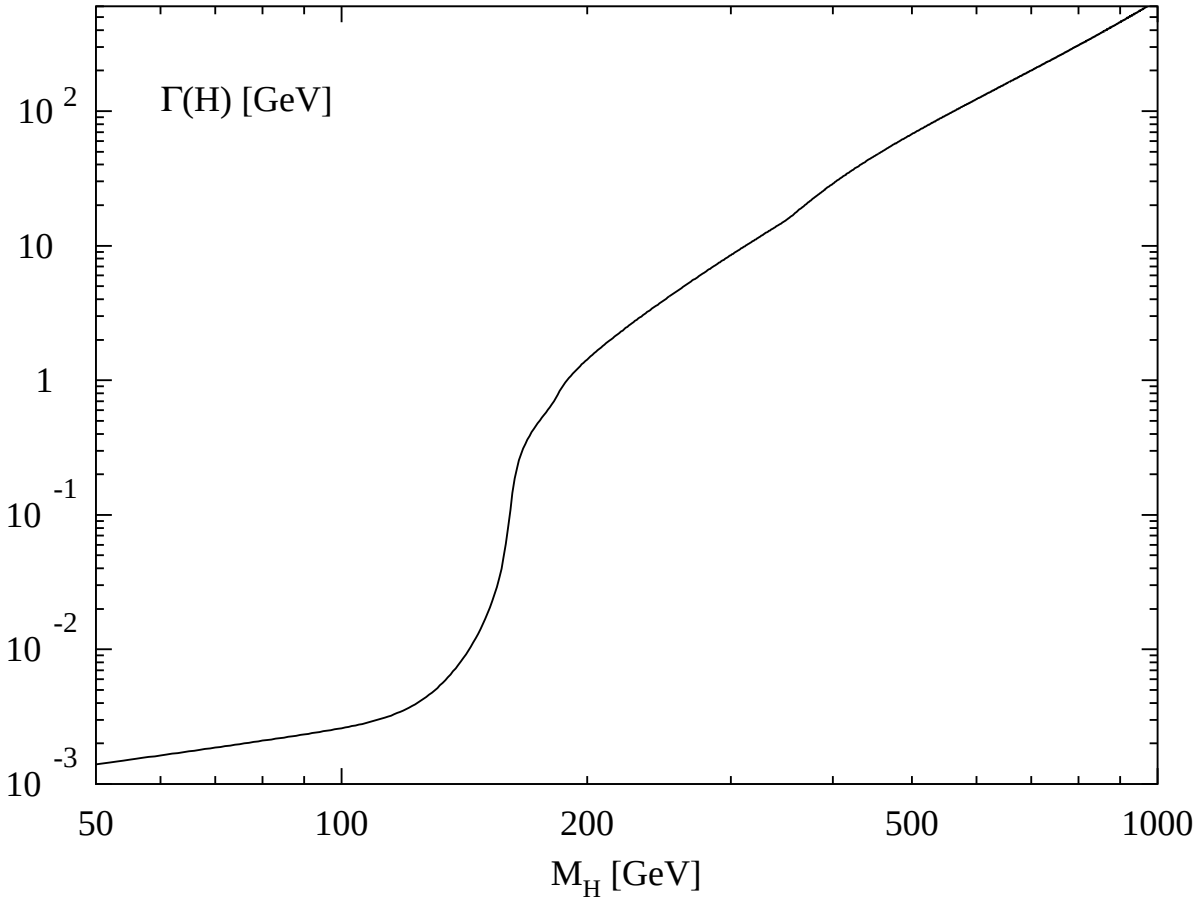

Figure 3: The total decay width (in GeV) of the Standard Model Higgs boson as a function of its mass. A top mass of $m_t = 175$ GeV/c^2 is assumed.

e^+e^- or pp colliders, the expected production cross section multiplied by the decay branching ratios are very small. Integrated luminosities of order 100 fb^{-1} are necessary, corresponding to runs of a year or more at the highest available luminosities, of order 10^{34} cm^{2}s^{-1}.

2.2 The Minimal Supersymmetric Standard Model

Supersymmetric extensions of the Standard Model are strongly motivated by the idea of providing a solution of the hierarchy problem in the Standard Model Higgs sector. They allow for a light Higgs particle in the context of GUTs [20], in contrast to the Standard Model, where the

extrapolation requires an unsatisfactory fine-tuning of the Standard Model parameters. Supersymmetric extensions does not exhibit any quadratic divergences, in contrast with the Standard Model Higgs sector.
In the minimal supersymmetric extension of the Standard Model (MSSM) [21], the Higgs sector contains two doublets. At tree level, the down and up quarks only couple to the neutral components of the Higgs doublet H_1 and H_2, respectively, preventing flavor-changing neutral current (FCNC) effects. The ratio of the vacuum expectation values of the two Higgs doublets, v_1 and v_2, is parametrized by $\tan\beta = v_2/v_1$. After the electroweak symmetry breaking mechanism, three of the eight degrees of freedom are absorbed by the Z and W gauge bosons, leading to the existence of five elementary Higgs particles. These consist of

- two charged H^+, H^- bosons,
- one CP-odd Higgs boson, A,
- and two CP-even, a light (h) and a heavy (H) Higgs boson.

At tree level all Higgs boson masses may be expressed as functions of $\tan\beta$, m_A and the W and Z boson masses, and an upper bound on the lightest CP-even Higgs boson mass is found, $m_H \leq M_Z |\cos 2\beta|$ [22]. This bound is modified by radiative corrections [23–27], which depend quartically on the top quark mass and logarithmically on the top squark masses [28, 29]. The upper mass limit preferred by supersymmetry is $m_h \lesssim 135$ GeV/c^2 [30–33]. In the MSSM the h boson will decay mainly to fermion pairs since the mass is smaller than about 135 GeV/c^2. The A boson also decays predominantly to fermion pairs, independently of its mass, since its coupling to vector bosons is zero at leading order.

2.3 Two Higgs Doublet Models

The existence and the structure of the Higgs sector is experimentally unknown. Up to now there is no evidence for supersymmetric particles. It is clearly desirable to explore the implications of more complicated Higgs models, both in the context of the Standard Model and in extended theories. The Two Higgs Doublet Model (2HDM) of the Standard Model is particularly attractive because it adds the fewest new parameters and it adds new phenomena (e.g. physical charged Higgs bosons).
The 2HDMs are characterized by five physical Higgs bosons as in the MSSM as a special case of 2HDMs. The important parameters for describing the 2HDM are the angles α and β, where α is the mixing angle in the neutral CP-even Higgs sector and $\tan\beta$ is the ratio of the vacuum expectation values of the two Higgs doublets. In the framework of 2HDM there are four different ways in which the Higgs doublets can couple to fermions [34]. The most common choice (Type II) is the structure assumed in the MSSM: one of the Higgs doublets couples both to up type quarks and to charged leptons, and the other doublet couples to down type quarks. The decay branching ratios of the Higgs boson to fermions depend not only on the masses, but also on the values of α, which is the mixing angle between the two fields and the physical Higgs boson states, and β. The coupling of the h to down-type quarks is proportional to

$$hd\bar{d} : -\sin\alpha/\cos\beta;$$

the coupling of the h to up-type quarks is proportional to

$$hu\bar{u} : \cos\alpha/\sin\beta;$$

the coupling of the A to down-type quarks is proportional to

$$Ad\bar{d} : \tan\beta;$$

and the coupling of the A to up-type quarks is proportional to

$$Au\bar{u} : \cot\beta.$$

In Type I models only one of the Higgs doublets couples to fermions. The coupling of the lightest CP-even boson h to a fermion pair is then proportional to $\cos\alpha$.
In the MSSM and 2HDM the couplings of the neutral Higgs bosons to quarks, leptons and gauge bosons are modified with respect to those of the Standard Model Higgs boson by factors which depend upon the mixing angle α and the ratio of the vacuum expectation values of the Higgs doublets $\tan\beta$.

3 Past: Higgs Bosons at LEP

LEP is the world's largest collider for electrons and positrons. Since the beginning of data-taking in 1989 experiments were performed to improve the understanding of the Standard Model of particle physics. The most accurate measurements of various parameters from the study of Z^0 production and decay, like mass, line shape and branching ratios to leptons and hadrons, angular asymmetries of the Z^0 decay products have been performed at LEP. Only weeks before LEP had to be shut-down to give space for a new generation of collider, the LHC, the LEP collaborations and the LEP Working Group for Higgs boson searches [35] have recently reported excesses of events that might be due to the production of a Higgs boson weighing about 115 GeV/c^2. A verification of this exciting interpretation of their events may have to wait for several years.
In this chapter we will summarize the results of the search for Higgs bosons in the Standard Model and its extensions obtained by the four LEP Collaborations.

3.1 The LEP Collider and the Detectors

LEP (Large Electron Positron Collider) is the largest collider for electrons and positrons with a circumference of 27 km. Collisions take place at four points where the particle detectors ALEPH [36], DELPHI [37], L3 [38] and OPAL [39] are located. Since the beginning of data-taking in 1989 until 1995 the centre-of-mass energy was around 91 GeV, which corresponds to the mass of the Z^0 boson. Per experiment around 4.5 million hadronic Z^0 decays have been observed. Precision tests of the Standard Model have been performed [40]. Since 1995 the centre-of-mass energy has been increased up to 209 GeV. This allows to search for new particles and for the Higgs boson in the Standard Model and extensions of it.
The basic structure of all four LEP detectors is rather similar. Detector components of different functionality surround the beam pipe in cylindrical layers. To achieve hermiticity the sequence

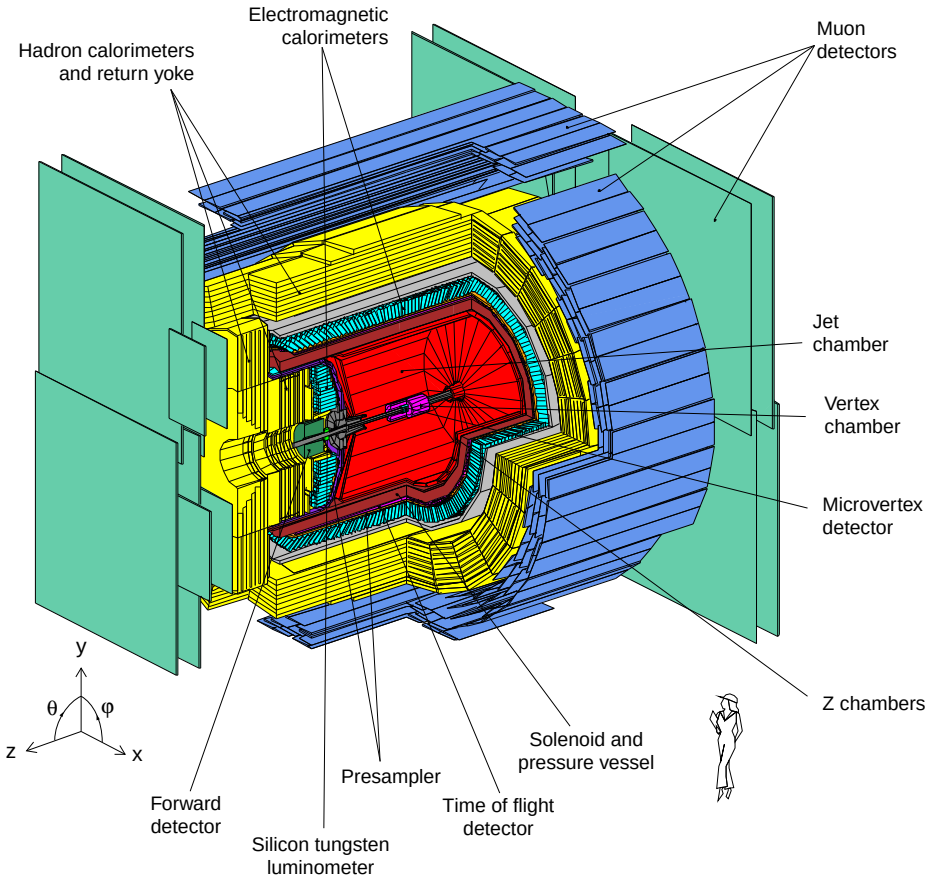

Figure 4: A 3-dimensional schematic view of the OPAL detector.

of layers is repeated at the endcaps. As a typical example the OPAL detector (Figure 4) will be described in the following.
A brief description of the apparatus is given here while a detailed description can be found in [39]. Particles emerging from the interaction region traverse a high precision silicon micro-vertex detector as innermost layer followed by three tracking chambers with larger volume. These tracking devices are located within a coil providing a homogeneous solenoidal field of 0.4 Tesla. The system allows for a precise reconstruction of primary and secondary vertices of the events, a momentum measurement with an accuracy of

$$\frac{\sigma_p}{p_T} = \sqrt{(0.02)^2 + (0.0015(\mathrm{GeV}^{-1}) \cdot p_t)^2}$$

and particle identification by multiple scattering of the energy loss.
The electromagnetic calorimeter is a homogeneous detector composed of 9440 (2264) lead glass blocks in the barrel (end-cap) region. The intrinsic energy resolution of the electro-magnetic calorimeter with its 22 radiation lengths is

$$\frac{\sigma_E}{E} \approx 0.2\% + \frac{6.3\%}{\sqrt{E[GeV]}}.$$

The return yoke for the magnetic flux from the magnet is used as the iron absorber of the hadron calorimeter. The depth is 4.8 nuclear interaction lengths. The energy resolution is about

$$\frac{\sigma_E}{E} \approx \frac{120\%}{\sqrt{E[GeV]}}.$$

The outermost part of the OPAL detector is formed by the muon detectors, drift chambers with a typical spatial resolution of 1.5 mm in the $r - \phi$ plane and 2 mm in the z direction.

3.2 Limits on the Higgs Boson Mass from Electroweak Precision Measurements

Several measurements at LEP, TeVatron and SLAC have reached a precision which is sensitive to higher order corrections of the electroweak theory. These corrections depend logarithmically on the Higgs boson mass. Assuming that the Standard Model as an effective theory is valid up to high energy scales it is possible to determine the Higgs boson mass from the size of electroweak radiative corrections to these precision measurements [41].
A global fit to the data available [42, 43] results in a value of the Higgs mass of

$$m_H = 98^{+58}_{-38}\ \mathrm{GeV}/c^2.$$

Translated into an upper limit at the 95% confidence level that yields to $m_H < 212$ GeV/c^2. In Figure 5 the observed value of $\Delta\chi^2 = \chi^2 - \chi^2_{min}$ as a function of m_H is plotted for the fit including all data. The lower limit on m_H of approximately 113 GeV/c^2 obtained from direct searches [35] has not been used in the determination of m_H.
Two values of the electromagnetic fine structure constant $\alpha(M_z^2)$ evaluated at a momentum transfer $Q^2 = m_Z^2$ have been used. The problem in the determination of $\alpha(M_z^2)$ arises from the uncertainty of the hadronic corrections $\Delta\alpha^{(5)}_{had}$. This correction can be derived by a dispersion

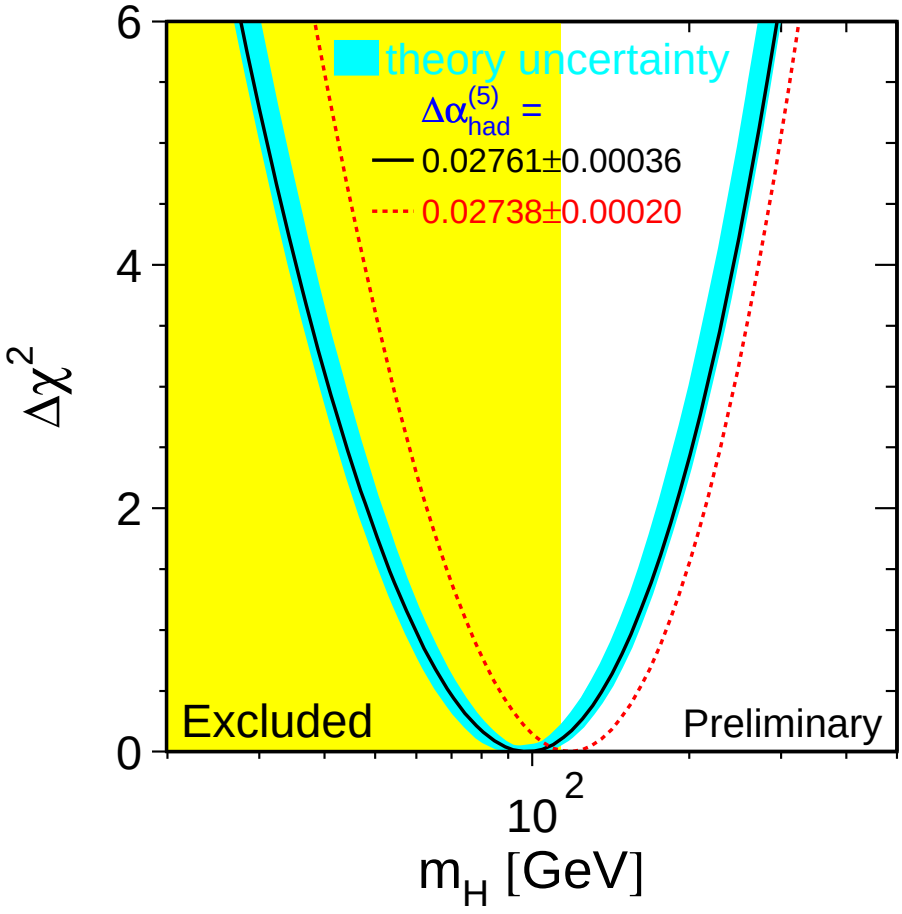

Figure 5: $\Delta\chi^2 = \chi^2 - \chi^2_{min}$ as a function of m_H. The line is the result of the fit using all electroweak data. The band represents an estimate of the theoretical error due to missing higher order corrections. The vertical band shows the 95% confidence level exclusion limit from the direct search at LEP.

relation from measurements of the hadronic cross-section in e^+e^- collisions at centre-of-mass energies in the region 1–10 GeV. A significant improvement of the accuracy has been obtained in the analysis of [44] by the inclusion of new data from the BES collaboration [45]. To demonstrate the impact of $\Delta\alpha^{(5)}_{had}$ on m_H Figure 5 also shows the χ^2 curve obtained when an evaluation with more theoretical assumptions [46].
By combining the information from precision measurements with the results from the direct search experiments carried out at LEP the probability that the Higgs boson weighs less than 116 GeV/c^2 comes to be around 35% while the 95% upper limit is located around 205–230 GeV/c^2 [47, 48].

3.3 Search for Neutral Higgs Bosons in the Standard Model

In the year 2000 - the final year of LEP running - the four LEP experiments have collected data at energies between 200 and 209 GeV, for approximately 850 pb^{-1} integrated luminosity with about 480 pb^{-1} above 206 GeV. The LEP working group for Higgs boson searches has combined these data with data sets collected earlier at lower energies. From combining the earlier data collected by the LEP experiments at centre-of-mass energies up to 202 GeV, a 95% confidence level lower bound of 107.9 GeV/c^2 has been obtained [49]. The probability that the whole data sample is compatible with originating exclusively from Standard Model background processes is found to be 0.4%.
The last few months of data-taking at LEP with centre-of-mass energies up to 209 GeV have given a tantalizing hint that the Higgs boson might indeed have a mass around 115 GeV/c^2. The technique and the results of the search at highest LEP energies will be described in the following.

3.4 Event Selection

In this section we present an update of the Standard Model Higgs boson search which includes the new data collected in the year 2000 at centre-of-mass energies up to 209 GeV.
At LEP the Standard Model Higgs boson is expected to be produced mainly via the Higgs-strahlung process $e^+e^- \rightarrow HZ$ and the WW fusion channel, $e^+e^- \rightarrow W^*W^* \rightarrow H\nu_e\bar{\nu}_e$ (see Figure 6). Contributions from the $WW \rightarrow H$ fusion channel are typically below 10% because the cross section for the Higgs-strahlung process scales as $1/s$ and dominates at low energies. The ZZ fusion mechanism, $e^+e^- \rightarrow Z^*Z^*e^+e^- \rightarrow He^+e^-$, also contributes to Higgs production, with a cross section suppressed by an order of magnitude compared to that for WW fusion.
The total production cross section near the kinematic edge is of the order of 50 to 500 fb, depending on how close m_H is to $\sqrt{s} - m_Z$. The Standard Model Higgs boson is expected to decay predominantly into $b\bar{b}$ pairs in the mass range of interest, with a branching ratio of 78% at $m_H = 110$ GeV/c^2. The second important decay mode is to tau pairs, with a branching ratio of approximately 7%. The searches performed by the four LEP collaborations encompass the usual HZ final state topologies, commonly called

- four-jet channel: $HZ \rightarrow b\bar{b}q\bar{q}$,
- missing energy channel: $b\bar{b}\nu\bar{\nu}$,

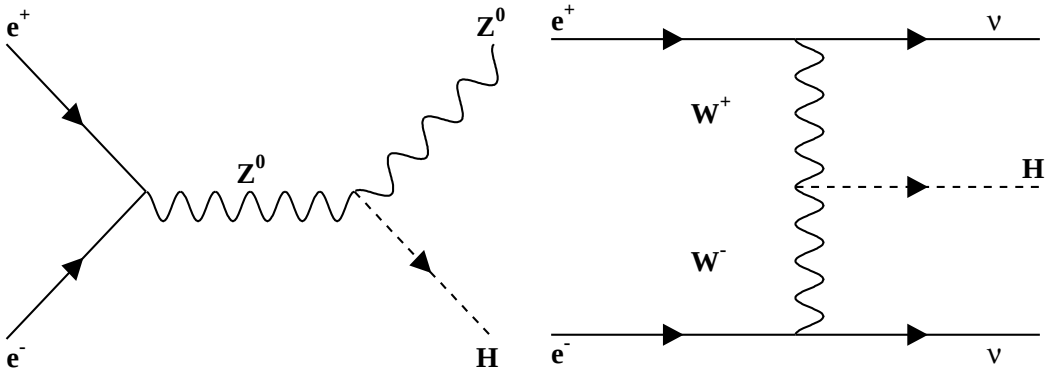

Figure 6: Production of the Higgs Boson in the Standard Model at LEP: Higgs-strahlung (left side) and WW-pair fusion (right side).

- leptonic channel: $b\bar{b}e^+e^-$ and $b\bar{b}\mu^+\mu^-$,
- and tau channel: $b\bar{b}\tau^+\tau^-$ and $\tau^+\tau^-q\bar{q}$.

Issues of critical importance to the four-jet channel are b-tagging, jet pairing and mass reconstruction. Information on the b-hadron lifetime, mass and semi-leptonic decays are combined into a neural net. The neural nets are calibrated with the data taken each year at the Z^0 peak and then checked at higher energies. High energy samples enriched in b-quarks can be obtained via the process $e^+e^- \rightarrow Z\gamma$; while samples enriched in non b-quarks can be obtained via the process $e^+e^- \rightarrow WW \rightarrow l\nu qq$. As an example the b-tagging performance at OPAL is described. All experiments perform these checks. The b-tagging variable $\mathcal{B}$ is evaluated for each jet to distinguish jets containing b-hadrons from those that do not [50]. Figure 7(a) shows the distribution of $\mathcal{B}$ for the calibration data. Comparisons between the data and the Monte Carlo simulation are shown in Figure 7(b) for jets which are found opposite to jets passing or failing the b-tagging requirement. The tagging efficiency for b-flavoured (udsc-flavoured) jets is modeled by the Monte Carlo simulation to within an accuracy of 2% (5%). Figure 7(c) shows the b-tagging variable $\mathcal{B}$ for jets opposite b-tagged jets in the 2000 sample, taken by OPAL. The efficiency for tagging udsc flavours is also checked by computing $\mathcal{B}$ for the jets in a sample of $WW \rightarrow l\nu qq$ obtained with the selection used to measure the W^+W^- cross section [51] as shown in Figure 7(d).

To reconstruct masses in the four-jet channel a 4C-kinematic fit is imposed, in which energy and momentum are conserved. Effectively the fifth constraint of HZ production is also imposed.
In the missing energy channel the energy flow and the jet reconstruction are two fundamental items to correctly reconstruct the Higgs mass. To improve the resolution it is possible to impose the recoil mass to be the Z^0 mass. The most difficult task is the treatment of the $q\bar{q}\gamma\gamma$ background. In case each of the two photons is emitted symmetrically by the electron and positron and they are lost in the beam pipe, the event is signal like. The only possibility to discriminate this background from the signal is to consider the acoplanarity of the two jets. The searches

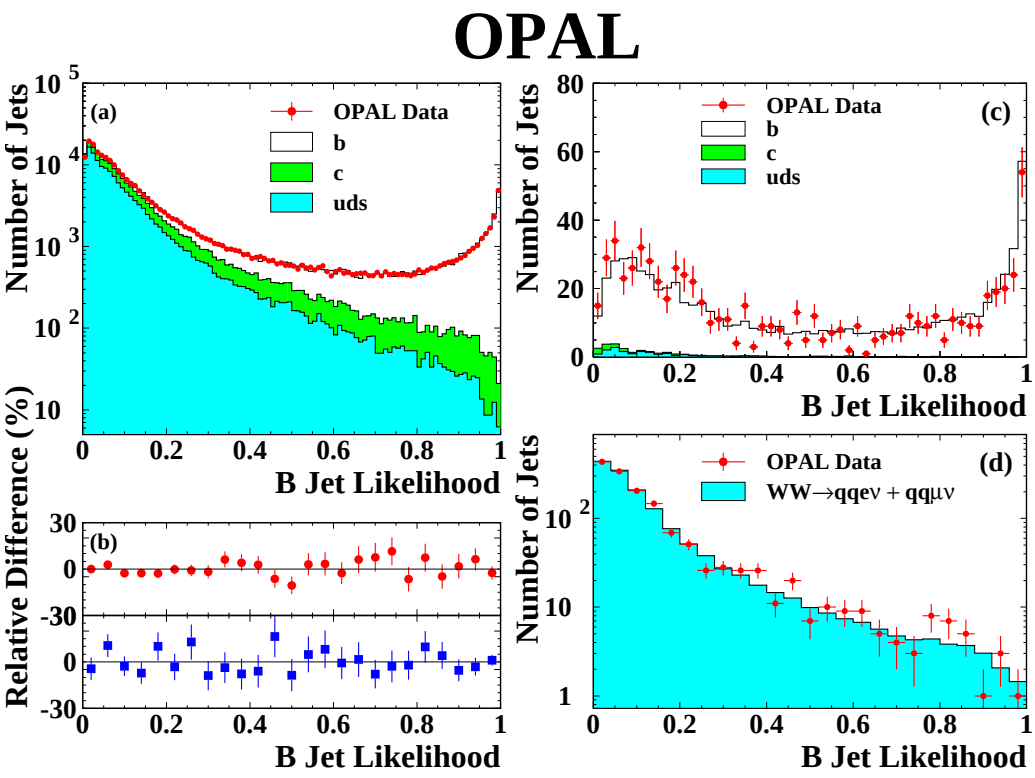

Figure 7: The b-tagging performance and modeling for (a–b) calibration data taken at $\sqrt{s} = m_Z$ in 2000, and (c–d) at $\sqrt{s}$ between 200–209 GeV in 2000. (a) The distribution of the b-tagging variable $\mathcal{B}$ for jets in data compared to the Monte Carlo expectation. (b) The bin-by-bin difference between data and Monte Carlo simulation for jets opposite non b-tagged jets (circles) and for jets opposite b-tagged jets (squares). (c) The b-tagging output, $\mathcal{B}$, for jets opposite b-tagged jets in a sample of $q\bar{q}\gamma$ events, and (d) for jets in a sample of $\mathrm{W^+W^-} \to \mathrm{q\overline{q}e^-\overline{\nu}_e}$ and $\mathrm{W^+W^-} \to \mathrm{q\overline{q}\mu^-\overline{\nu}_\mu}$ events (and charge conjugates). The histogram in (d) shows the distribution from the four-fermion Monte Carlo samples.

in the missing energy channel are optimized for Higgs-strahlung, but are also sensitive to the $WW \to H$ fusion process.
In the final states with charged leptons (leptonic and tau channels) the background contamination can be reduced to a smaller contribution than it is possible for the other final states for the same signal efficiency. Using constrained fits, the mass resolution can reach values of 2-3 GeV/c^2, and the typical problems of jet pairing of the four jet final states, or of energy flow of the missing energy channel are avoided.
The background processes can have cross sections of order of magnitude greater than those for the Higgs production (Figure 8):

- The two photon background can be easily reduced as their topology is very different from the signal.
- Another background arises from radiative returns to the Z^0 boson. Initial state radiation reduces the effective $\sqrt{s}$ to the Z^0 pole energy and produces boosted Z^0 events. These events are backgrounds to analyses requiring missing energy.
- Further background is the W-pair production $e^+e^- \to W^+W^-$. These produce four-jet final states, or jets and a lepton+missing energy, or two leptons and missing energy. The production of b-quarks in W decays is highly suppressed and therefore analyses with b-tagging achieve a good rejection of this background.
- The primary irreducible background to Higgs boson searches is the Z-pair production, $e^+e^- \to Z^0Z^0$. These events may have four jets, two jets and missing energy, two jets and two like-flavour but opposite-sign leptons, four leptons, or two leptons and missing energy. They have a high b quark content and therefore cannot be suppressed with b-tags.

The $Z\gamma$ and WW events will be the main background for all channels.
The cross sections σ of the fermion-pair and boson-pair production as well as for the Higgs-strahlung production at different Higgs boson masses as a function of the centre-of-mass energy $\sqrt{s}$ are compared in Figure 8. The energy dependence for the signal process shows the expected threshold behavior for the Higgs-strahlung process at $\sqrt{s} = m_Z + m_H$. At LEP1 energies a virtual Z^* boson and a Higgs boson has been produced in the Higgs-strahlung process, at LEP a real Z boson and a Higgs boson.
The analyses are often divided into two main steps: preselection cuts and the construction of a discriminant variable. In the preselection steps, the aim is to reduce events coming from background processes with different topological characteristics from signal events. The $\gamma\gamma$ background can be reduced to a negligible level and the 2-fermion and 4-fermion events are reduced by about a factor 15, keeping a high efficiency for the signal events.

3.5 Statistics and Definitions

The following steps consist of constructing a single variable that combines the most discriminating observables between background and signal events by means of a likelihood ratio or Neural Network techniques. The statistical procedure adopted for the combination of the data

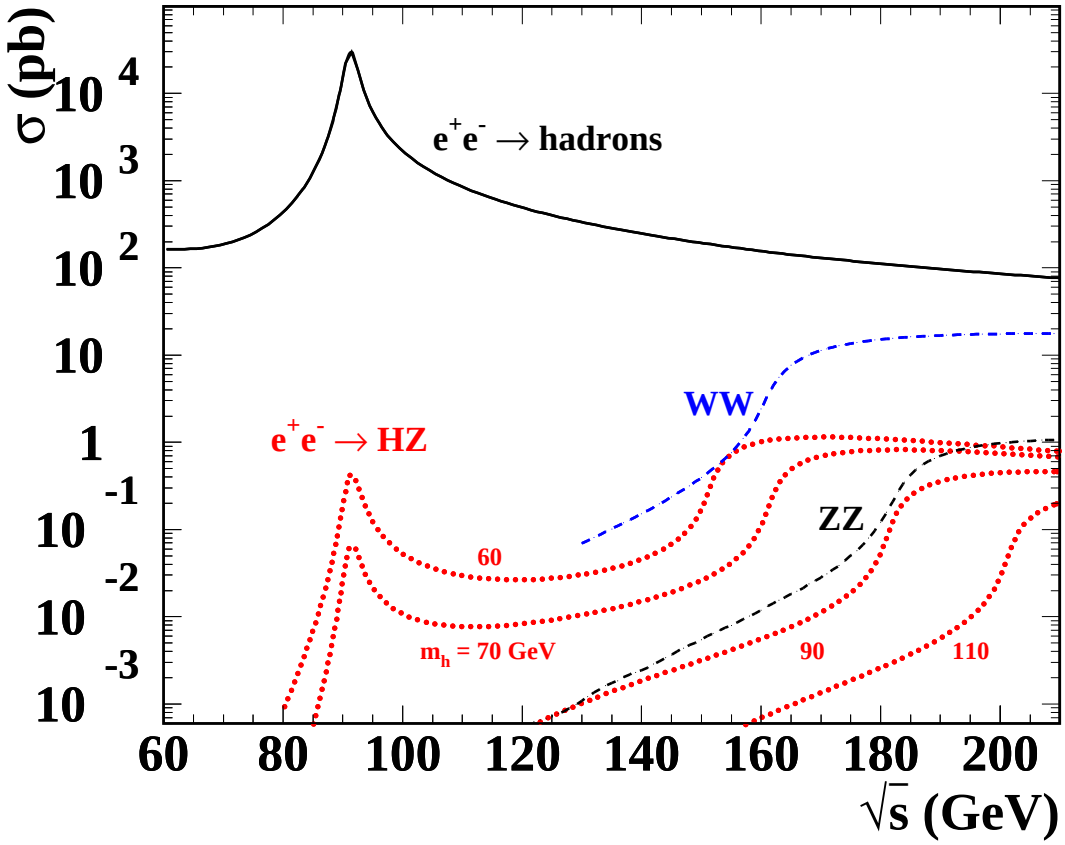

Figure 8: Cross section of $q\bar{q}$, W^+W^-, ZZ and HZ production in e^+e^- interactions as function of the centre-of-mass energy $\sqrt{s}$. The cross sections for the process $e^+e^- \to HZ$ are displayed for Higgs boson masses m_H=60–110 GeV/c^2. The background processes are shown with a dashed or a solid line, the signal process is shown with a dotted line.

and the definitions of the confidence levels CL_b, CL_{s+b} and CL_s by which the search results are expressed, will be stated here.
In the Standard Model as well as in the MSSM, the signal and background rates are predicted channel by channel. The corresponding search results can thus be combined for a better overall sensitivity. Furthermore, datasets from different LEP energies and experiments can also be added. The combined LEP data are used to test two hypotheses: the background-only (b) hypothesis, which assumes no Higgs boson to be present in the mass range investigated, and the signal+background (s+b) hypothesis, where Higgs bosons are assumed to be produced according to the model under consideration. A global test-statistic X is constructed which allows the experimental result $\mathrm{X}_{observed}$ to be classified between the b-like and s+b-like situations. It utilizes the number of selected events and various distributions which provide discrimination between signal and background (e.g.,the reconstructed mass or b-tag variables). The test-statistic takes into account experimental details such as detection efficiencies, signal-to-background ratios, resolution functions, and provides a single value for a given model hypothesis (e.g., the test-mass m_H in the Standard Model).
To set the scale for X, a large number of Monte Carlo experiments are generated, separately for the b and the s+b hypotheses, and separately for each model hypothesis (e.g., m_H). The resulting distributions of X(m_H) are normalized to become probability density functions, and integrated to form the confidence levels $CL_b(m_H)$ and $CL_{s+b}(m_H)$. The integration starts in both cases from the b-like end and runs up to $\mathrm{X}_{observed}$; thus $CL_b(m_H)$ and $CL_{s+b}(m_H)$ express the probabilities that the outcome of an experiment is more b-like or less s+b-like, respectively, than the outcome represented by the set of selected events.
When performing a search with small expected signal rates, it may happen that the observed number of candidates is far below the expected background level. In such cases the limit may extend beyond the range of sensitivity of the search, To prevent a priori such unphysical, but formally valid, results from occurring, the ratio

$$CL_s(m_H) = CL_{s+b}(m_H)/CL_b(m_H)$$

as a conservative approximation to the signal confidence one might have obtained in the absence of background is considered. The 95% CL lower limit for the Standard Model Higgs mass is defined here as the lowest value of the test mass m_H which yields $CL_s(m_H)$=0.05.
The quantity $1 - CL_b(m_H)$ is an indicator for a possible signal: a Standard Model Higgs boson with true mass m_0 would produce a pronounced drop in this quantity for $m_H \approx m_0$. Values of $1 - CL_b < 5.7 \times 10^{-7}$ ($1 - CL_b < 2.7 \times 10^{-3}$) would indicate a 5 σ (3 σ) discovery. These confidence levels may be computed using Monte Carlo techniques [52], or by various convolution methods [53]. Additional information is taken into account in the likelihood ratio $Q = L_{s+b}/L_b$, where L_b is the likelihood of the background hypothesis, and L_{s+b} is the likelihood when a specific Higgs boson signal is added to the background. The likelihood ratio measures the compatibility of the experiment with a particular signal mass hypothesis:

$$Q = \frac{L_{s+b}}{L_b} = \frac{e^{-(s+b)}}{e^{-b}} \prod_{i=1}^{n_{obs}} \frac{s f_s(X_i) + b f_b(X_i)}{b f_b(X_i)}$$

where s and b are the total numbers of signal and background events expected. Neglecting the f_s and f_b terms, this is simply the ratio of the Poisson probabilities to observe n_{obs} events for

the signal-plus-background and background-only hypotheses. The functions f_s and f_b are the probability densities that a signal or background event will be found in a given final state with the set of values X_i which includes the reconstructed mass and possibly a second discriminant.

The likelihood ratio is traditionally shown in the form $-2\ln Q$ (the log-likelihood estimator) because of the relationship between the likelihood ratio and chi-squared distributions, and because when the logarithm is taken, individual events contribute as a sum of event weights, $\ln(1 + sf_s/bf_b)$, which can be examined individually. The negative log-likelihood ratio for

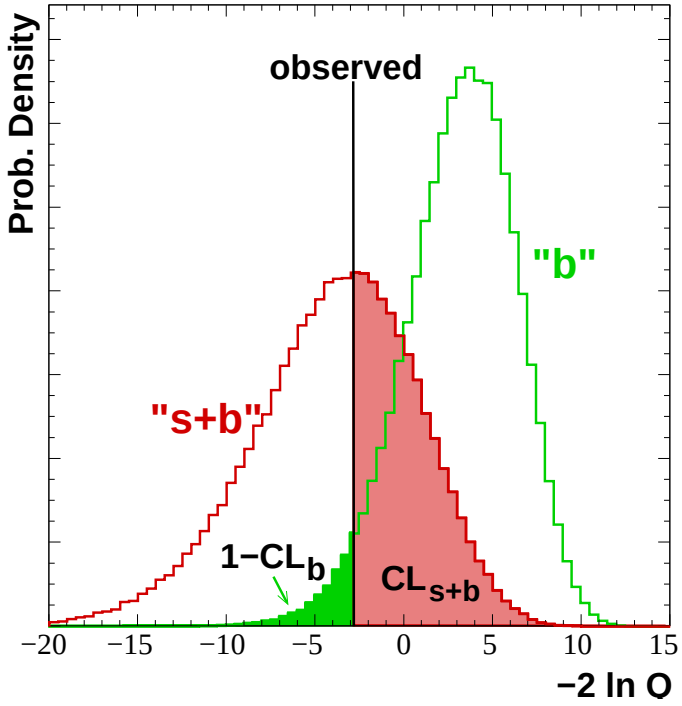

Figure 9: Negative log-likelihood ratio for an arbitrary test-mass. Vertical line: observed in data. Light grey curve: expected from the background-only hypothesis. Dark grey curve: expected from the signal-and-background hypothesis. Indicated by the light grey area is the 1-CL$_b$ confidence level and by the dark grey area the CL$_{s+b}$ confidence level.

an arbitrary test-mass is shown in Figure 9. The light grey area indicates the confidence level 1-CL$_b$ for the background-only hypothesis, the dark grey area indicates the confidence level CL$_{s+b}$ for the signal-and-background hypothesis.

3.6 Results

Before the final results from the four LEP experiments will be presented the results of the single experiments will be described.

3.6.1 Results from the ALEPH Collaboration

ALEPH has found an excess of 3 σ beyond the background expectation, consistent with the production of the Higgs boson with a mass of 114 GeV/c^2 [54]. Much of this excess is seen in the four-jet analyses where three high purity events are selected. As described in Reference [55], the Higgs boson search was conducted using both a Neural Network based stream (NN) and a cut-based stream (cut). Alternative analyses are used in the searches for four-jet and for missing energy final states, while the searches are identical in both streams for the lepton pair and tau lepton final states. In particular, a b-tagging Neural Network described in Ref. [56] is used, based upon the b-hadron lifetime, mass and semi-leptonic decays. In the four-jet cut-based analysis the pairing of the jets is based upon the decay angles of the Z and Higgs bosons. The NN analysis includes these two variables in the Neural Network and selects the jet pairing with the largest Neural Network output value, thereby effectively also using the b-tagging and Z boson mass information. In the four-jet analysis, a 4C kinematic fit is performed, in which energy and momentum conservation are imposed. The reconstructed Higgs boson mass m_{REC} is calculated as $m_{12}+m_{34}-m_Z$, where m_{12} and m_{34} are the fitted Z and Higgs boson masses. In the missing energy final state, the Higgs boson mass is reconstructed by a rescaling of the hadronic jets such that the missing mass is the Z boson mass. In the lepton pair final state, it is calculated as the mass recoiling against the pair of leptons. In the tau lepton final state, it results from a kinematic fit, with the Z mass constraint imposed either on the tau pair or on the hadronic system.

For the NN (cut) searches, a total of 134 (95) events are selected in the data, while 128.7 (87.6) events are expected from Standard Model background processes. In the observed distribution of $1-CL_b$ a large deviation from 0.5 - the expected value if the data are consistent with background only hypothesis - can be seen, consistent with an excess over the background hypothesis, which is maximal for a Higgs boson mass of 116 GeV/c^2. The probability of having such a large excess is 1.5×10^{-3} and 1.1×10^{-3} for the NN and cut streams, respectively. The significance of this excess is 3.0 σ and 3.1 σ relative to the expected background in the NN and cut streams. The Signal Estimator Method [57] is used to derive a 95% confidence level lower limit on the Standard Model Higgs boson mass of 111.1 GeV/c^2 (110.6 GeV/c^2) with an expected limit of 114.2 GeV/c^2 (113.8 GeV/c^2) for the NN (cut) stream.

One of the three high purity four-jet candidates is shown in Figure 10. The reconstructed Higgs boson mass is 114.3 GeV/c^2. Both of the Higgs boson jets are very well b-tagged with well measured displaced vertices and b-tagging neutral net values of 0.999. The measured invariant mass of the two non b-tagged jets is 92.1 GeV/c^2, consistent with a Z boson.

The observed distribution of $-2\ln Q$ is shown as a function of the hypothesized Higgs boson mass in Figure 11. The likelihood ratio is traditionally shown in the form $-2\ln Q$ (the log-likelihood estimator) because of the relationship between the likelihood ratio and chi-squared distributions, and because, when the logarithm is taken, individual events contribute as a sum of event weights, $\ln(1+\frac{sf_s}{bf_b})$, which can be examined individually. The most likely Higgs boson mass corresponds to the minimum, observed near 114 GeV/c^2.

In order to determine the impact of any given candidate event on the excess its contribution to the logarithm of the likelihood ratio is calculated as a function of the Higgs boson mass. All of the five four-jet events with weights larger than 0.4 in either the NN or cut analysis were selected with a centre-of-mass energy greater than 206 GeV. The largest contribution to the excess in the

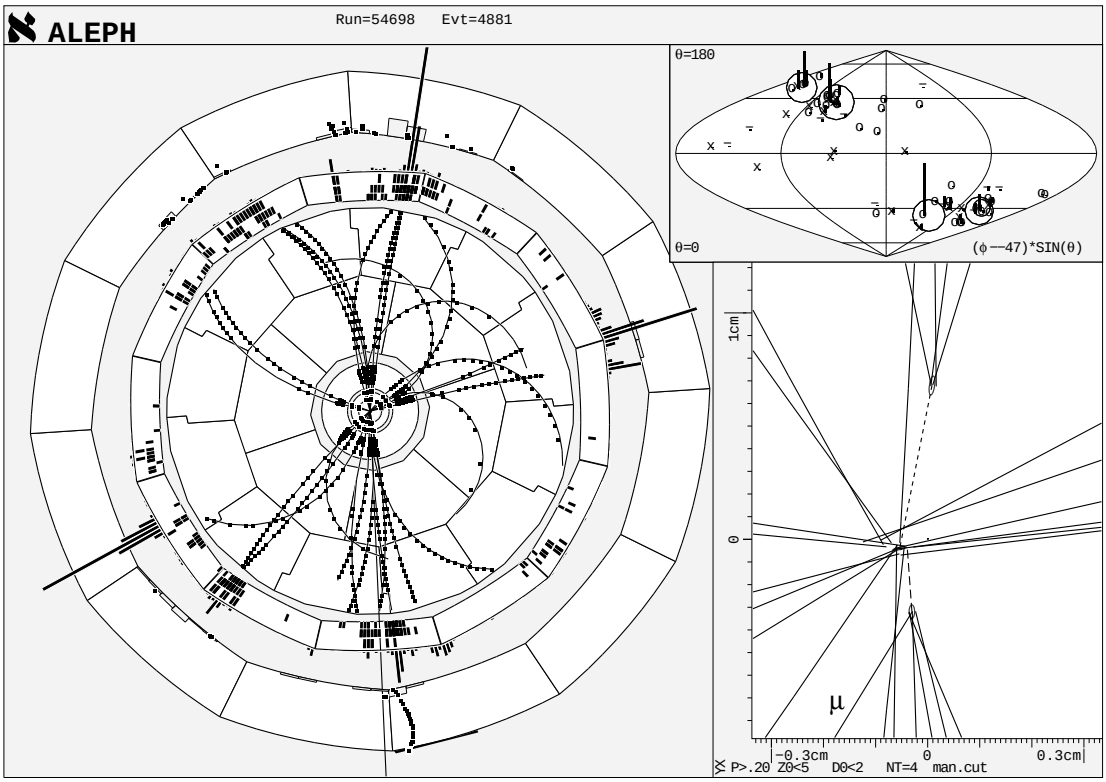

Figure 10: ALEPH four-jet Higgs boson candidate with a reconstructed Higgs boson mass of 114.3 GeV/c^2. The two Higgs boson jets are well b-tagged.

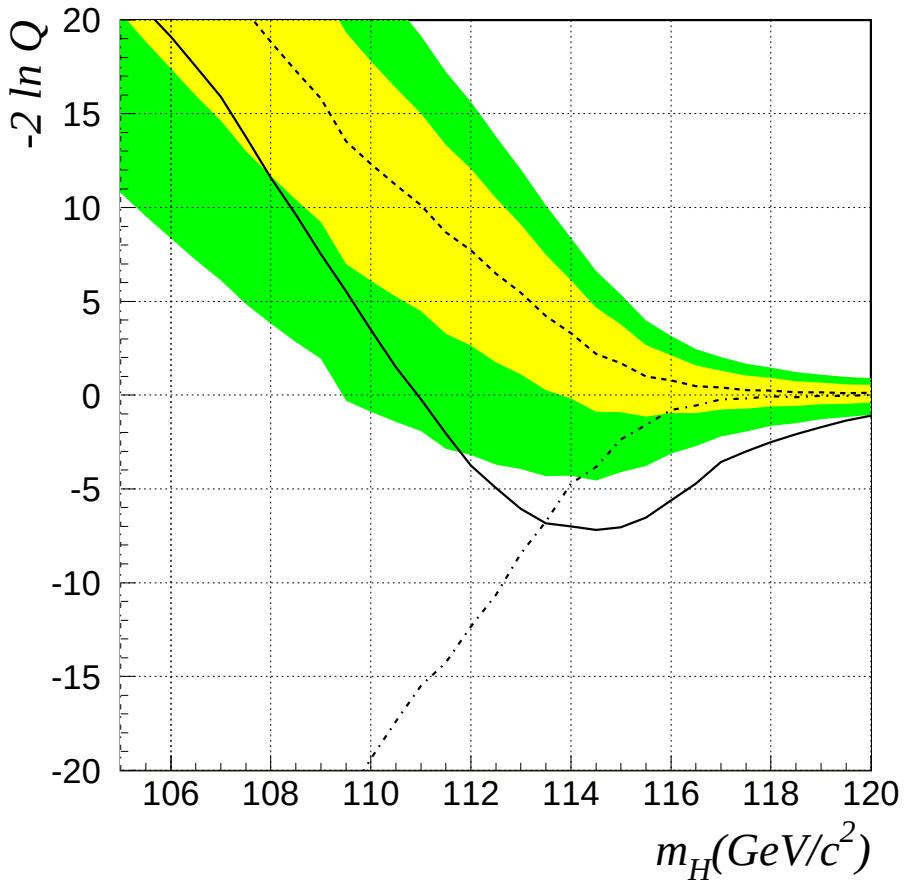

Figure 11: The log-likelihood estimator $-\ln Q$ for the NN stream as a function of the mass of the Higgs boson for the observation (solid) and background-only expectation (dashed) as seen by the ALEPH experiment. The light and dark grey regions around the background expectation represent the one and two sigma bands, respectively. The dash-dotted curves show the medians of the log-likelihood estimator as a function of the Higgs boson mass for the signal hypothesis.

NN stream comes from three four-jet events which have Neural Network output values larger than 0.99. The four-jet analysis uses only the reconstructed Higgs boson mass as discriminant, which causes the three 114 GeV/c^2 events to receive the same weights, whereas the four-jet NN analysis uses the Neural Network output as second discriminant. The stability of the excess can be investigated by increasing the purity of the event selections. The selection criteria of all analyses are tightened to give a signal ($m_H = 114$ GeV/c^2) to background ratio (s/b) of 1.5 for events with a reconstructed Higgs boson mass greater than 109 GeV/^{2}. To obtain a high purity selection in the four-jet NN-analysis, the cut on the Neural Network output is tightened. The purity of the four-jet cut selection is increased by tightening cuts on the b-tagging and the fitted Z boson mass. In the high mass region above 109 GeV/c^2, both the NN and cut streams select the same three four-jet candidates. All three candidates are collected at a centre-of-mass energy of 206.7 GeV. The reconstructed Higgs boson masses of these three candidates are
110.0 GeV/c^2, 112.9 GeV/c^2 and 114.3 GeV/c^2.

3.6.2 Results from the DELPHI Collaboration

The DELPHI Collaboration has not observed any evidence for a Higgs boson signal in the kinematically allowed mass range [58]. A 95% confidence lower mass limit of 114.3 GeV/c^2 has been set, to be compared with an expected limit of 113.5 GeV/c^2. The negative log-likelihood ratio is shown in Figure 12.
The limit on the Standard Model Higgs boson mass is set combining the data taken in the year 2000 with those taken at lower energies, namely 161 and 172 GeV, 183 GeV, 189 GeV and 192-202 GeV. The data collected by the DELPHI detector in the year 2000 corresponds to 224.1 pb^{-1}.
Compared to previous analyses [59] the following improvements have been introduced: The four-jet channel benefits from a better tuned b-tagging procedure and although it keeps the same event variables in the analysis, the discriminant Neural Network has been optimized for the high mass hypotheses. The missing energy channel includes a tighter preselection and additional variables in the likelihood, resulting in a better background rejection for a Higgs boson with high mass.
The result is not incompatible with the existence of a Higgs boson with a mass of 115 GeV/c^2. The confidence level CL$_s$(m_H=115 GeV/c^2) for this hypothesis is 12%.

3.6.3 Results from the L3 Collaboration

L3 has also reported Higgs boson candidates in the 212.5 pb^{-1} data collected in the year 2000 [60]. An excess of candidates for the process $e^+e^- \rightarrow Z^* \rightarrow HZ$ is found for Higgs boson masses near 114.5 GeV/c^2. For an assumed Higgs boson of this mass, the confidence level to be consistent with a background only hypothesis is calculated to be 0.09, equivalent to 1.7 σ from the background expectation. The confidence level to be consistent with signal plus background is 0.62.
The most significant $H\nu\bar{\nu}$ event is found where 0.16 background events and 0.38 signal events are expected (see Figure 13. This event was recorded at a centre-of-mass energy of 206.6 GeV. The event presents two nearly back-to-back jets with a large amount of missing energy and

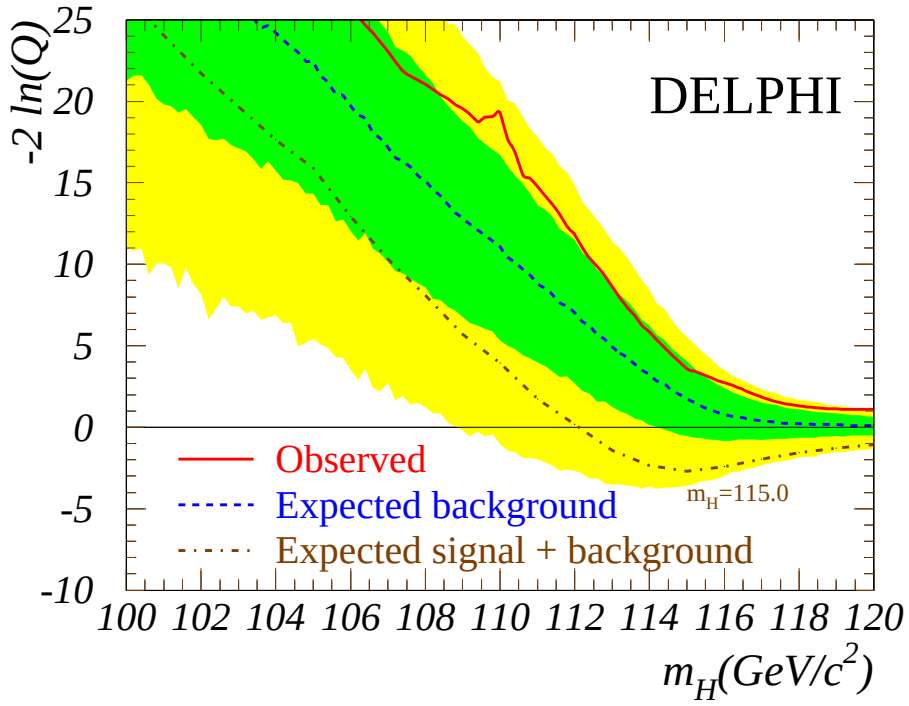

Figure 12: The log-likelihood estimator $-2\ln Q$ comparing the consistency of the data with the signal+background hypothesis with the consistency of the data with the background-only hypothesis as seen by the DELPHI experiment. The observation for the data is shown with a solid line. The dashed line indicates the median background expectation and the dark (light) shaded band shows the $\pm 1\sigma (\pm 2\sigma)$ variation. The median signal expectation is shown with a dot-dashed line.

very little missing momentum, compatible with the production of the Higgs boson and the Z boson nearly at rest. The visible mass is 111 GeV/c^2 and the event has a missing mass of 94 GeV/c^2. Assuming a Z boson recoiling against the Higgs, the fitted mass is 114.4 GeV/c^2 with a resolution of 3 GeV. The event has a high b-tag value and the acollinearity is 3 degrees . One jet has a very clear secondary vertex 7 mm from the primary, with a large visible mass. The main sources of background for this event are double radiative production of an off-shell Z boson and Z pair production.

3.6.4 Results from the OPAL Collaboration

OPAL has been performed the search based on the full data sample collected at $\sqrt{s} \approx$ 192-209 GeV in 1999 and 2000 [50].
The same final states as used by ALEPH are taken into account. The most important tool is again the b-tagging. The performance of the b-tagging is checked with high-purity samples of $q\bar{q}(\gamma)$ by selecting hadronic events with the mass of the $q\bar{q}$ system near m_Z. There is no evidence of mismodeling of the tagging rates within the statistical precision of the tests.
The preselection requirements in the four-jet channel are identical to those of [61]. After the preselection, a likelihood selection based on eight variables is applied. For each selected candidate, two of the jets are associated to the Higgs Boson using a likelihood method based on the kinematic fit result and the b-tagging information. The mass determined by a HZ 5C kinematic fit for the chosen jet pair gives the reconstructed mass of the Higgs boson candidate m_H^{rec}. Because of the kinematic fit, $m_H^{rec} < \sqrt{s} - m_Z$. The data are examined for their consistency with the background-only hypothesis and various Higgs boson mass hypotheses. The data favor slightly the Higgs boson production hypothesis for high masses, but are also consistent with the pure background hypothesis. The largest deviation with respect to the expected Standard Model background in the confidence level for the background hypothesis (1-CL$_b$), is observed for a Higgs boson mass of 107 GeV/c^2 with a minimum (1-CL$_b$) of 0.02, but the observed excess is less significant than expected for a Standard Model Higgs boson with a 107 GeV/c^2 mass. The observed low value of (1-CL$_b$) at 107 GeV/c^2 is caused by candidates which have relatively high weights at around 105-110 GeV/c^2.
The observed $-2\ln Q$ is shown as a function of the test mass m_H in Figure 14. The maximum deviation from the background expectation is observed near m_H=107 GeV/c^2, but this observation is not consistent with the expected Standard Model cross section for this signal hypothesis. Also shown are the 68% and 95% probability contours centered on the median expectation.
A lower mass bound on the Standard Model Higgs boson of 109.7 GeV/c^2 is obtained at the 95% confidence level while the median expectation for the background-only hypothesis is 112.5 GeV/c^2. For a Higgs boson mass in the 114-116 GeV/c^2 range, (1-CL$_b$) is approximately 0.2 which corresponds to 1.2 σ above the background expectation.

3.6.5 Combined Results from the four LEP Experiments

The four LEP experiments have collected about 2.5 fb^{-1} of e^+e^- collision data at energies between 189 and 209 GeV, of which 543 pb^{-1} are at energies above 206 GeV. The data have been combined and examined for their consistency with the Standard Model background hypothesis

a)

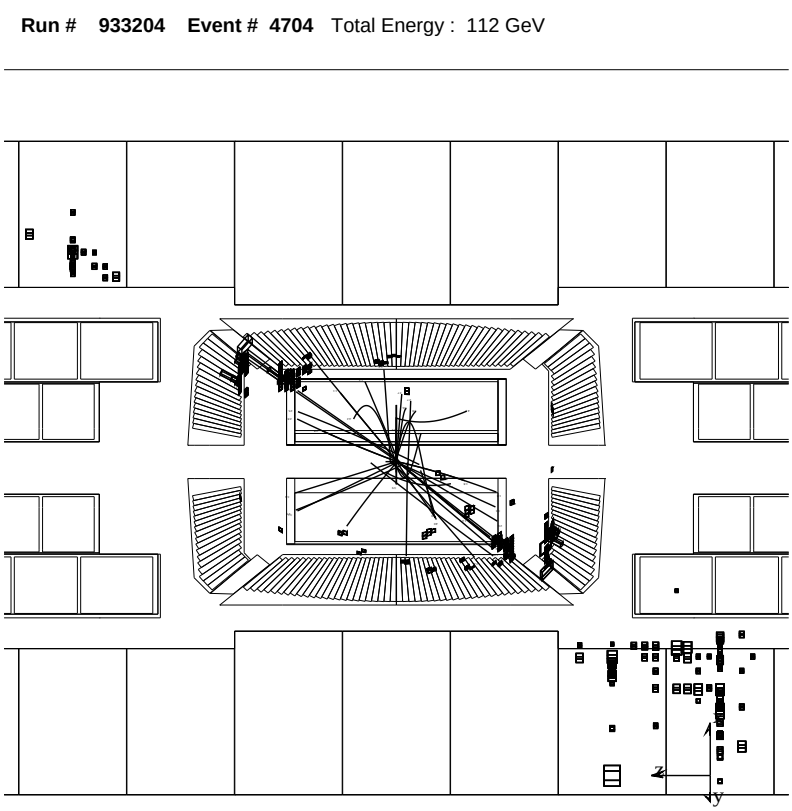

b)

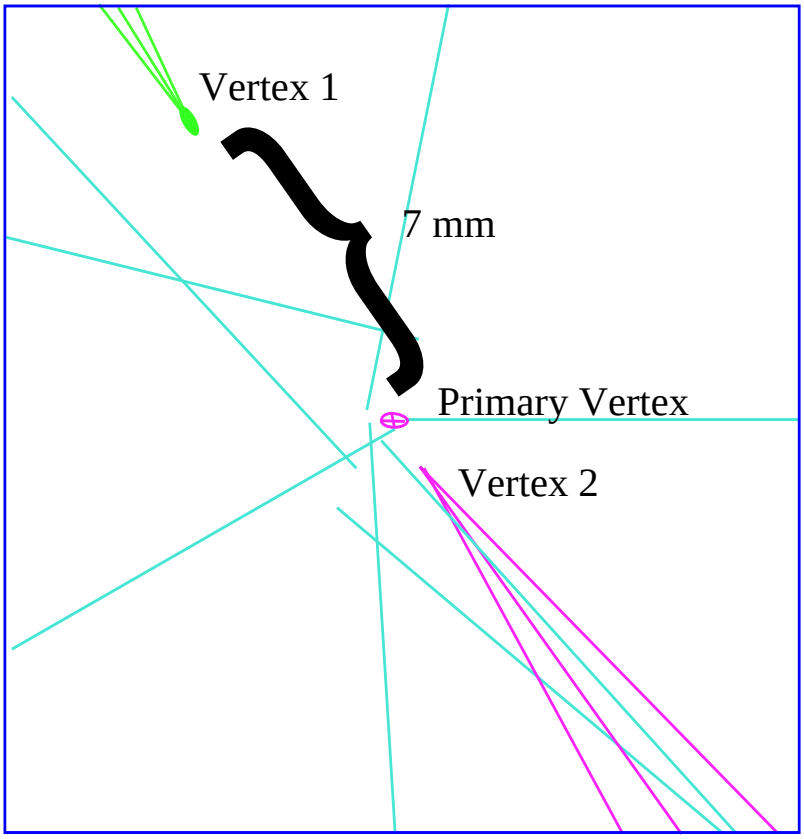

Figure 13: a.) L3 $H\nu\bar{\nu}$ Higgs boson candidate at a centre-of-mass energy of 206.6 GeV. b.) Close-up of the vertex region of this event.

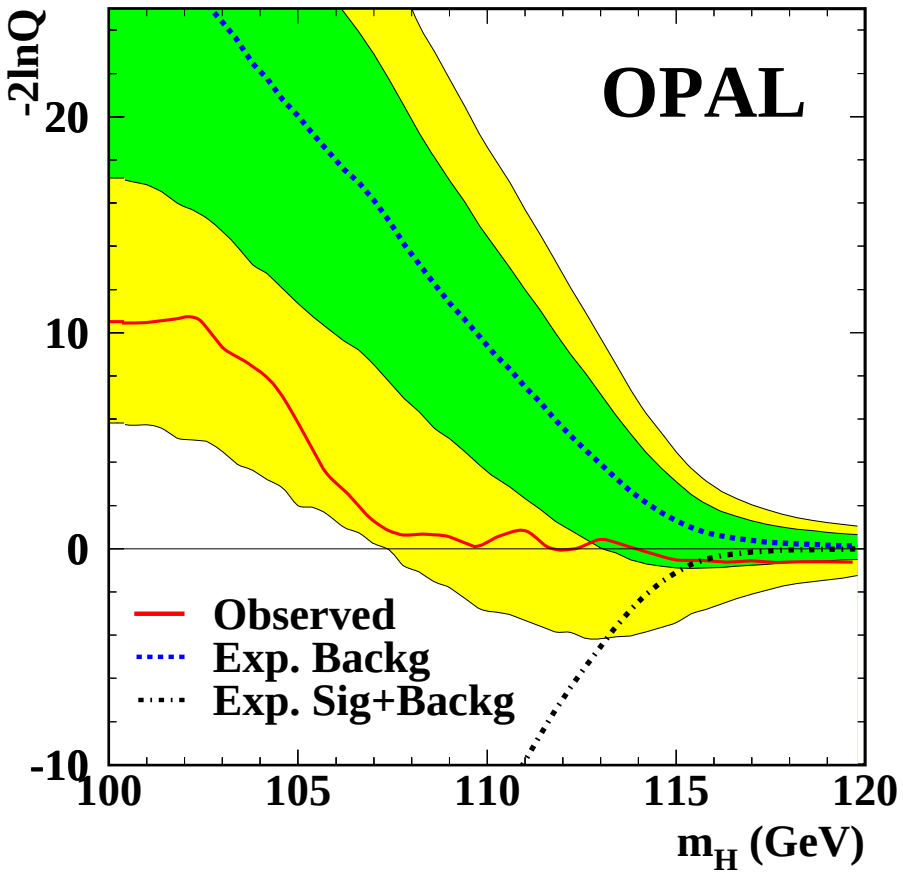

Figure 14: The log-likelihood estimator $-2\ln Q$ comparing the consistency of the data with the signal+background hypothesis with the consistency of the data with the background-only hypothesis as seen by the OPAL experiment. The observation for the data is shown with a solid line. The dashed line indicates the median background expectation and the dark (light) shaded band shows the $\pm 1\sigma\,(\pm 2\sigma)$ variation. The median signal expectation is shown with a dot-dashed line.

and various Higgs boson mass hypotheses. Assuming a mass of 114/115/116 GeV/c^2 and taking into account the selection efficiencies of the four experiments, one expects in the present combined search 28.6/19.2/12.8 Higgs boson signal events together with 797.1/785.3/780.9 background events; from the data samples 778/758/755 events are selected and take part in the LEP-wide combination.

Figure 15 shows the log-likelihood estimator as a function of m_H for the combined LEP results. The solid line represents the observation. The dashed/dash-dotted lines show the median

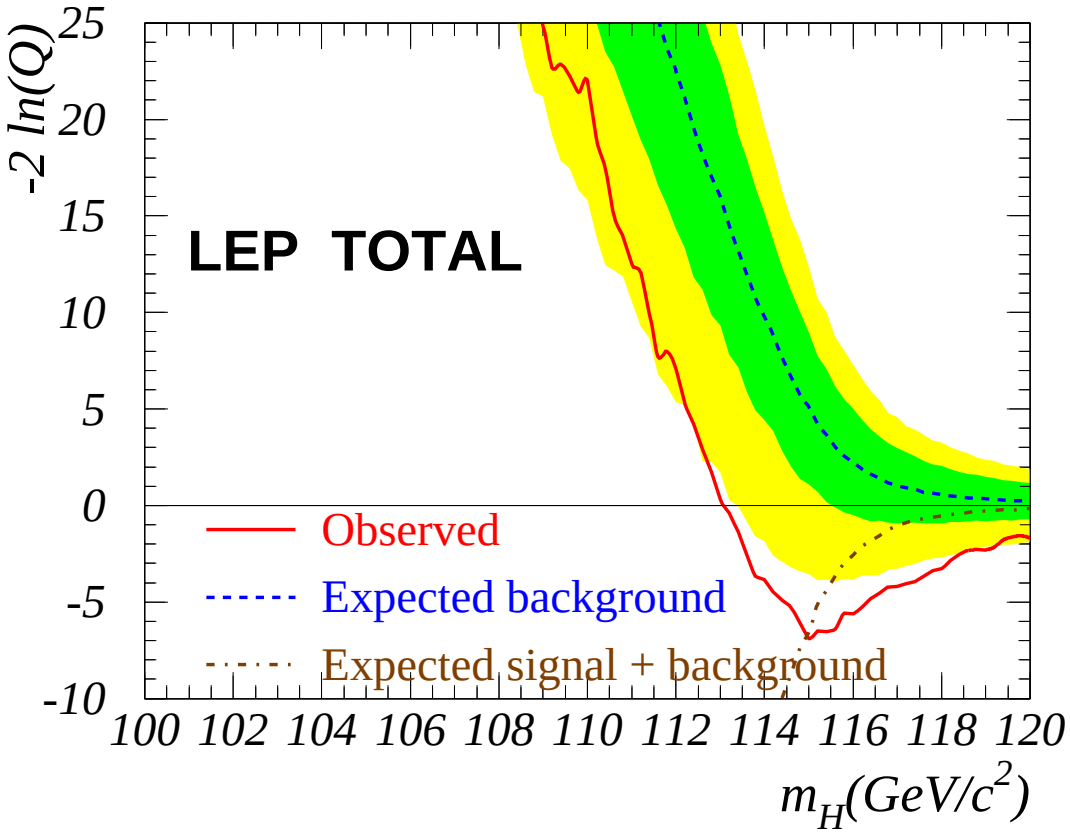

Figure 15: The log-likelihood estimator $-2\ln Q$ as a function of the Higgs boson mass m_H. Dashed line: median expected from the background-only hypothesis, with the one (dark grey) and two (light grey) standard deviation bands. The dashed-dotted line shows the median signal+background expectation. The solid line represents the observation.

background/signal+background expectations. The maximal significance for a signal is derived from the minimum of the negative log-likelihood ratio. The position of the minimum is consistent with a Standard Model Higgs boson with a mass of $\approx$ 115.0 GeV/c^2. Figure 16 shows a comparison of the log-likelihood ratio observed in the data (vertical line) with the distributions expected in the background-only (light-grey curve) and the signal-and-background (dark grey curve) hypotheses, for a $m_H = 115$ GeV/c^2 using the combined LEP data sample. The data clearly favor the signal-and-background hypothesis to the background-only hypothesis.

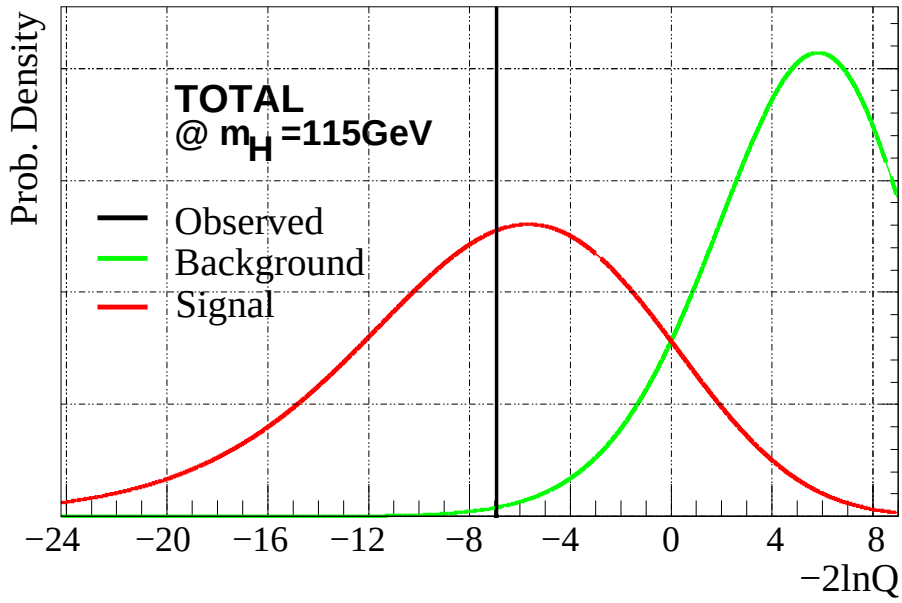

Figure 16: Negative log-likelihood ratio for a $m_H = 115$ GeV/c^2 Higgs boson. The observed value of $-2\ln Q$ which corresponds to the data is indicated by the vertical line with the distributions expected in the background-only (light-grey curve) and the signal-and-background (dark grey curve) hypotheses.

The excess at $m_H = 115$ GeV/c^2 has been examined in subsets of the data obtained by subdividing the total data set by experiments (Figure 17) and by decay channels (Figure 18). The

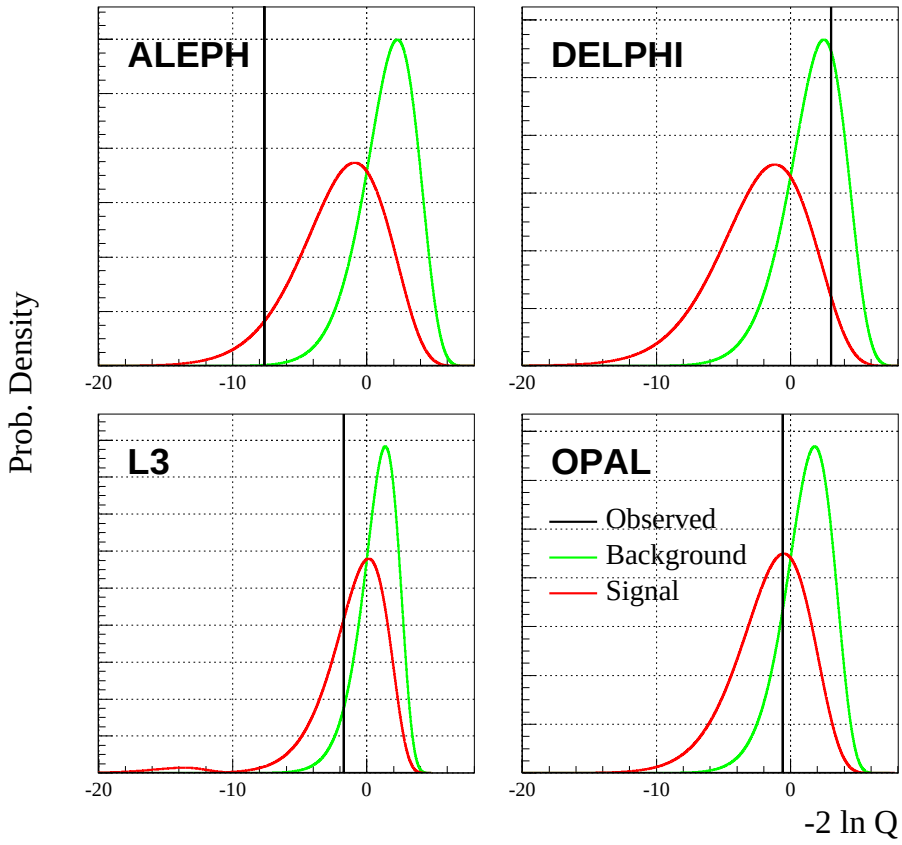

Figure 17: Negative log-likelihood ratio for a $m_H = 115$ GeV/c^2 Higgs boson subdivided by experiments. In each case, the observed value of $-2\ln Q$ is indicated by the vertical line with the distributions expected in the background-only (light-grey curve) and the signal-and-background (dark grey curve) hypotheses.

comparison indicates what has been discussed in the previous section: ALEPH favors the signal-and-background hypothesis over the background-only hypothesis. DELPHI, L3 and OPAL are all consistent with the signal-and-background hypothesis or the background-only hypothesis. Only for DELPHI the background-only hypothesis is preferred over the signal-and-background hypothesis. The combined four-jet channels and the missing energy channels are more signal- than background-like while the lepton channels and the tau channels indicate no preferences.

In Table 1 the compatibility of the data with the background-only hypothesis (1-CL$_b$) and the significance at $m_H = 115$ GeV/c^2 is presented for each experiment. The values given for 1-CL$_b$ are taken from [35]. All four collaborations have published papers including the total data sample. The 1-CL$_b$ values changed slightly from 6.5×10^{-4} to 2.7×10^{-3} [54], 0.68 to 0.77 [58], 6.8×10^{-2} to 9.0×10^{-2} [60] and 1.9×10^{-1} to 2.0×10^{-1} [50]. A new combined

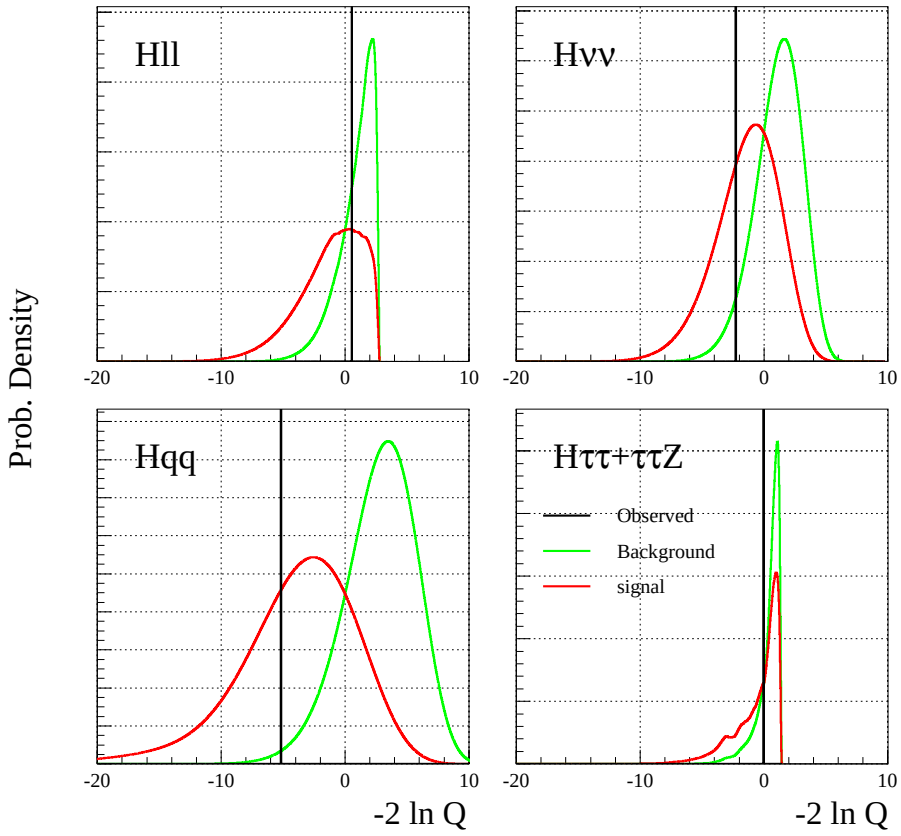

Figure 18: Negative log-likelihood ratio for a $m_H = 115$ GeV/c^2 Higgs boson subdivided by decay channels. In each case, the observed value of $-2\ln Q$ is indicated by the vertical line with the distributions expected in the background-only (light-grey curve) and the signal-and-background (dark grey curve) hypotheses.

limit of all four LEP collaborations using all available data is not available yet. The final LEP Higgs working group results are expected by end of the year 2001.

Experiment	1–CL$_b$	Significance	observed limit	expected limit
ALEPH	6.5×10^{-4}	3.4 σ	111.1 GeV/c^2	114.2 GeV/c^2
DELPHI	0.68	bkgd-like	114.3 GeV/c^2	113.5 GeV/c^2
L3*	6.8×10^{-2}	1.8 σ	113.0 GeV/c^2	110.9 GeV/c^2
OPAL	1.9×10^{-1}	1.3 σ	109.7 GeV/c^2	112.5 GeV/c^2
LEP	4.2×10^{-3}	2.9 σ	113.5 GeV/c^2	115.3 GeV/c^2

Table 1: Confidence level 1–CL$_b$, significance at $m_H = 115$ GeV/c^2 and observed and expected mass limit for the four LEP experiments and for the combined data sample. For the ALEPH experiment the results for the neural net stream is given. * The observed and expected limit from the L3 collaboration is using only data taken until begin of October 2000 [62].

Table 2 shows the candidates seen at LEP using data taken in the year 2000 with a weight greater than 0.3 at a Higgs boson mass of 115 GeV/c^2. The two most significant candidates are in the four-jet channel, the candidate with the third highest weight is a $H\nu\bar{\nu}$ candidate. The breakdown by channel is close to that expected from the theoretical branching ratios. Four LEP experiments have seen signal-like events with a weight greater than 0.3 and the events have been seen in all four search channels. Figure 19 shows the LEP combined compatibility as a function of the

(s/b)$_{115}$	M_{rec} (GEV/c^2	Channel	Experiment
4.7	114	Hqq	ALEPH
2.3	112	Hqq	ALEPH
2.0	114	$H\nu\bar{\nu}$	L3
0.9	110	Hqq	ALEPH
0.6	118	He^+e^-	ALEPH
0.5	113	Hqq	OPAL
0.5	111	Hqq	OPAL
0.5	115	$H\tau^+\tau^-$	ALEPH
0.5	115	$H\nu\bar{\nu}$	ALEPH
0.49	114	$H\nu\bar{\nu}$	L3
0.47	115	Hqq	L3
0.45	97	Hqq	DELPHI
0.40	114	Hqq	DELPHI
0.32	104	$H\nu\bar{\nu}$	OPAL

Table 2: Selected candidates seen at LEP with a Signal-over-background weight (s/b)$_{115} > 0.3$.

Higgs boson mass. The excess of events observed can be interpreted as an indication for the production of a Standard Model Higgs boson with a mass of 115 GeV/c^2.
The cross section is compatible with a Standard Model Higgs boson at a mass of $m_H = 115.0^{+1.3}_{-0.9}$ GeV/c^2. This excess is concentrated mainly in the data sets with centre-of-mass en-

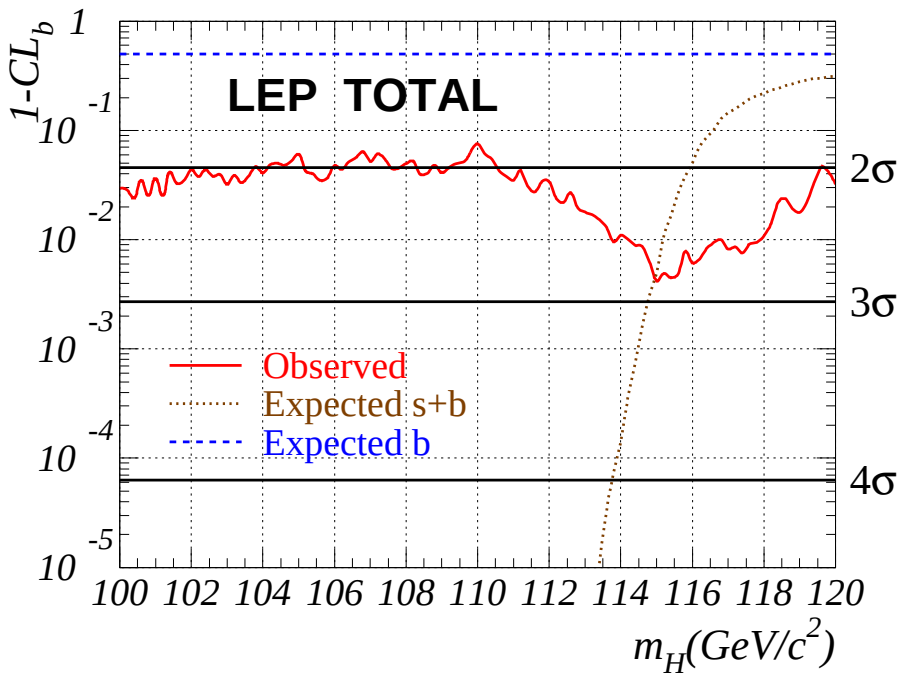

Figure 19: Confidence level 1-CL$_b$ as a function of the test mass m_H for the combined LEP data sample. The horizontal lines indicate deviations of 2 σ, 3 σ and 4 σ from the background hypothesis. Solid line: observation; dashed/dotted lines: expected probability for the background/signal+background hypotheses.

ergies higher than 206 GeV. It has a probability of $4.2\times\ 10^{-3}$ to be due to a local statistical fluctuation of the Standard Model background, corresponding to a significance of $2.9\,\sigma$. The integral of the signal+background probability density distribution from the observed value to $+\infty$, CL_{s+B}, is a measure of compatibility with the signal+background hypothesis. The behavior of CL_s=CL_{s+b}/CL_b as a function of the test mass is shown in Figure 20. The test mass for which the

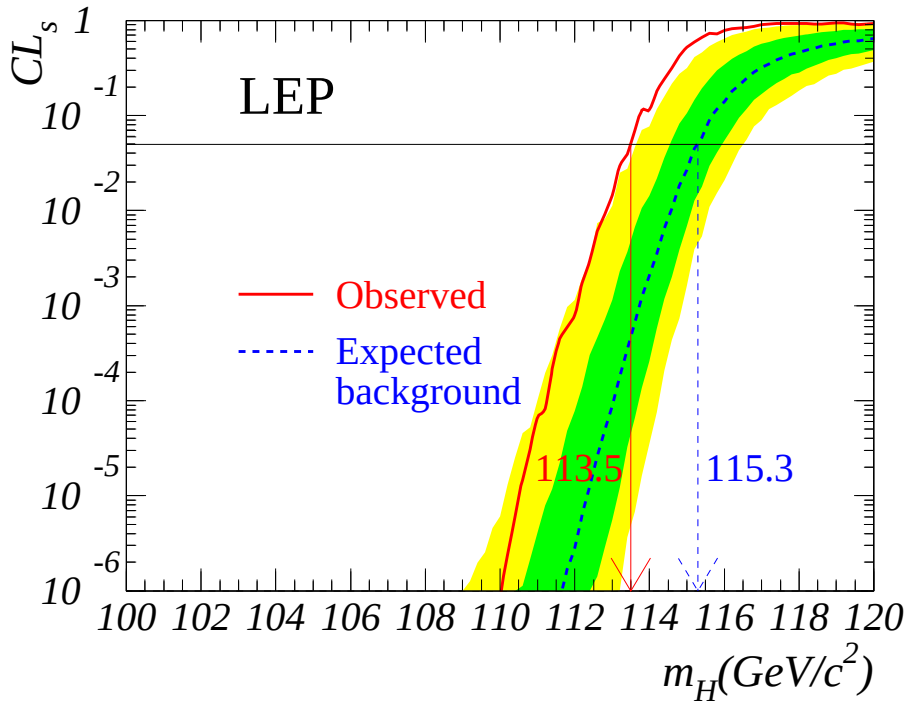

Figure 20: Confidence level CL_s for the signal+background hypothesis. The solid line shows the observation, the dashed line the median background expectation. The dark/light shaded bands around the median expected line correspond to the $\pm 1\sigma$/ $\pm\ 2\sigma$ spreads from a large number of background experiments.

value CL_s=0.05 is crossed designates the 95% confidence level lower bound for the mass of the Higgs boson. With a confidence level of 95% a lower bound on the Standard Model Higgs boson of 113.5 GeV/c^2 is set, while a median value of 115.3 GeV/c^2 is expected from background.

3.7 Implications of a Higgs Boson at 115 GeV/c^2

The possible existence of a light Higgs boson at around 115 GeV/c^2 implies that the Standard Model remains valid at most up to scales limited by about 10^6 GeV [16, 17, 63]. Above 10^6 GeV the effective Higgs potential is destabilized by the radiative corrections due to the relatively heavy top quark, that can not be counterbalanced by those due to a relatively light Higgs boson alone, necessitating the appearance of new physics. Extended non-perturbative models of new physics, such as Technicolour, cannot accommodate a relatively light Higgs boson [64]. Technicolour models generally also include light pseudo-scalar particles, but these can not be produced

copiously in association with a Z boson [65]. On the other hand, a relatively light Higgs boson favors generically a perturbative scenario for electroweak symmetry breaking. In the minimal supersymmetric extension of the Standard Model (MSSM) a Higgs boson weighing less than about 130 GeV/c^2 is expected.
A possible observation of a Higgs boson weighing around 115 GeV/c^2 constrains significantly the sparticle spectrum in models with conservation of R parity, so that the lightest neutralino χ may constitute the cold dark matter postulated by astrophysicists and cosmologists [66] and models which assume also CP conservation for the tree-level MSSM parameters. The principle uncertainty in predicting the sparticle mass spectrum is due to the lack of precision in the measurement of the top quark mass m_t.

3.8 Search for Neutral Higgs Bosons in the MSSM

To solve the hierarchy problem in the Standard Model Higgs sector the Minimal Supersymmetric extension of the Standard Model (MSSM) is one of the possible solutions. In the MSSM, the Higgs-strahlung process $e^+e^- \to hZ^0$ proceeds as it does in the Standard Model, but its rate is suppressed by the factor $\sin^2(\beta-\alpha)$. The WW- and ZZ fusion processes of the Standard Model also proceed with a rate suppressed by the same factor relative to the Standard Model rate. Heavy Higgs-strahlung, $e^+e^- \to HZ^0$, also occurs if it is kinematically possible, and has the Standard Model production cross section suppressed by the factor $\cos^2(\beta-\alpha)$; this process is also considered in the scans described below. The process $e^+e^- \to hA$ also occurs when kinematically allowed, and its production cross section is the Standard Model rate suppressed by the factor $\cos^2(\beta-\alpha)$ and the phase space available, taking into account the centre-of-mass energy and the masses of the h and the A.
The presence of an MSSM Higgs boson signal is tested using a constrained model with seven parameters, M_{SUSY}, M_2, μ, A, $\tan\beta$, m_A and $m_{\tilde{g}}$. All of the sfermion masses are set to M_{SUSY} at the electroweak scale. M_2 is the SU(2) gaugino mass parameter at the electroweak scale, and M_1 is derived from M_2 using the GUT relation $M_1 = M_2 \cdot (5\sin^2\theta_W/3\cos^2\theta_W)$, where θ_W is the weak mixing angle. The supersymmetric Higgs boson mass parameter is denoted μ, and $\tan\beta$ is the ratio of the vacuum expectation values of the Higgs field doublets. The parameter A is the common trilinear Higgs-squark coupling parameter, assumed to be the same for up-type squarks and for down-type squarks. The largest contributions to m_h from radiative corrections arise from stop loops, with much smaller contributions from sbottom loops. The gluino mass $m_{\tilde{g}}$ affects loop corrections from both stops and sbottoms. The mass of the top quark is taken to be 174 GeV/c^2.
Three different benchmark scenarios [67] are considered in the search for the neutral Higgs bosons of the MSSM using LEP data collected at energies up to 209 GeV [68]. The first ("no mixing" scenario) assumes that there is no mixing between the scalar partners of the left-handed and the right-handed top quarks, with the following values and ranges for the parameters: $M_{SUSY} = 1$ TeV, $M_2 = 200$ GeV, $\mu = -200$ GeV, $X_t(\equiv A - \mu\cot\beta) = 0$, $0.4 < \tan\beta < 50$ and 4 GeV $< m_A <$ 1 TeV. The gluino mass $m_{\tilde{g}}$ is set to 800 GeV. Masses of the m_A boson below 4 GeV are not considered because of the rapidly changing branching ratios for m_A boson decay due to kinematic cutoffs. The second scenario ("m_h -max") is designed to yield the maximal value of m_h in the model. This scenario corresponds to the most conservative range of

excluded $\tan\beta$ values. The same parameters are chosen as for the no-mixing scenario, except for the stop mixing parameter $X_t = 2M_{SUSY}$ using the conventions of the two-loop diagrammatic calculation of [69]. The third scenario ("large μ" scenario) is a scan with parameters chosen to be $M_{SUSY} = 400$ GeV, $\mu = 1$ TeV, $M_2 = 400$ GeV, $m_{\tilde{g}} = 200$ GeV, $4 \leq m_A \leq 400$ GeV, $X_t = -300$ GeV. This third scenario is designed to illustrate choices of MSSM parameters for which the Higgs boson h does not decay into pairs of b quarks due to cancellations from SUSY-QCD loops. This situation occurs at $\tan\beta > 20$ and for $120 < m_A < 220$ GeV. The dominant decay mode of the h for these points is to $\tau^+\tau^-$, and the Higgs-strahlung search in the tau channel is the only channel with sensitivity to these points. For the no-mixing and m_h -max scenarios, the two-loop diagrammatic approach of [69] is used to compute the relations between the SUSY parameters, m_h, m_A, $\tan\beta$, and the production cross-sections and decay branching ratios. For the large μ scenario, the one-loop renormalization-group improved calculation of [70] is used. These two calculations give consistent results [71], although small differences still exist. For example, in the m_h -max scenario, the calculation of [69] gives a more conservative upper edge of the excluded region of $\tan\beta$, while the calculation of [70] gives a slightly more conservative lower edge.

The 95% exclusion contours for the m_h -max scenario in four projections, in the (m_h,m_A), the (m_h,$\tan\beta$), the (m_A,$\tan\beta$)and in the ($m_{H^\pm}$,$\tan\beta$) plane, are shown in Figure 21.

Figure 22 shows the $1 - CL_b$ significance contours as functions of h mass and A mass for the m_h-max scenario. An excess is seen at (m_h,m_A)$\sim$ (83,83) GeV/c^2, with a significance level slightly in excess of 2σ. This is due to candidates seen by the OPAL collaboration in data taken at 189 GeV in the $\tau^+\tau^- b\bar{b}$ channel [61] which have not been confirmed by later running or in other experiments; the significance has gradually decreased as additional luminosity has been accumulated. Another excess is seen near (m_h,m_A)$\sim$ (90,90) GeV/c^2, due to candidates in the OPAL four-jet channel in the 196 GeV data [72], which also does not appear in other samples. The current 95% CL exclusion limits from LEP (shown also in the same figure) rule out both of these possibilities as an MSSM signal. The results are based on data collected at $\sqrt{s}$ $\approx$200–209 GeV and are combined with data collected earlier at lower centre-of-mass energies. For the search in the $e^+e^- \to hZ$ process the Standard Model searches presented separately by the four collaborations in [50, 54, 58, 60] are used, combined with the searches for the $e^+e^- \to hA$ process described in [73–76]. The observed mass limits for the m_h-max scenario are 91.0 GeV/c^2 for m_h and 92.9 GeV/c^2 for m_A, the expected mass limits are 94.6 GeV/c^2 for m_h and 95.0 GeV/c^2 for m_A if $\tan\beta$ is larger than 1.2. In the no-mixing scenario the limits are slightly (<0.5 GeV/c^2) higher. For the m_h-max scenario, values of $\tan\beta$ between 0.48 and 2.38 are excluded, while for the no-mixing scenario, values of $\tan\beta$ between 0.76 and 9.6 are excluded.

3.9 Search for Neutral Higgs Bosons in Models with Two Scalar Field Doublets

In 2HDMs the couplings and production cross sections are modified with respect to the Standard Model. Depending on the choice of parameters (m_h, m_A, $\tan\beta$,α) a decay into b-quarks can be highly suppressed. Previous analyses mainly focused on the information from b-quarks and thus are not sensitive in regions with diminishing or even vanishing decay rates to b-quarks.

OPAL has published a paper [77] about searches for the neutral Higgs bosons h^0 and A^0 which

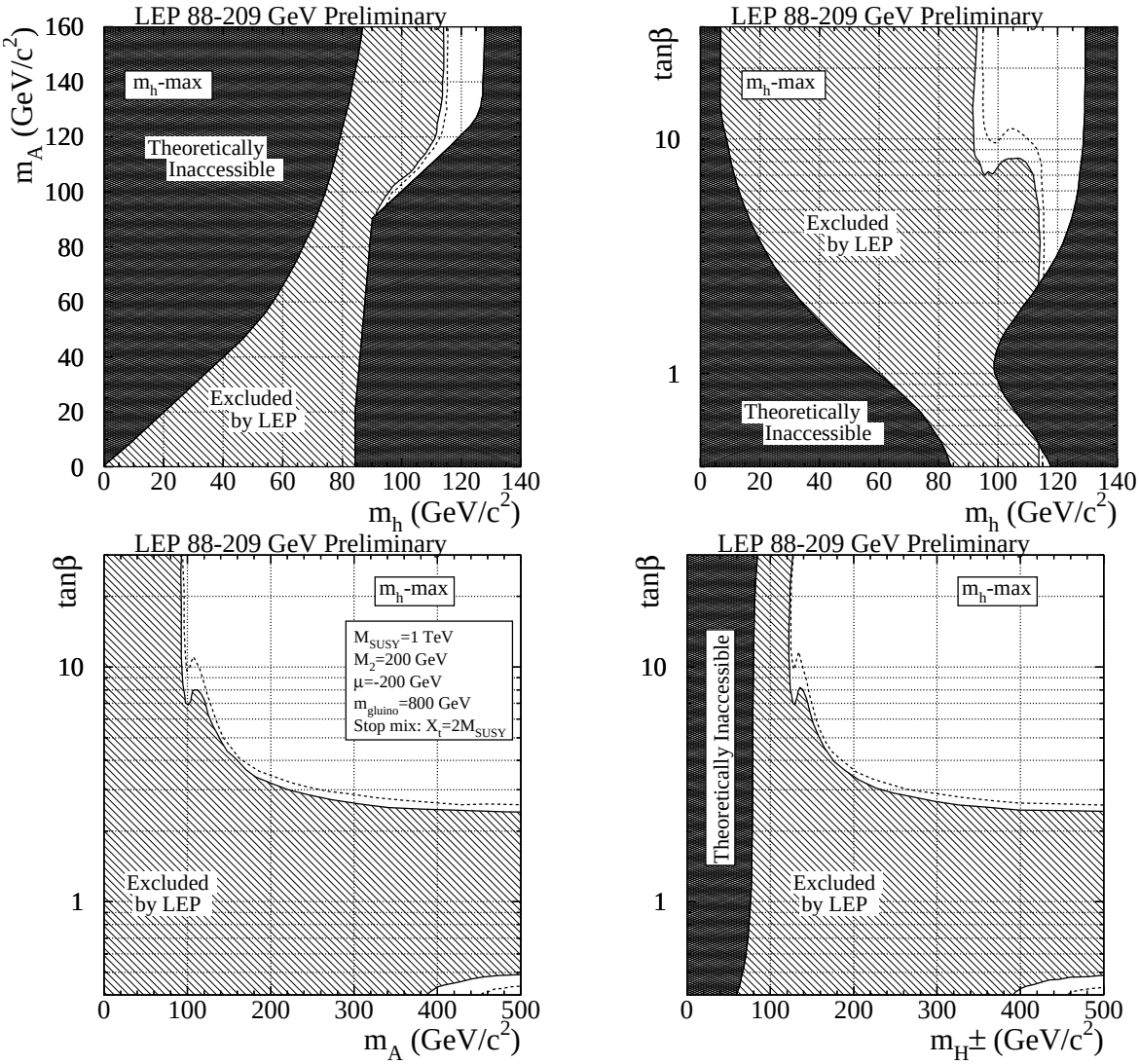

Figure 21: The MSSM exclusion for the m_h-max benchmark scenario described in the text. This figure shows the excluded (diagonally hatched) and theoretically disallowed (cross-hatched) regions as functions of the MSSM parameters in four projections: (upper left) the (m_h,m_A) plane, (upper right) the (m_h,$\tan\beta$) plane, (lower left the (m_A,$\tan\beta$) plane and (lower right) the ($m_{H^\pm}$,$\tan\beta$) plane. The dashed lines indicate the boundaries of the regions to be excluded at the 95% confidence level if only Standard Model background processes are present.

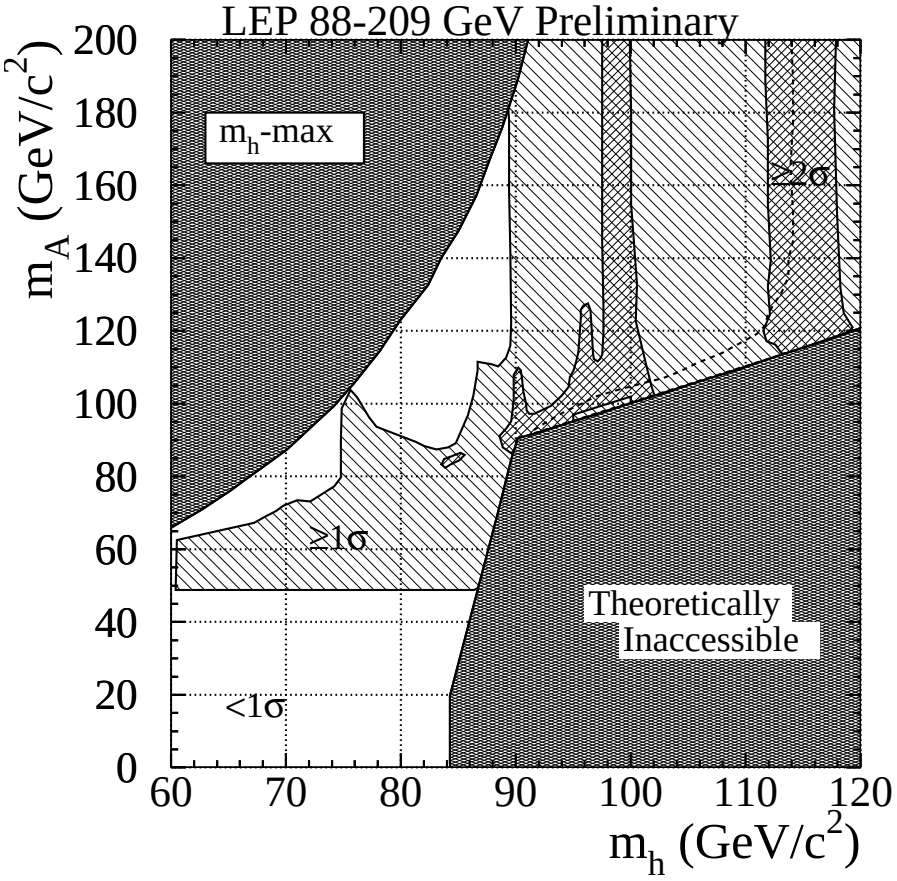

Figure 22: The distribution of the confidence level CL_b in the (m_h, m_A) plane for the m_h-max scenario. In the white domain, the observation either shows a deficit or is less than 1σ above the background prediction, while in the domains labelled $\geq 1\sigma$ and $\geq 2\sigma$, the observation shows an excess above the Standard Model background prediction by the indicated amount. If at a point (m_h, m_A) in the plane, two values of $\tan\beta$ are allowed by the benchmark model, the choice of $\tan\beta$ with the larger CLb is shown. Results from the hZ searches are combined with the results of the Ah searches. Vertical structures are due to features in the hZ search results, while structure on the $m_h = m_A$ line arises from the Ah searches. The 95% CL exclusion contours is shown with the dashed line; points to the right and below the dashed line are not excluded. These regions can also be seen in Figure 21.

has been used to obtain limits on the Type II Two Higgs Doublet Model (2HDM(II)) with no CP-violation in the Higgs sector and no additional particles besides the five Higgs bosons. The analysis combines approximately 170 pb^{-1} of data collected with the OPAL detector at $\sqrt{s} \approx 189$ GeV with previous runs at $\sqrt{s} \approx m_Z$ and $\sqrt{s} \approx 183$ GeV. The searches are sensitive to the h^0, $A^0 \to q\bar{q}, gg, \tau^+\tau^-$ and $h^0 \to A^0A^0$ decay modes of the Higgs bosons. For the first time, the 2HDM(II) parameter space is explored in a detailed scan, and new flavour independent analyses for both the Higgs-strahlung process, $e^+e^- \to hZ$, and the pair-production process, $e^+e^- \to hA$, are applied to examine regions in which the neutral Higgs bosons decay predominantly into light quarks or gluons. The results of all the individual search channels at the studied centre-of-mass energies are combined statistically to provide 95% confidence level limits in a model-independent interpretation in which no assumption is made on the structure of the Higgs sector. The interpretation of the searches for the neutral Higgs bosons in the 2HDM(II) is done by scanning the parameter space of the model. Every (m_h, m_A, $\tan\beta$,α) point determines the production cross section and the branching ratios to different final states. The region $1 \lesssim m_h \lesssim 44$ GeV/c^2 and $12 \lesssim m_A \lesssim 56$ GeV/c^2 is excluded at 95% confidence level independent of α and $\tan\beta$ with the scanned parameter space. The search results have been updated by adding data collected at LEP at centre-of-mass energies up to 209 GeV [76]. Assuming the Standard Model hZ^0 cross-section and BR($h \to$hadrons)=1.0, a lower bound on the mass of the h Boson is derived. The observed lower limit on m_h is 101.8 GeV/c^2 with an expected limit of 107.3 GeV/c^2. The 95% confidence level upper limits on the production cross section are shown as a function of the scalar neutral Higgs boson mass m_{S^0} in Figure 23. The ALEPH Collaboration has also performed a flavour-independent search for the Higgs-strahlung process in e^+e^- collisions [78]. ALEPH has found a 95% confidence level lower mass limit of 109.4 GeV/c^2 for a cross-section equal to that of the Standard Model and a 100% hadronic branching fraction. A similar search has been performed by L3 with an 95% confidence level lower mass limit of 106.9 GeV/c^2 [79]. Flavour independent searches are also sensitive to set limits in models in which Higgs bosons might not couple to b quarks [80].

3.10 Search for Fermiophobic Higgs Bosons

In 2HDMs of Type I only one of the two Higgs doublets is allowed to couple to fermions. The coupling of the lightest Higgs boson to a fermion pair is then proportional to $\cos\alpha$. If $\alpha = \pi/2$ this coupling vanishes and the lightest Higgs boson becomes a fermiophobic Higgs boson.
ALEPH [81], DELPHI [82], L3 [83] and OPAL [76] performed searches for a Higgs boson, decaying into two photons, considering all decay modes of the Z^0 boson in the Higgs-strahlung process. No signal has been found and confidence limits were derived in the framework of possible extensions of the Standard Model. The observed lower limits are 104.3 GeV/c^2 (L3) and 105.4 GeV/c^2 (ALEPH), 105.5 GeV/c^2 (OPAL) and 107 GeV/c^2 (DELPHI) assuming Standard Model cross sections and fermiophobic decays. DELPHI has extended the search to the pair-production process Ah with two or four photons plus jets or missing energy in the final state and excluded a region in the (m_h, m_A) plane.
The L3 collaboration [84] presented a lower mass limit on the standard fermiophobic Higgs model considering four different channels of the process $hZ \to WW^*f\bar{f}$. The results of the analysis was combined with the results from the fermiophobic $h \to \gamma\gamma$ analysis. The observed

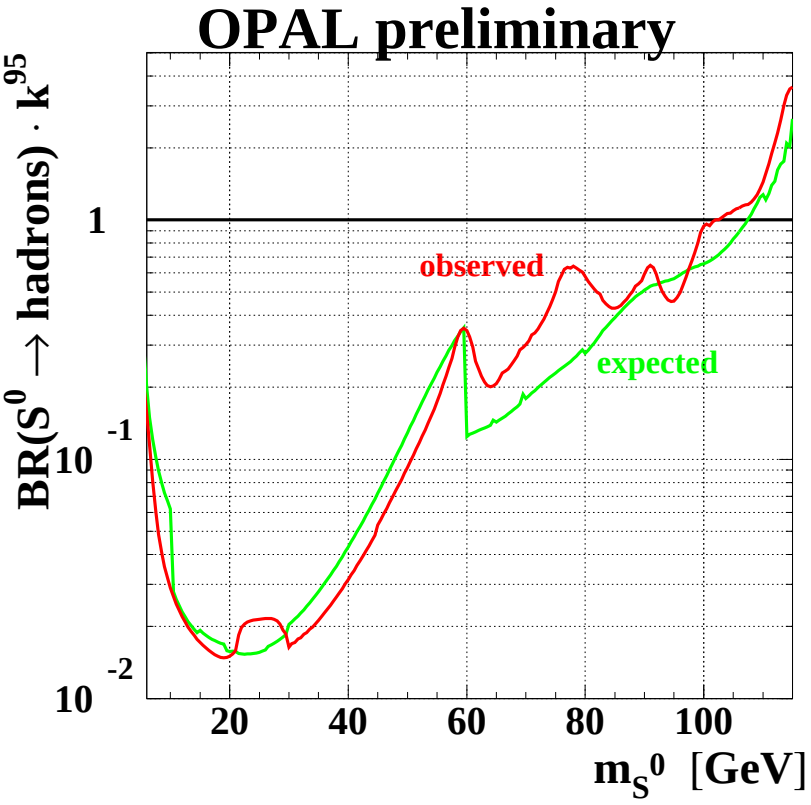

Figure 23: The 95% confidence level upper limit on the cross section of the associated production of a Z^0 and a scalar neutral Higgs boson in units of the Standard Model Higgs-strahlung cross section as a function of the scalar neutral Higgs boson mass S^0. The hadronic branching ratio of the S^0 is assumed to be 100%.

limit is 104.8 GeV/c^2.

3.11 Search for Charged Higgs Bosons

At LEP energies charged Higgs bosons are expected to be produced mainly through the process $e^+e^- \rightarrow H^+H^-$. In the MSSM and at tree-level the $H^\pm$ is constrained to be heavier than the $W^\pm$ bosons but loop corrections can drive the mass to lower values. Since the sensitivity of current searches is limited to the range below $M_{W^\pm}$ due to the background from $e^+e^- \rightarrow W^+W^-$, any signal for H^+H^- would indicate either new physics beyond the MSSM or a rather extreme set of MSSM parameter values.

The present searches for charged Higgs bosons are placed in the general context of 2HDM models where the mass is not constrained. At tree level the production cross-section is fully determined by the $H^\pm$ mass [85]; here they are provided by HZHA version 3 [86]. The searches are carried out under the assumption that the two decays $H^+ \rightarrow c\bar{s}$ and $H^+ \rightarrow \tau^+\nu$ exhaust the H^+ decay width; however, the relative branching ratio is not predicted. Thus, the searches encompass the following H^+H^- final states: $(c\bar{s})(\bar{c}s)$, $(\tau^+\nu)(\tau^-\bar{\nu})$ and the mixed mode $(c\bar{s})(\tau^-\bar{\nu})$+$(\bar{c}s)(\tau^+\nu)$. The combined search results are presented as a function of the branching ratio BR($H^+ \rightarrow \tau^+\nu$). Details of the searches of the individual experiments can be found in [76, 87–89]. These are summarized in Table 3, together with the 95% confidence level lower bounds, expected and observed. In the Table the mass mass limits are quoted separately for BR($H^+ \rightarrow \tau^+\nu$)=0,1, and a limit independent of the branching ratio. It should be noted that L3 observes an excess of events in the pure hadronic and the semi-leptonic channels in the mass region around 68 GeV/c^2 [89]. This behavior is reproduced when the combination protocol is applied to the L3 data only, but is not seen when applied to the ALEPH, DELPHI and OPAL data. The excess of events at L3 around $m_{H^\pm}$=68 GeV/c^2 is compatible with a 4.4 σ fluctuation in the background [90]. The excess is visible in the $c\bar{s}\bar{c}s$ and in the $c\bar{s}\tau^-\bar{\nu_\tau}$ mass distributions around 68 GeV/c^2. Figure 24 [90] (left side) shows the combined background-subtracted mass distribution for these two Higgs decay channels, where the events are corrected for the efficiency of their respective analyses. The figure also shows the expected distribution for a 68 GeV/c^2 Higgs with BR($H^\pm \rightarrow \tau\nu$)=0.1. The statistical significance of the excess is almost constant for values of BR($H^\pm \rightarrow \tau\nu$) between 0.1 and 0.2. The data are 1 σ below what is expected for a Higgs signal at this mass. Again, this difference is not strongly dependent on the value of the branching fraction. The background confidence level (1-CL$_b$) is displayed in Figure 24(right side) for the data, for the expectation in the absence of a signal and for a 68 GeV/c^2 mass Higgs signal. The combined lower 95% confidence level bound for charged Higgs bosons decaying only into $H^+ \rightarrow c\bar{s}$ and $\tau^+\nu$ is 78.5 GeV/c^2. The mass limits expected and observed are shown in Figure 25. To obtain the limits, the branching ratio BR($\tau^+\nu$) has been scanned in steps of 0.05, and the limit setting procedure is repeated for each step. In the hadronic channel and for masses close to $m_{W^\pm}$, the sensitivity is suppressed by the $W^+W^- \rightarrow e^+e^-$ background. There is a regain of sensitivity at higher masses, as signalled by the excluded islands above 84 GeV/c^2.

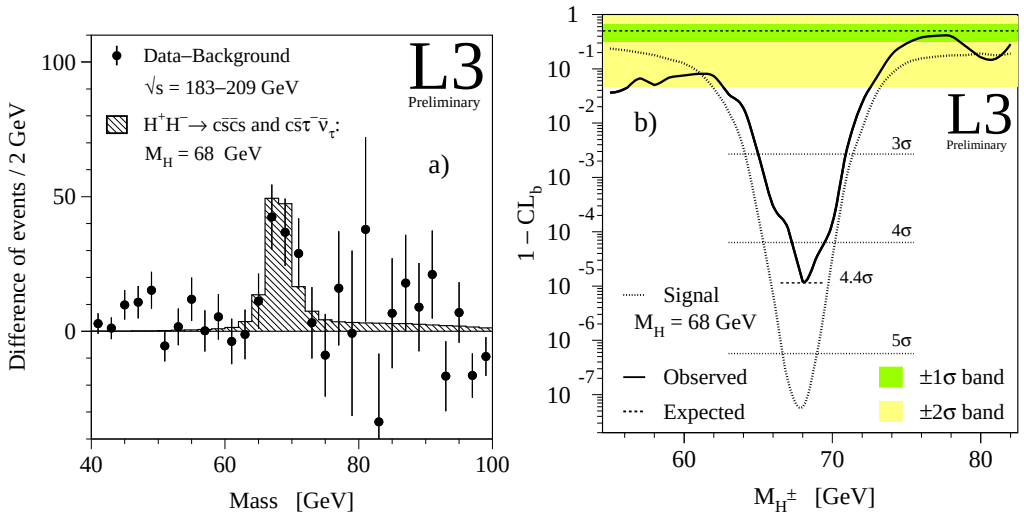

Figure 24: a.) Combined background-subtracted mass distributions for the $H^+H^- \to c\bar{s}\bar{c}s$ and $c\bar{s}\tau^-\bar{\nu_\tau}$ decay channels. The expected distributions for a 68 GeV/c^2 Higgs with BR($H^\pm \to \tau\nu$)=0.1 is shown by the hatched histogram. b.) the background confidence level, 1-CL$_b$, as a function of the Higgs mass with BR($H^\pm \to \tau\nu$)=0.1. The solid line shows the values computed from the observed results and the dashed line the expectation for the background only hypothesis. The dotted line is the curve expected for a 68 GeV/c^2 Higgs signal at this value of the branching ratio.

Int. Luminosity (pb^{-1}):	217.2	225.1	217.8	217.4
Backg. exp. / Events obs. (*)				
$(c\bar{s})(\bar{c}s)$	997.7/968	412.8/387	884.5/961	424.2/439
$(c\bar{s})(\tau^+\nu)$	118.0/127	190.8/173	172.1/171	203.5/224
$(\tau^+\nu)(\tau^-\bar{\nu})$	22.0/17	23.8/25	40.6/36	331.7/315
Events in all channels	1137.7/1112	627.4/585	1097.3/1168	959.4/978
Limit exp.(median)/obs.				
for B=0	78.1/80.7	77.0/77.4	77.1/77.2	77.1/76.2
for B=1	86.9/83.4	89.3/85.4	83.0/84.9	86.5/84.5
for any B	76.9/78.0	75.4/73.8	75.0/67.1	74.5/72.2

Table 3: Individual search results for the $e^+e^- \to H^+H^-$ final states. The numbers of events correspond to the data sets taken at energies between 200 and 209 GeV. (*) The OPAL selection is mass-dependent; the numbers are given for $m_{H^\pm}$=80 GeV/c^2.

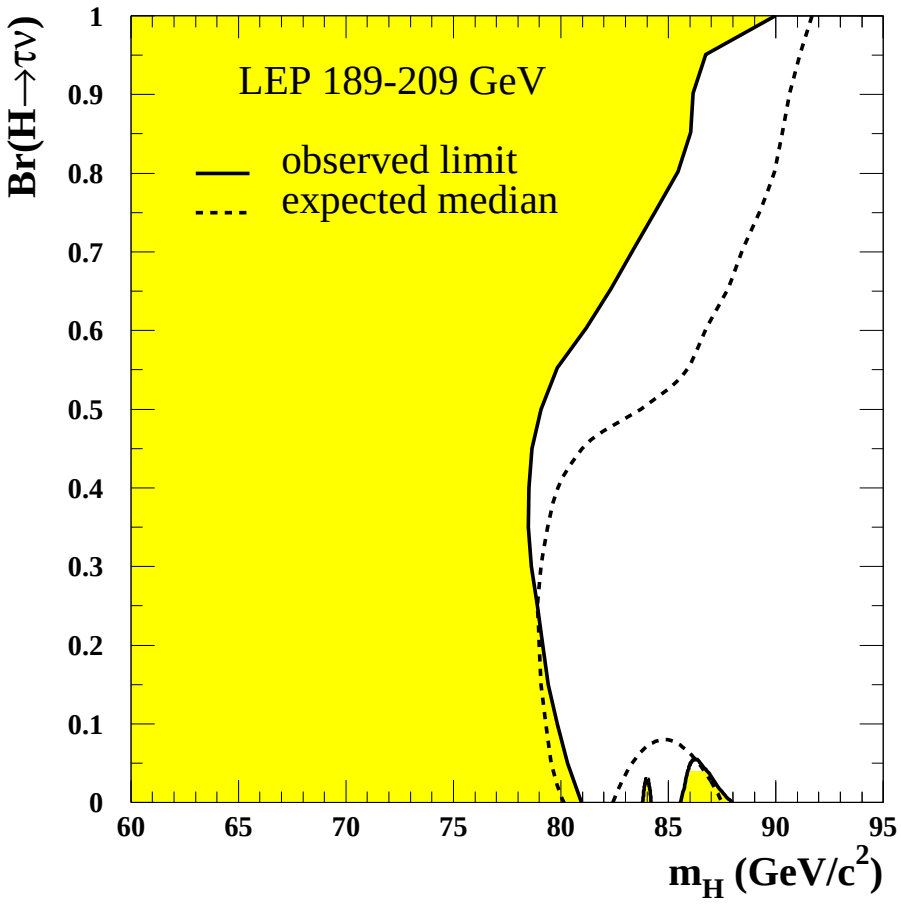

Figure 25: The 95% confidence level bounds on $m_{H_\pm}$ as a function of the branching ratio $H^+ \to \tau^+\nu$, combining the data collected by the four LEP experiments at energies from 189 to 209 GeV. The expected exclusion limits are indicated by the dashed line and the observed limits by the solid line. The shaded area is excluded at the 95% confidence level.

4 Present: Higgs Bosons at the upgraded TeVatron

What LEP has seen in the data in the final year of running in 2000 is quite consistent with the production of a Standard Model Higgs boson with a mass around 115 GeV/c^2. However, the statistical significance of the effect, although in agreement with that expected from such a signal, is just about to reach 2.9 σ, which is still too low to claim that a statistical fluctuation of the background (with a probability of 0.4%) is excluded.
The next place to look for a Higgs boson will be the TeVatron with the two experiments CDF [91] and DØ [92] at Fermilab. Two experiments, CDF and DØ, each collected approximately 125 pb^{-1} of data during the period Run I in the years 1992–1996. Among the highlights from Run I are the discovery of the top quark [93, 94] and measurements of its mass and production cross section; the precise determination of the mass of the W boson, a first measurement of the self-couplings of the electroweak gauge bosons and extensive studies of QCD.

4.1 The TeVatron Collider and the Detectors

The TeVatron is a $p\bar{p}$ collider that operated until 1996 at a centre-of-mass energy of $\sqrt{s}$=1.8 TeV. Then the TeVatron accelerator has been upgraded to increase its centre-of-mass energy to $\sqrt{s}$=2.0 TeV and to ultimately achieve a luminosity of $2{\cdot}10^{32}$ cm^{-2}s^{-1}. CDF and DØ are also being upgraded to take advantage of the higher luminosity. Data-taking for Run II started in March 2001. Projections for the integrated luminosity in Run II amount to 2 fb^{-1} for the two first years of data-taking and reach another factor of five to ten up to the year 2006.
The CDF upgrade [95] includes a new silicon vertex tracker, a new wire drift chamber, a time-of-flight detector, new end-plug calorimeters, extended muon systems, and new front-end electronics, trigger, and the data acquisition system. The goals of the silicon system with 722k channels are double b-tagging coverage to $|\eta| \leq 2$, 3D imaging of the vertex to improve dead-time-less triggering on displaced tracks, and an improved impact parameter resolution.
The major DØ upgrades [96] include a $793k$ channel silicon micro-strip vertex detector, a central fiber tracker, a 2 T solenoid with a radius of 60 cm, enhanced muon systems, and a completely new front-end electronics, trigger and data acquisition system. DØ will retain its existing hermetic LAr calorimeter which has a resolution of

$$\sigma_E/E \sim 15\%/\sqrt{E}$$

for electrons,

$$\sigma_E/E \sim 50\%/\sqrt{E}$$

for pions.

4.2 Higgs Boson Searches in Run I

CDF has searched for the process $p\bar{p} \to b\bar{b}X \to b\bar{b}b\bar{b}$ with 91 pb^{-1} of Run I data. This reaction is particularly important in the MSSM where the Yukawa couplings between the Higgs scalars and the b quarks are enhanced for large $\tan\beta$ values with respect to the Standard Model. Four-jet events with at least three of them b-tagged are required to select the event sample. In addition, a mass dependent E_T cut on the three highest-E_T reconstructed jets in the event is also imposed.

Dominant background is QCD heavy flavour production with other contributions from fake triple tags, $t\bar{t}$ and W/Z+jets. A cut on the b-tagged di-jet angular distribution further increases the significance of the signal by eliminating the gluon splitting QCD component of the sample. The observed number of data events is in agreement with the expected Standard Model contributions. Figures 26 and 27 show the 95% confidence level excluded regions in the $\tan\beta$ versus M_h and M_A plane respectively. Results are shown for two stop mixing scenarios, no mixing and maximal mixing, and for a SUSY mass scale of 1 TeV [97].

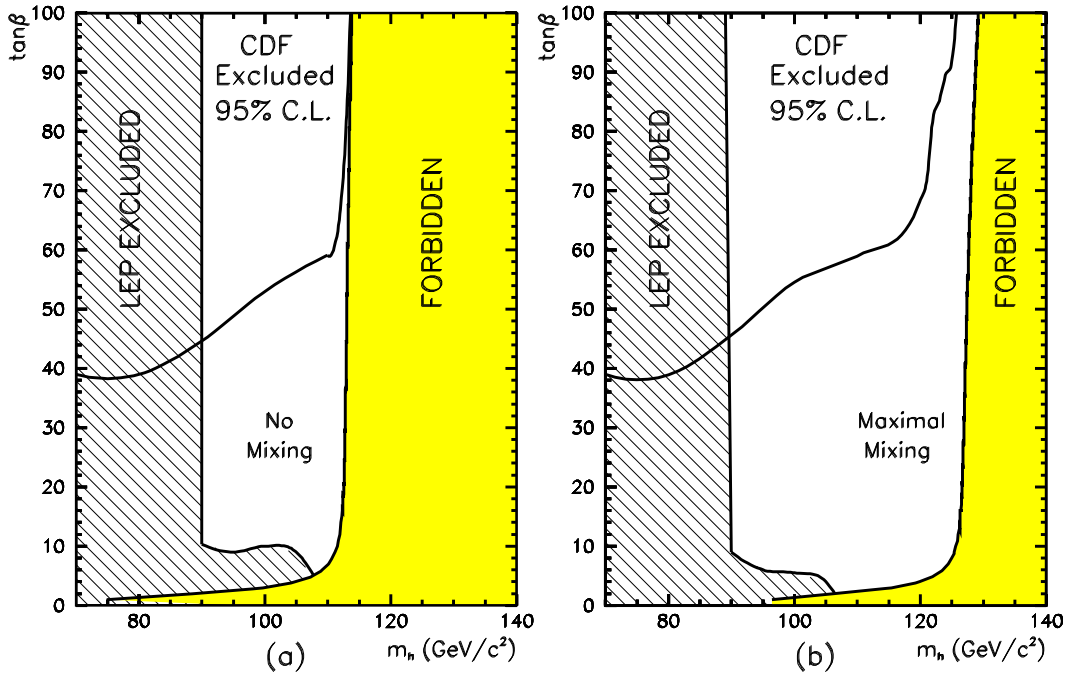

Figure 26: CDF 95% confidence level excluded region in the parameter space $M_h - \tan\beta$ for the two stop mixing scenarios: (a) no mixing, and (b) maximal mixing. Also shown are the theoretically forbidden region and the LEP exclusion region for their no mixing and m_h^{max} scenarios. [98].

Both CDF and DØ have searched for the Standard Model Higgs boson through associated production with a vector boson. The searches are restricted to the mass region below $\sim$ 140 GeV/c^2 where the $H \to b\bar{b}$ dominates. The decay mode of the vector boson dictates the final signature. CDF has published results for the signatures $WH \to l\nu b\bar{b}$ ($l = e, \mu$) and $VH \to q\bar{q}b\bar{b}$ ($V = W, Z$) [99–101]. More recently the channels $ZH \to \nu\bar{\nu}b\bar{b}$ and $ZH \to l^+l^-b\bar{b}$ ($l = e, \mu$) have also been investigated. Individual and combined 95% confidence level upper limits on the production cross sections for VH ($V = W, Z$) are shown in Figure 28. DØ has also searched for $WH \to l\nu b\bar{b}$ and $ZH \to \nu\bar{\nu}b\bar{b}$ events. The limits on $\sigma \times$BR are still more than one order of magnitude higher than the Standard Model prediction but show that these searches are possible and limited only by luminosity, provided the experiments have excellent b-tagging and b-jet energy resolution. Both CDF and DØ have improved their detectors with precisely these

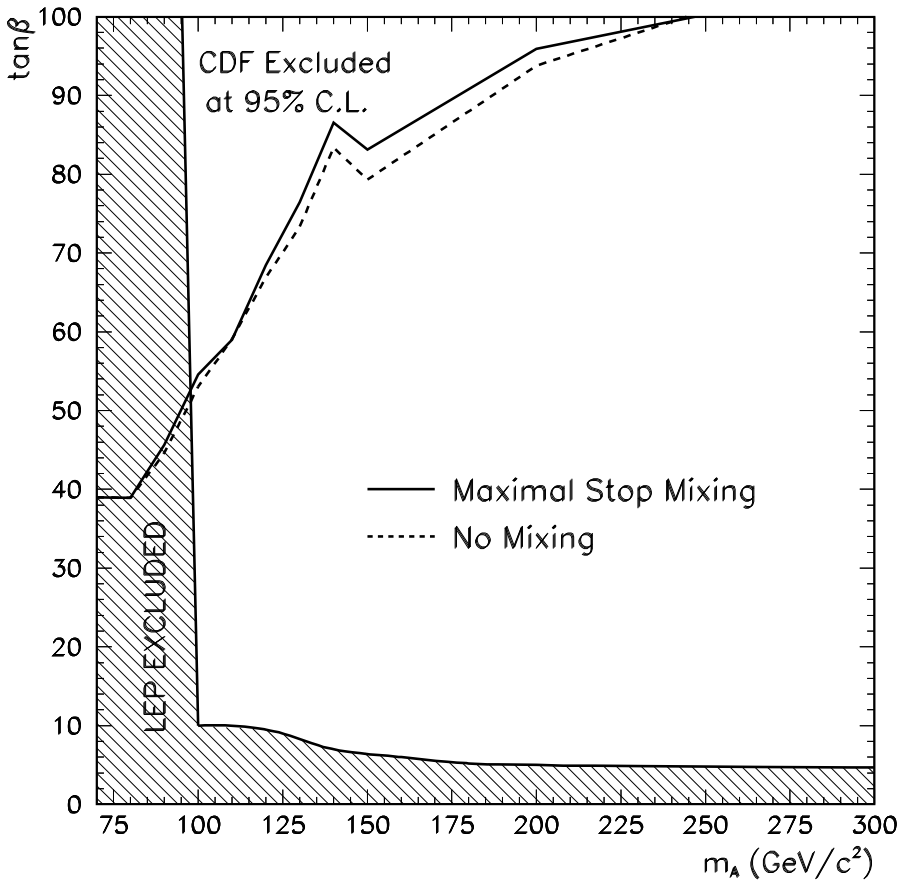

Figure 27: CDF 95% confidence level excluded region in the parameter space $M_A - \tan\beta$ for the two stop mixing scenarios: no mixing (dashed line) and maximal mixing (solid line). Also shown are the theoretically forbidden regions and the LEP exclusion region for the no mixing and maximal mixing scenario [98].

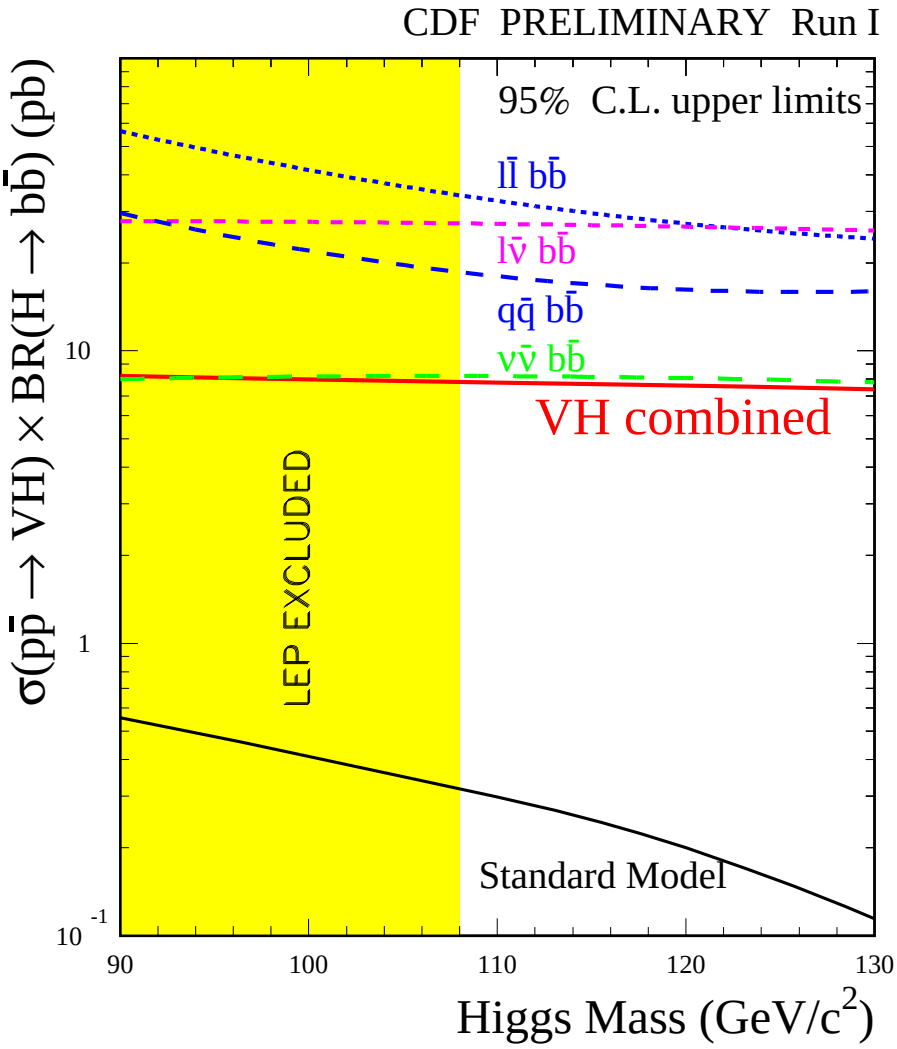

Figure 28: CDF Run I individual and combined 95% confidence level upper limits on $\sigma(VH) \times BR(H \rightarrow b\bar{b})$ as a function of signal mass. The four dashed curves show the limits from the individual search channels, and the solid curve labeled 'VH combined' shows the limit from combining all four channels. The expectation from Standard Model Higgs production is shown by the solid curve labeled Standard Model.

capabilities in mind.

The search for the charged Higgs boson of the MSSM is an especially interesting search since the TeVatron is the only facility that can take advantage of the $t \to H^{\pm} b$ mode, provided that the $H^{\pm}$ mass satisfies $M_{H^{\pm}} < M_{top} - M_b$. This decay competes with the Standard Model decay $t \to W^{\pm} b$.

The DØ Collaboration has searched for a charged Higgs boson [102] lighter than the top quark. Such a charged Higgs is contained in Two Higgs Doublet Models, for example, in Supersymmetric extensions of the Standard Model. The standard analysis leading to the measurement of the top cross section assumes the top decays 100% of the time to a W boson and a b quark. In a scenario with a light charged Higgs boson, one or both of the top quarks could decay into a charged Higgs boson and a b quark. It is assumed that this is the only alternative decay mode available to the top and the effects it would have on the acceptance of the standard analysis to the lepton plus jets final states are studied. The acceptance depends on the mass of the charged Higgs boson and on $\tan\beta$ as well as on the mass of the top quark. This analysis scans the plane defined by the mass of the Higgs and $\tan\beta$ with the pair production cross section and the mass of the top quark as parameters. Based on the number of events observed by DØ , for a top quark mass of 175 GeV/c^2 and a top production cross section of 5.53 pb, the analysis excludes $\tan\beta$ <0.97 or $\tan\beta$ >40.9 for a charged Higgs boson mass of 60 GeV/c^2. Within the range of 0.3< $\tan\beta$ <150, no lower limit can be set on $\tan\beta$ for a charged Higgs boson larger than 124 GeV/c^2, and no upper limit for M_{H^+} >153 GeV/c^2.

Direct searches from CDF [103] look for $H^+ \to \tau\nu$ using τ identification via its hadronic decays and they thus are sensitive only in the large $\tan\beta$ region. Indirect searches, performed by CDF and DØ [102] - as described above - are more powerful and look for suppression of Standard Model $t\bar{t}$ decays, caused by $t \to H^+ b$ decays. Observed rates of dilepton and lepton+jets events in the top sample depends on BR($t \to H^+ b$), while the Standard Model predictions for $\sigma_{t\bar{t}}$ are independent of $H^{\pm}$ production. Exclusion regions in the m_{H^+} versus $\tan\beta$ plane have been derived with sensitivity in both low and high $\tan\beta$ region as shown in Figure 29.

4.3 Standard Model Higgs Boson Searches in Run II

Higgs bosons at TeVatron [104] will be produced mainly in the gluon fusion process which proceeds primarily through a top quark triangle loop , with cross sections of roughly 1.0 to 0.1 pb for 100 GeV/c^2 $\leq m_H \leq$ 200 GeV/c^2 (see Figure 30). The two-loop QCD corrections enhance the gluon fusion cross section by about 60-100%. Unfortunately it is very difficult to make use of this production process in the Higgs boson search because of the overwhelming QCD background.

The most promising Standard Model Higgs boson discovery mechanism at the TeVatron for $m_H \leq$ 130 GeV/c^2 consists of $q\bar{q}$ annihilation into a virtual V^* ($V = W or Z$), in which the virtual $V^* \to VH$ followed by $H \to b\bar{b}$ and the leptonic decay of the V. The cross section for $q\bar{q} \to W^{\pm}H$ reaches values of 0.3 to 0.02 pb for 100 $\leq m_H \leq$ 200 GeV. The corresponding $q\bar{q} \to ZH$ cross-section is roughly a factor of two lower over the same Higgs mass range. The QCD corrections to $\sigma(q\bar{q} \to VH)$ coincide with those of the Drell-Yan process and increase the cross sections by about 30%.

The Higgs boson decays dominantly to the most massive kinematically allowed final state. For

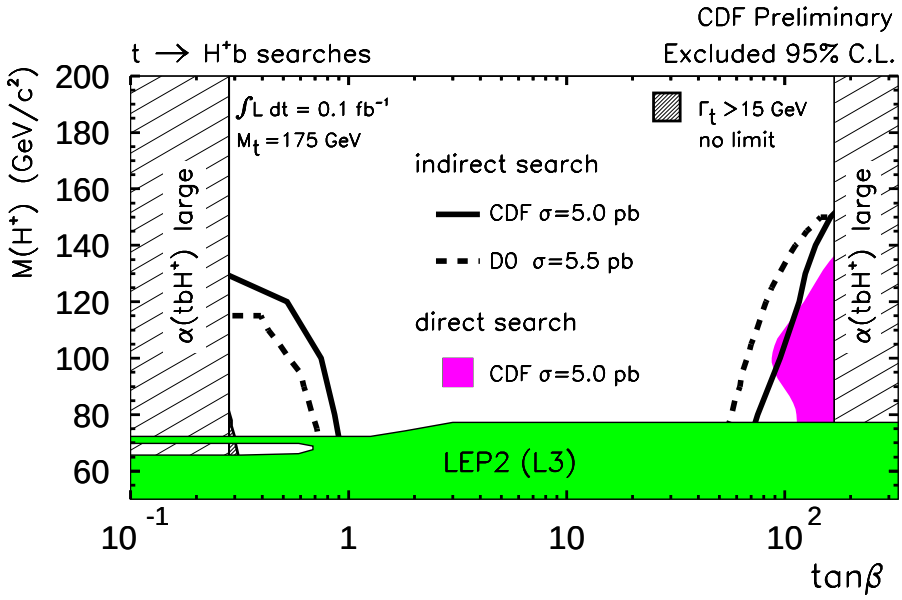

Figure 29: The 95% confidence level exclusion boundaries in the ($\tan\beta$,M_{H^+}) plane for m_t=175 GeV/c^2 for the charged Higgs boson searches from CDF and DØ .

$M_H < 135$ GeV/c^2, the dominant decay mode is $H \to b\bar{b}$ with a branching ratio of roughly 80%. For $m_H > 135$ GeV/c^2, the dominant mode is $H \to WW^{(*)}$, where one W is maybe off the mass shell. Thus, searches for lower mass Higgs will seek final states with at least two b jets, and the higher mass searches will have multiple (possibly virtual) W bosons.

4.3.1 $H \to b\bar{b}$

The dominant process for the production of Higgs bosons in $p\bar{p}$ collisions is $gg \to H$. Unfortunately, even with maximally efficient b-tagging this channel is swamped by QCD di-jet production. The more promising channels are $p\bar{p} \to WH$ and $p\bar{p} \to ZH$ final states [106]. The possible final states are: (1) $p\bar{p} \to WH \to l\nu b\bar{b}$, (2) $p\bar{p} \to ZH \to \nu\bar{\nu}b\bar{b}$, (3) $p\bar{p} \to ZH \to l^+l^-b\bar{b}$, (4) $p\bar{p} \to WH \to q\bar{q}b\bar{b}$ or $p\bar{p} \to ZH \to q\bar{q}b\bar{b}$. The primary backgrounds to these channels are $W + b\bar{b}$ and $Z + b\bar{b}$ with the $b\bar{b}$ pair from gluon radiation, single top-quark production and top-quark pair production.
For the production process $p\bar{p} \to WH, ZH$ the leptonic decays of W, Z provide a good trigger and the $H \to b\bar{b}$ signal is visible with adequate b-tagging.
Final states with a high p_T electron (e) or muon (μ) and a neutrino from the decay of the W boson and a $b\bar{b}$ pair from the decay of the Higgs boson are considered. To model the expected response of CDF and DØ run II detectors the SHW program [107] is used, which provides a fast, approximate simulation of the trigger, tracking, calorimeter clustering, event reconstruction and b-tagging. SHW is a parametrized simulation, details of event-by-event detector response are missing. This means that systematic effects and hardware-related background and misidentifications are largely neglected. Their impact can be estimated, however, from extrapolations of

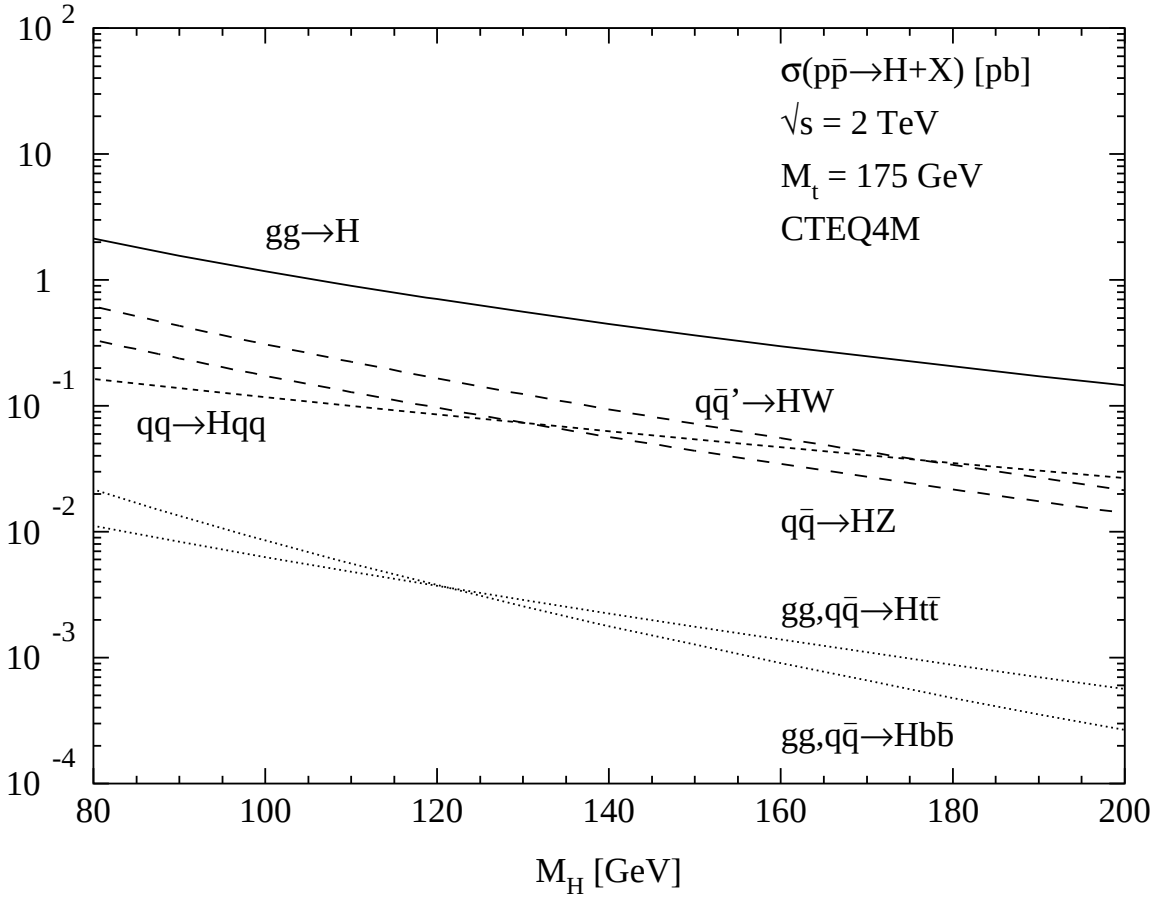

Figure 30: Cross section for various Higgs production processes in $p\bar{p}$ collisions at $\sqrt{s}$=2 TeV as a function of Higgs boson mass. From Ref. [105].

Run I results, and thus are not completely ignored.
Experimental considerations, such as trigger threshold and the need to restrict data to the phase space in which the detector response is well understood, dictate a set of loose cuts on the event variables:

- the transverse momentum of the isolated lepton $p_T^l > 15$ GeV/c
- the pseudo-rapidity of the lepton $|\eta| < 2$
- the missing transverse energy in the event $E_T^{miss} > 20$ GeV
- two or more jets in the event with $E_T^{jet} > 10$ GeV and $|\eta_{jet} < 2$.

Since the Higgs decays into a $b\bar{b}$ pair the requirement that two jets are b-tagged is imposed. A powerful tool used to suppress the $Wb\bar{b}$ background is the invariant mass of the b-tagged jets, which is expected to peak at the Higgs boson mass, whereas one expects a broad distribution for the background. Variables to discriminate between the signal and the backgrounds have been defined like the invariant mass of the b-tagged jets, the sum of the transverse energies of all selected jets, sphericity, etc. Then Neural Networks have been used. The most problematic background is the WZ production which is kinematically identical for Higgs boson masses close to the Z mass. Table 4 summarizes the results for the searches in the WH channel.

$WH \to l\nu bb$		$ZH \to l^+l^-bb$		$ZH \to \nu\nu bb$	
M_H (GeV/c^2)	$\sigma\times$BR(fb)	M_H (GeV/c^2)	$\sigma\times$BR(fb)	M_H (GeV/c^2)	$\sigma\times$BR(fb)
90	119.0	90	20.3	90	40.6
100	85.4	100	14.8	100	29.6
110	62.3	110	10.9	110	21.8
120	45.3	120	8.22	120	16.4
130	34.1	130	6.25	130	12.5
Backgrounds					
$Wb\bar{b}$	3500.0	$Zb\bar{b}$	350.0	$Zb\bar{b}$	700.0
WZ	164.8				
tbq	800.0	tbq	800.0	tbq	800.0
	σ (fb)		σ (fb)		σ (fb)
		ZZ	1235.0	ZZ	1235.0
tb	1000.0	tb	1000.0	tb	1000.0
$t\bar{t}$	7500.0	$t\bar{t}$	7500.0	$t\bar{t}$	7500.0

Table 4: Cross section times branching ratio for the WH and ZH processes which have been studied, for various M_H and for given backgrounds. For tb, $t\bar{t}$ and ZZ processes the total cross section is given.

For the di-lepton channel and the missing transverse energy channel a strategy similar to that described for the single-lepton channel is used.
For the upcoming high luminosity run (15 fb^{-1} integrated luminosity) the production of a Standard Model Higgs boson in association with a top quark pair is investigated [108]. But the signal

rate is low and a factor of three more of integrated luminosity would be needed to increase the significance of this search in the $t\bar{t}H$ channel with $H \to b\bar{b}$ for masses up to about 140 GeV/c^2 to 5σ per experiment.

4.3.2 $H \to WW^{(*)}$

In this section analyses designed for final states in which the Higgs boson decays to WW [109] instead of $b\bar{b}$ are described. Above 135 GeV/c^2 the decay into WW pairs is the dominant Higgs boson decay mode. Three final states are considered:

- (1) Three leptons $l^{\pm}l'^{\pm}l^{\mp}$, arising primarily from $p\bar{p} \to WH \to WWW$,
- (2) Di-leptons and neutrinos, $l^+l^-\nu\bar{\nu}$, from $p\bar{p} \to H \to WW$ and
- (3) like-sign di-leptons plus jets, $l^{\pm}l^{\mp}jj$, from $p\bar{p} \to WH \to WWW$ and $p\bar{p} \to ZH \to ZWW$.

The dominant backgrounds are Standard Model production of WW, WZ, ZZ, and $W(Z)$+jets and $t\bar{t}$ and multi-jet events with misidentification arising from detector effects.
As for the low mass analyses, the initial selections are based on simple variables related to the kinematics of the decay products. However, to reach a useful sensitivity, the analyses then use either requirements typically relating angular correlations arising from spin differences between signal and background and likelihood methods. The signal to background ratio is good (up to .45) but the low rate of a possible Higgs boson signal limits the statistical significance. The control of the systematic uncertainties will be challenging in this channel.
The tri-lepton signal is smaller than the like-sign leptons plus jets signal by about a factor of 3 due to the difference of the W decay branching fractions to $l = e, \mu$ and two jets. The signal rates for $WH \to b\bar{b}l\nu$ drop dramatically for a $m_H > 150$ GeV/c^2. In the pure leptonic channel ($H \to WW \to l\nu l\nu$) it is difficult to reconstruct m_h due to the two missing neutrinos but the QCD background is much lower compared to the $l\nu jj$ decay channel [110].

4.3.3 Overall Sensitivity

Before turning to channel-by-channel sensitivities as a function of Higgs boson mass and luminosity it is worthwhile to describe the results concerning the key Higgs search detector parameters:

- Missing E_T resolution was excellent in Run I and no gains are foreseen in this area.
- Lepton identification efficiency in CDF and DØ is mainly governed by geometrical acceptance. Improvements are being made in the muon systems of both detectors.
- Tagging of b-quarks plays an important role in any Standard Model Higgs boson search. However, the signal significance ($S/\sqrt{B}$) grows at a faster rate if the invariant mass resolution for pairs of b jets is improved than if the b-tagging efficiency is increased. This highlights the importance of a good understanding of the b-jet scale.

The sensitivity to a Standard Model Higgs boson from a combination of CDF and DØ expectations, as measured by signal over the square-root of background ($S/\sqrt{B}$) for various decay channels, as a function of the Higgs boson mass, is presented in Figure 31 for an integrated luminosity of 1 fb^{-1} per experiment. The mass reach of the TeVatron experiments is significantly improved by considering final states produced when the Higgs boson at higher masses decays to real or virtual boson pairs. Good improvements in sensitivity over purely cut-based analyses can be expected when using techniques such as neural net analyses. But it is clear that 1 fb^{-1} per experiment is not sufficient for a Higgs boson discovery. This is quantified in Figure 32

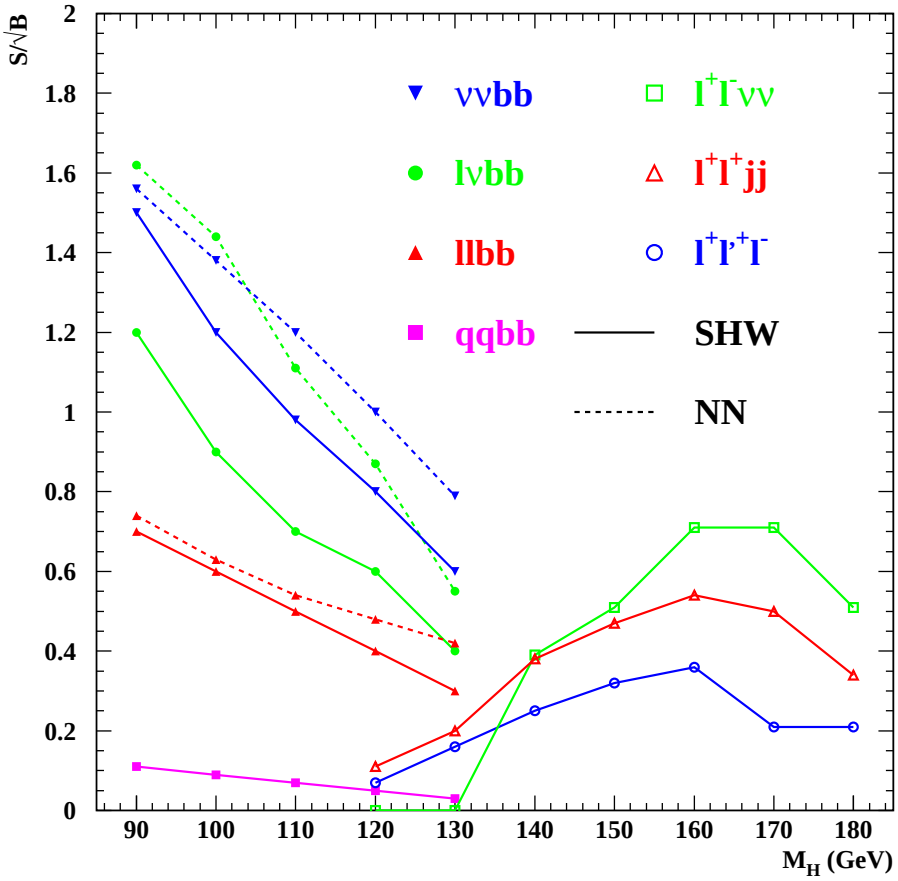

Figure 31: Sensitivities for a combination of CDF and DØ expectations in the main Standard Model Higgs boson final states. Results are given for 1 fb^{-1} delivered to each experiment. Points connected by solid lines correspond to cut-based analyses, the dashed lines indicate results using a neural net.

where the combined CDF and DØ 95% confidence level limits, 3 σ evidence and 5 σ discovery thresholds for a given integrated luminosity delivered to each experiment are plotted as a function of Higgs mass. With the minimal Run II integrated luminosity of 2 fb^{-1}, the TeVatron will not be able to extend the LEP Higgs mass limit of 113.5 GeV/c^2. With more than 15 fb^{-1} per experiment, a Standard Model Higgs boson could be excluded up to about 180 GeV/c^2. First

hints of a real Higgs signal (3 σ) would only appear beyond what has already been excluded for an integrated luminosity of at least 8 fb^{-1} per experiment. With 15 fb^{-1} per experiment a Higgs boson with a mass up to 120 GeV/c^2 could be detected with 5 σ significance. A Bayesian combination method [111] has been used to combine all channel and both experiments. A 10% $m_{b\bar{b}}$ resolution has been assumed. For the analysis in the $H \rightarrow b\bar{b}$ channel a neural network technique has been used. As systematic error the minimum of 10% or $1/\sqrt{\int \mathcal{L}dt \times B}$, where B is the expected background in 1 fb^{-1} and $\int \mathcal{L}dt$ is the integrated luminosity, has been used.

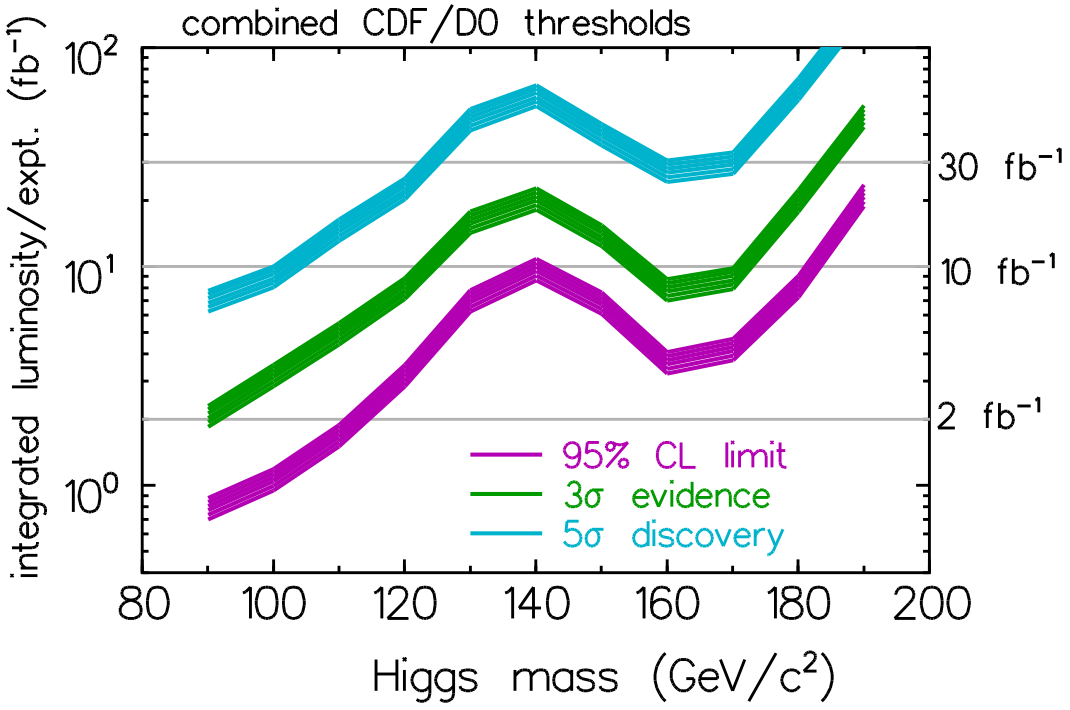

Figure 32: Standard Model Higgs sensitivity predicted for a combination of CDF and DØ expectations as a function of Higgs mass and integrated luminosity delivered to each experiment. Limits (at 95% confidence level), 3 σ evidence and 5 σ discovery curves are plotted. The bands represent an uncertainty of 30% arising from $m_{b\bar{b}}$, Efficiency ϵ_b and the background uncertainties. The curves shown are obtained by combining the $l\nu b\bar{b}$, $\nu\bar{\nu}b\bar{b}$ and $l^+l^-b\bar{b}$ channels using a neutral network selection in the low-mass region ($90 \lesssim m_H \lesssim 130$ GeV/c^2), and the $l^\pm l^\mp jj$ and $l^+l^-\nu\bar{\nu}$ channels in the high-mass region ($130 \lesssim m_H \lesssim 190$ GeV/c^2).

4.4 Searches for the MSSM Higgs Bosons in Run II

The searches for the Standard Model Higgs boson can be interpreted more generally in the framework of an extended Higgs sector. Generically, extended Higgs sectors contain additional scalar states beyond the Standard Model Higgs boson with different couplings from those found in the Standard Model.

The simplest approach to search for the MSSM neutral Higgs bosons at TeVatron is to use the search channels for Standard Model production of $VH, (V = W, Z)$ [104,112]. Where the cross section is lower than that of the corresponding MSSM production, one can exclude or discover the MSSM Higgs boson at that mass. The first step is to calculate for each Higgs boson mass and for a given integrated luminosity the value R of the ratio of the production cross section at which one can expect to exclude or discover the Higgs boson to the Standard Model cross section. For different m_A and $\tan\beta$, then, one compares the values of R thus obtained to the theoretical values at those parameter values. Figure 33 shows the values of R for 95% confidence level limits and 5 σ discovery as a function of the Higgs boson mass, based on the low-mass Standard Model Higgs boson search channels WH and ZH.

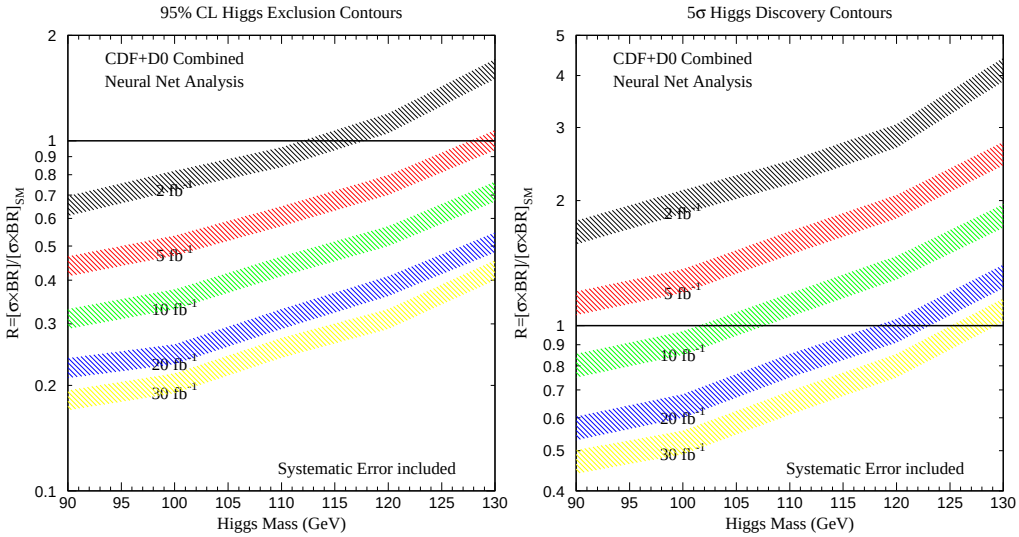

Figure 33: The ratio $R = \sigma(q\bar{q}' \to V\phi)BR(\phi \to b\bar{b})/\sigma(q\bar{q}' \to Vh_{SM})BR(h_{SM} \to b\bar{b})$ as a function of the Higgs boson mass. Each shaded region represents the minimal value of R necessary at a given Higgs boson mass to (a) exclude a Higgs boson signal at 95% confidence level, for the integrated luminosity per detector as indicated (combining the statistical power of both experiments). The thickness of the bands, extending upwards from the estimated thresholds, indicate the uncertainties in b-tagging efficiency, background, mass resolution and other effects [104].

Figure 34 shows the regions of the MSSM parameter space $\tan\beta$ versus m_A in which one can exclude or discover the Higgs boson, as a function of the delivered integrated luminosity per experiment, combining the data from both experiments. In Figure 34 results for two different sets of parameters are shown: The upper plots using a maximal mixing benchmark scenario ($\mu = -0.2$, $X_t = \sqrt{6}$, $A_b = A_t$, $M_{SUSY} = 1$ TeV, $M_{\tilde{g}} = 1$ TeV), the lower plots using parameters ($A = -\mu$ =1.5 TeV, $A_b = 0$, $M_{SUSY} = 1$ TeV, $M_{\tilde{g}} = 1$ TeV). As the figure shows, with 5 fb^{-1} one can exclude most of the parameter space for maximal stop mixing; to discover the MSSM Higgs boson in most of the space at 5 σ significance requires about 20 fb^{-1}. However for the case $A = -\mu = 1.5$ TeV the difficult region for large $\tan\beta$ extends due to the

suppression of the $Vb\bar{b}$ coupling.
In the MSSM, the basic $b\bar{b}\phi, \phi = h, H, A$ couplings are proportional to $1/\tan\beta$ at large $\tan\beta$, and thus can lead to enhanced production of MSSM neutral Higgs bosons in conjunction with a $b\bar{b}$ pair. If, for example, the value of $\tan\beta$ is near $m_t/m_b \sim 35$, then the production of $ab\bar{b}$ is enhanced by over a factor of 1000 compared with the Standard Model production of $Hb\bar{b}$. Thus by searching for events with $b\bar{b}b\bar{b}$ final states, one can be sensitive to a large range of the MSSM parameter space (see Figure 34).
Within MSSM models, new Higgs production modes exist, some with couplings proportional to $\tan^2\beta$. For sufficiently large values of $\tan\beta$ these become the dominant production modes. One such mode is $p\bar{p} \to \phi b\bar{b}$ with $\phi = h, H, A$. A study to evaluate the sensitivity reach for this mode in Run II has been performed. This results in final states containing four b-flavoured jets. The analysis [104] typically requires four jets, three of which satisfy b-tag requirements. All possible mass combinations of b-jets are computed, and the resulting distribution is examined for a peak near the generated Higgs boson mass. The 95% exclusion contours in the $\tan\beta$ versus m_A plane are shown in Figure 35 for several integrated luminosities. These results indicate that assuming $\tan\beta$=40, the sensitivity reach is about 160 GeV/c^2 at 95% confidence level with an integrated luminosity of 2 fb^{-1} extending up to 225 GeV/c^2 with 10 fb^{-1}. This channel serves as the most important mode for discovering or ruling out the MSSM Higgs at large $\tan\beta$.
The search for charged Higgs bosons at TeVatron as described in a previous section can be continued in Run II. If there is a charged Higgs boson lighter than the top quark, its presence can be detected by a so-called disappearance search [104] if $\tan\beta$ is substantially different from $\sqrt{m_t/m_b}$, prompting a direct search to confirm discovery: In a disappearance search, one employs selection criteria optimized to detect the Standard Model decay of $t\bar{t}$. Such criteria are expected to have relatively low efficiency for decays involving $t \to H^+b$. The top quark pair-production cross section is not expected to be significantly affected by the presence of a charged Higgs boson. Consequently, if data agree well with Standard Model based predictions for $\sigma_{t\bar{t}}$, regions of parameter space where BR($t \to H^+b$) is large can be excluded because in those regions one would expect fewer events than seen in data.

5 Near Future: Higgs Bosons at LHC

When LHC will start it may still not be clear if a light Higgs boson with a mass below 120 GeV/c^2 exists. LEP stopped data-taking with the final result of a 2.9 σ evidence for a Higgs boson with a mass around 115 GeV/c^2. TeVatron will be able to exclude a Higgs boson at this mass at the 95% confidence level with 2 fb^{-1} per experiment (end of the year 2003). If a Higgs boson in the mass range 115–120 GeV/c^2 exists, however, TeVatron would need $\sim$ 15 fb^{-1} per experiment for a 5 σ discovery. The projected luminosity for LHC in 2007 is 10 fb^{-1}, sufficient for a 5 σ discovery of a Higgs boson in the mass range 115–120 GeV/c^2.

5.1 The LHC Collider and the Detectors

LHC (Large Hadron Collider) is a pp accelerator with a circumference of 27 km which will be built in the existing LEP tunnel. For the year 2006 first collisions of 7 TeV protons with 7 TeV

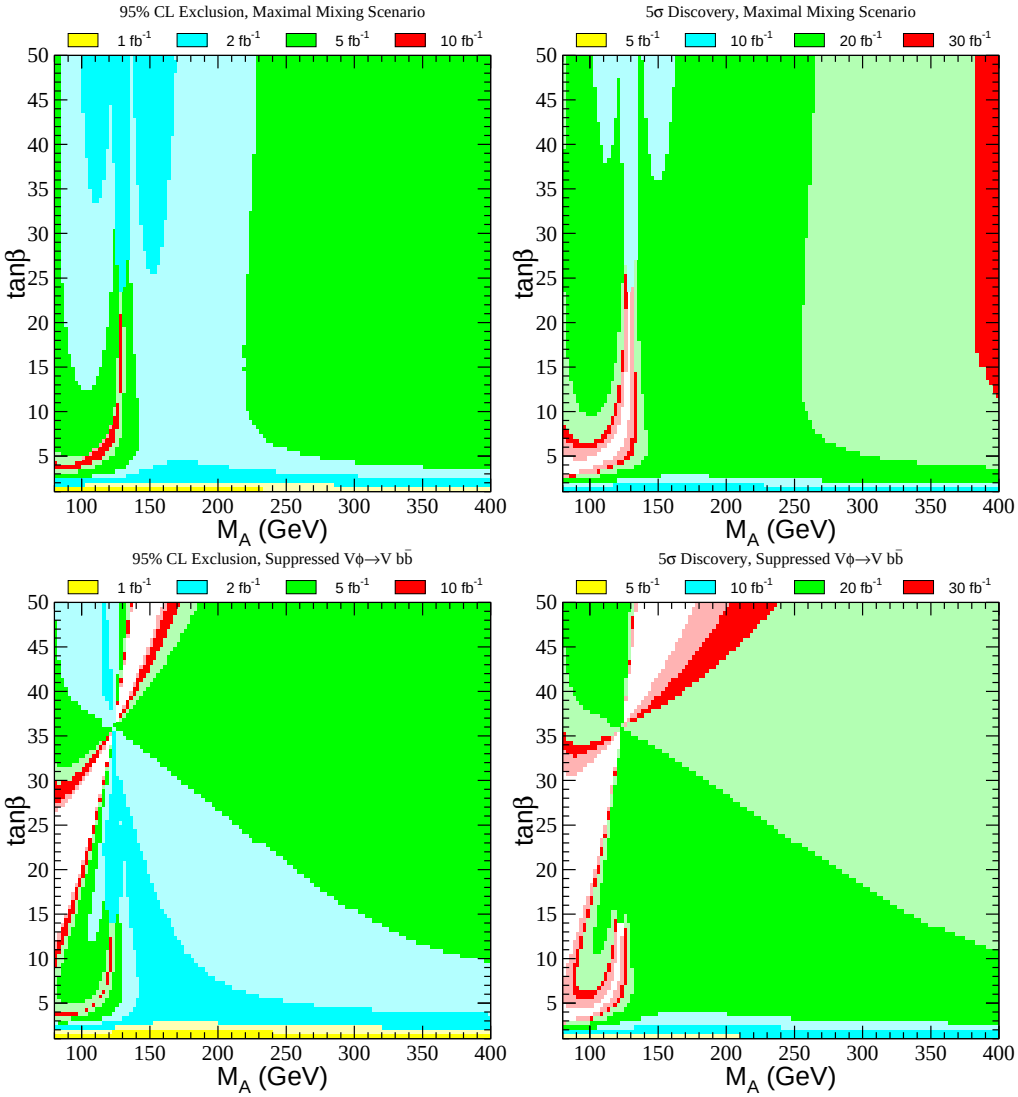

Figure 34: In each of the two scenarios, the 95% confidence level exclusion regions and the 5 σ discovery regions are shown for two different search channels: (i) shaded regions correspond to V+Higgs (where V=W or Z and the associated Higgs boson is one of the two CP-even Higgs scalars of the MSSM-h or H), and (ii) regions in the upper left-hand corner of the graphs bounded by the solid lines correspond to $b\bar{b}$ Higgs boson production (where the associated neutral Higgs boson is either h, H or A). Different integrated luminosities are explicitly shown by the color coding. Note that the same colors correspond to different integrated luminosities in the 95% CL and 5 σ plots. For search channel (ii), the two sets of lines (for a given color) correspond to the CDF and D0 simulations, respectively. The region below the solid black line near the bottom of the plot is excluded by the absence of observed $e^+e^- \to Z + h$ events at LEP.

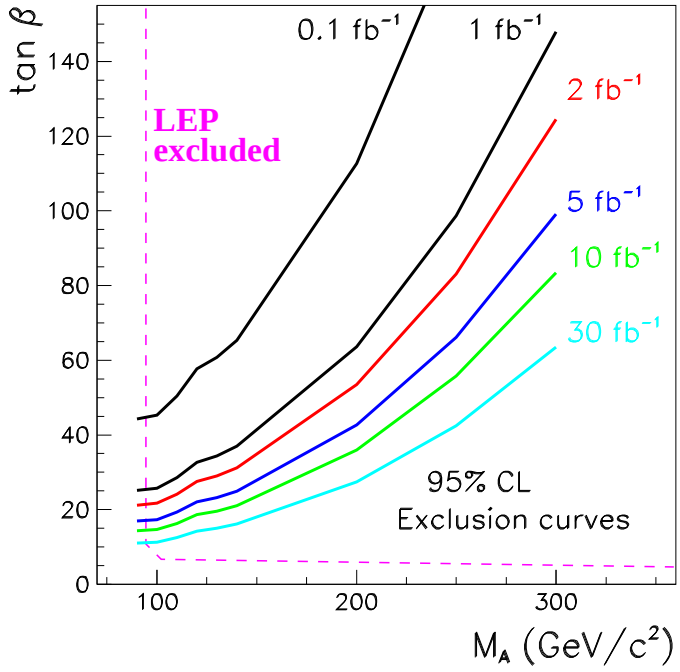

Figure 35: 95% confidence level exclusion curves for $p\bar{p} \to \phi b\bar{b} \to b\bar{b}b\bar{b}$ with $\phi = h, H, A$. The curves show the sensitivity reach for the MSSM neutral Higgs bosons in the $\tan\beta$ and m_A parameter space. The LEP Excluded region is also shown for comparison. The results are shown for the maximal mixing scenario. The excluded region is above the curve at high $\tan\beta$ and low m_A values.

protons are planned. Two general purpose experiments - ATLAS [113] and CMS [114] - are under construction.
The LHC offers a wide range of physics opportunities [115] and the search for the Higgs boson or more generally the origin of particle masses are definitively a major focus of interest. The motivation of this accelerator, however, goes far beyond the Standard Model. Complementary information will come from the search for new particles, with an excellent discovery potential for supersymmetry, a promising accuracy for the study of W boson and top quark properties and couplings and last but not least the high b-quark production rate which is expected to give new insights in the problem of CP-violation.
A broad spectrum of detailed physics studies [116, 117] specified the design of the detectors as presented in their Technical Proposals [113, 114].
As an example the ATLAS detector will be described in the following. The overall detector layout is shown in Figure 36. The basic design criteria of the detector include a very good electromagnetic calorimetry for electron and photon identification, high-precision muon momentum measurements, efficient tracking at high luminosity and a large acceptance in pseudorapidity.
The inner detector is contained within a cylinder of length 7m and a radius of 1.15 m, in a solenoidal magnetic field of 2 T. Pattern recognition, momentum and vertex measurements, and electron identification are achieved with a combination of high-resolution semiconductor pixel and strip detectors in the inner part of the tracking volume, and straw-tube tracking detectors with transition radiation capability in the outer part.
Highly granulated liquid-argon (LAr) electromagnetic (EM) sampling calorimetry, with excellent performance in terms of energy and position resolution, covers the pseudo-rapidity range $|\eta| < 3.2$. In the end-caps, the LAr technology is also used for the hadronic calorimeters, which share the cryostats with the EM end-caps. The same cryostats also house the special LAr forward calorimeters which extend the pseudo-rapidity coverage to $|\eta| < 4.9$. The overall calorimeter system provides the very good jet and E_T^{miss} performance of the detector. The LAr calorimetry is contained in a cylinder with an outer radius of 2.25 m and extends longitudinally to $\pm$6.65 m along the beam axis.
The calorimeter is surrounded by the muon spectrometer [118]. The air-core toroid system, with a long barrel and two inserted end-cap magnets, generates a large magnetic field volume with strong power within a light and open structure. Multiple-scattering effects are thereby minimized, and excellent muon momentum resolution is achieved with three stations of high-precision tracking chambers. The muon instrumentation also includes as a key component trigger chambers with very fast time response. The muon spectrometer defines the overall dimensions of the ATLAS detector. The outer chambers in the barrel are at a radius of about 11 m. The half-length of the barrel toroid coils is 12.5 m, and the third layer of the forward muon chamber, mounted on the cavern wall, is located about 23 m from the interaction point.
The primary goal of the experiment is to operate at high luminosity (10^{34} cm^{-2} s^{-1}) with a detector that provides as many signatures as possible.

5.2 Standard Model Higgs Boson Searches

Figure 37 shows the different Feynman graphs for the production of Higgs bosons at LHC.
Higgs boson production at the LHC is dominated by the gluon fusion mechanism $gg \rightarrow H$,

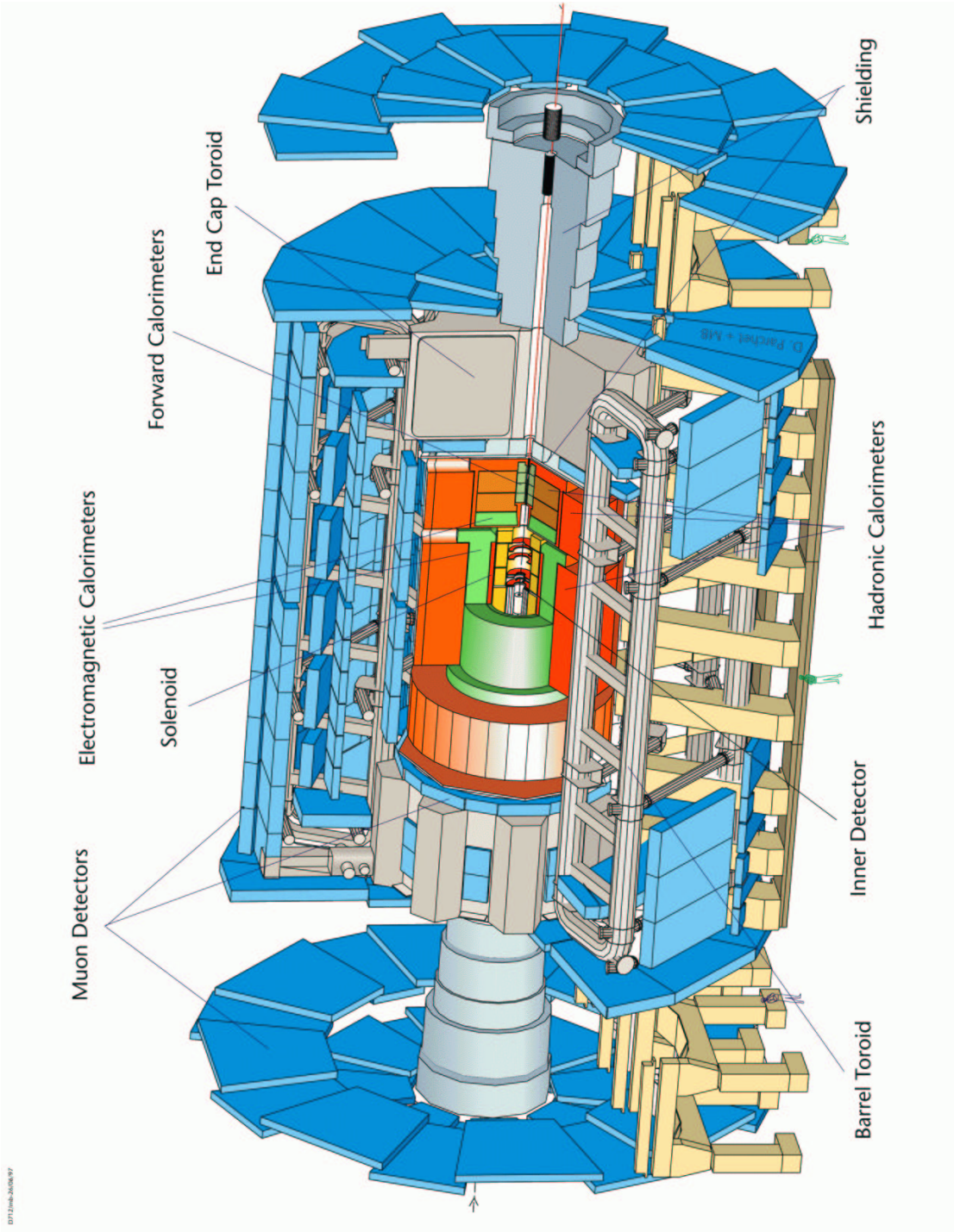

Figure 36: 3-dimensional schematic view of the ATLAS detector.

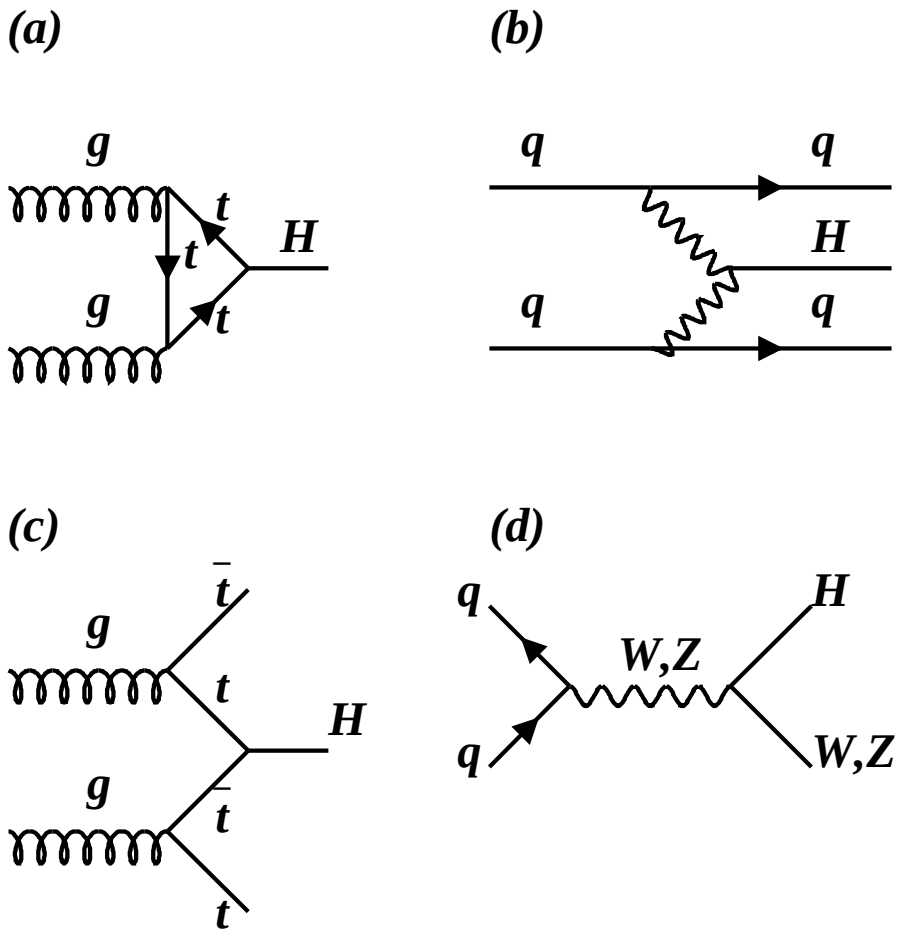

Figure 37: Production mechanism for Higgs bosons at LHC: (a) gluon-gluon-Fusion, dominant at low Higgs boson masses, (b) vector boson fusion, dominant at high Higgs boson masses, (c) associated $t\bar{t}H$ production, about 50 times smaller than gluon-gluon fusion, (d) associated WH fusion, about 50 times lower than vector boson fusion. For cross sections of these processes at LHC see Figure 38.

which is mediated by top and bottom triangle loops. This production process is directly sensitive to the $t\bar{t}H$ coupling. This can be inferred from Figure 38, which presents all relevant Higgs production cross sections as a function of the Higgs mass. The two-loop QCD corrections increase the production cross section by 60-90%, so that they can no longer be neglected [119]. For large Higgs boson masses the vector boson fusion mechanism $WW, ZZ \rightarrow H$ becomes competitive, while for intermediate Higgs boson masses it is about an order of magnitude smaller than gluon fusion [120–122]. This process is sensitive to the Higgs coupling to the weak vector bosons. The ratio of the two cross sections provides the information how the Higgs couples to fermions and bosons. The QCD corrections are small and thus negligible [123]. Higgs-strahlung $W^*/Z^* \rightarrow HW^*/Z^*$ plays a role only for $m_H < 100$ GeV/c^2. The QCD corrections are moderate, so that this process is calculated with reliable accuracy [124]. Another interesting production process for Higgs bosons is the associated Higgs production: $q_i\bar{q}_j \rightarrow WH$ or $q_i\bar{q}_j \rightarrow ZH$, where an off-shell vector boson is produced and radiates a Higgs boson. The last production mechanism is the Higgs bremsstrahlung: $gg, q_i\bar{q}_j \rightarrow t\bar{t}H$ where top quarks are produced and radiate a Higgs boson. The two last production mechanisms have a cross section about 100 times smaller than the gluon fusion process.

The strategy to find the Higgs boson changes depending on its mass [115]. For Higgs boson masses below 130 GeV/c^2 the most significant channels are the decays $H \rightarrow \gamma\gamma$ and $H \rightarrow b\bar{b}$. Between 130 and 180 GeV/c^2 the decay channels $H \rightarrow ZZ^* \rightarrow$4l and $H \rightarrow WW^* \rightarrow l^+\nu l^-\bar{\nu}$ are the expected discovery channels. For larger masses up to 400 GeV/c^2 $H \rightarrow ZZ^* \rightarrow$4l provides the easiest discovery signature. For higher Higgs boson masses, additional signatures involving hadronic W and Z decays have been investigated and promising signals have been obtained. These channels will be discussed in detail in the following sections.

Physics processes have been simulated with the PYTHIA [125] Monte Carlo program, including initial- and final-state radiation, hadronization and decays. The signal and background production cross sections are affected by uncertainties due to higher order corrections, structure function parameterizations and event generation. The higher-order QCD corrections to the production cross sections are not known for all signal and background processes. Therefore, the present Higgs studies at ATLAS have consistently and conservatively refrained from using k-factors, resorting to Born-level predictions for both signal and backgrounds. The studies performed by the CMS collaboration are using k-factors. The k-factors, i.e. higher order corrections are of the order of 1.6-1.9 for $gg \rightarrow H$. The uncertainties from parton density functions and NNLO cross sections are estimated to be smaller than 20%.

5.2.1 $H \rightarrow \gamma\gamma$

The decay H$\rightarrow \gamma\gamma$ is a rare decay mode, only detectable in a limited Higgs mass region where the production cross-section and the decay branching ratio are both relatively large. It is a promising channel for a Higgs search in the mass range of 100$< m_H <$150 GeV/c^2. Excellent energy and angular resolution are required to observe the narrow mass peak above the irreducible prompt $\gamma\gamma$ continuum. Powerful particle identification capability is needed to reject the large jet background.

The direct production of a low mass Higgs is dominated by the gg fusion process. The irreducible background consists of genuine photon pairs via the following three processes: Born ($q\bar{q} \rightarrow \gamma\gamma$),

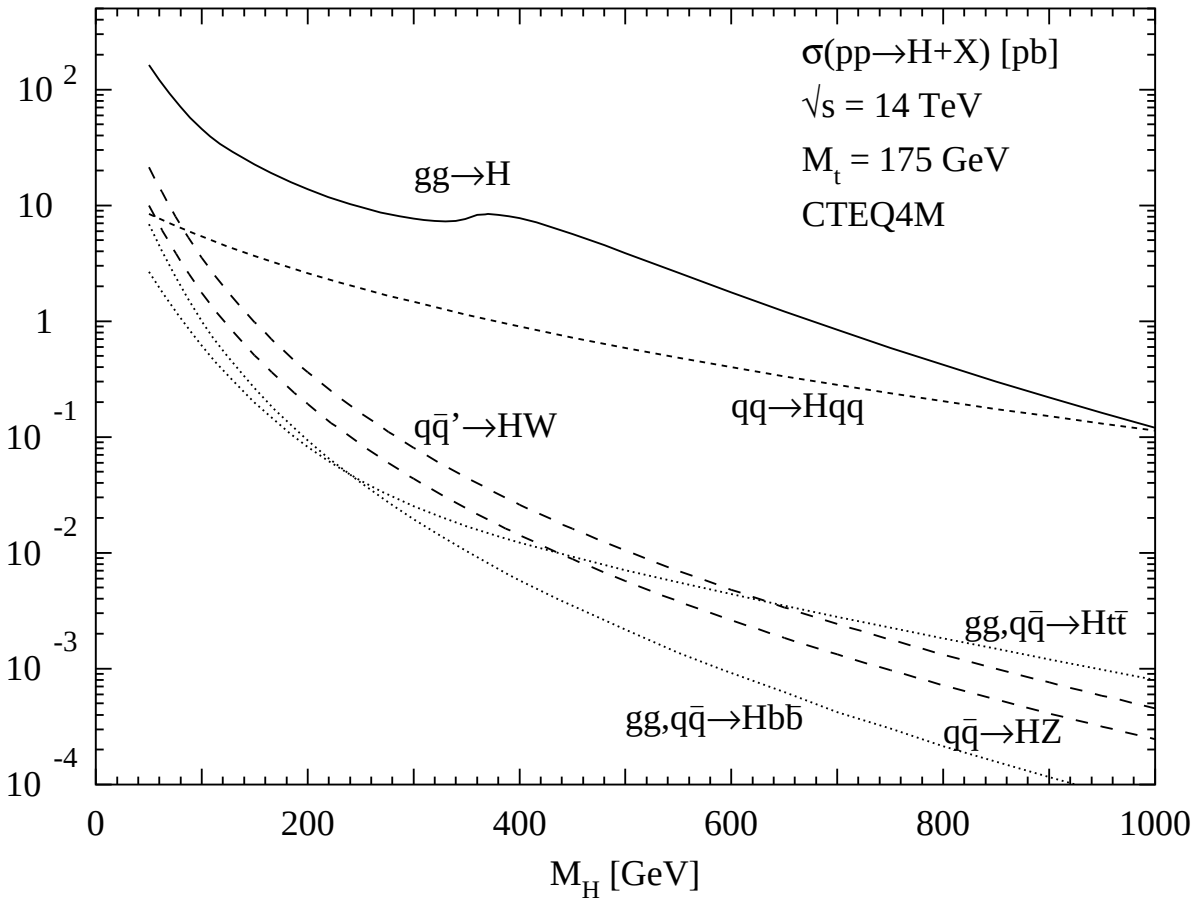

Figure 38: Cross section for various Higgs production processes in *pp* collisions at $\sqrt{s}$=14 TeV as a function of Higgs boson mass. From Ref. [126].

box ($g \rightarrow \gamma\gamma$), and quark-bremsstrahlung ($qg \rightarrow q\gamma \rightarrow q\gamma\gamma$). The production cross section for the sum of the Born and box processes is of the order of 1 pb/GeV/c^2 in the two-photon mass range around 100 GeV/c^2. After isolation cuts, this background amounts to about 50% of the combined Born plus box contribution. The reducible background consists of $jet-jet$ and $\gamma-jet$ events in which one or both jets are misidentified as photons, as well as $Z \rightarrow e^+e^-$ decays, where both electrons are mistaken as photons. Since the production cross sections for these processes are many orders of magnitude larger than the signal cross sections, excellent photon/jet and photon/electron discrimination are required. The expected $H \rightarrow \gamma\gamma$ signal significances, defined for each mass point as $S/\sqrt{B}$ where S and B are the numbers of accepted signal and background events in the chosen mass window of $\pm 1.4\ \sigma$ for an integrated luminosity of 100 fb^{-1} ranges from 2.4 to 6.5 σ in the mass range $80 < m_H < 130$ GeV/c^2. In addition to the signal events from direct production, events from the associated production of a Higgs boson with a W or Z boson or a $t\bar{t}$ pair have been included in the signal. As an example for the signal reconstruction, Figure 39 shows the expected signal from a Higgs boson with $m_H = 120$ GeV/c^2 after an integrated luminosity of 100 fb^{-1} (high luminosity). The $H \rightarrow \gamma\gamma$ signal is clearly visible above the smooth background, which is dominated by the irreducible $\gamma\gamma$ background.

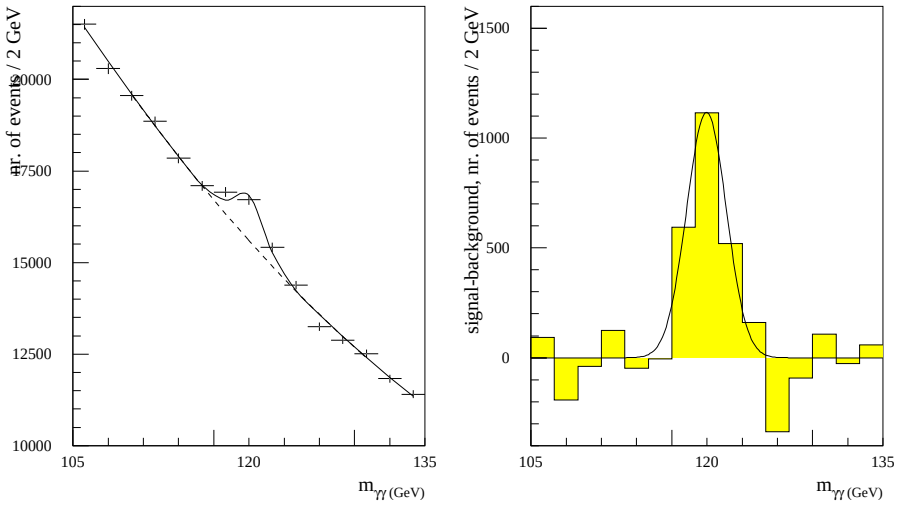

Figure 39: Expected H$\rightarrow$ $\gamma\gamma$ signal for $m_H = 120$ GeV/c^2 for an integrated luminosity of 100 fb^{-1}. The signal is shown on top of the irreducible background (left) and after background subtraction (right).

The production of the Higgs in association with a W or a Z boson or with a $t\bar{t}$ pair can be used in addition to the direct $\gamma\gamma$ decay mode to search for a low mass Higgs boson. The production cross section for the associated production is almost a factor 50 lower than for the direct production, leading to much smaller signal rates. If the associated W/Z boson or one of the top quarks is required to decay leptonically, thereby leading to final states containing one isolated lepton and two isolated photons, the signal-to-background ratio can nevertheless be substantially improved with respect to the direct production. In addition, the vertex position can be unambiguously determined by the lepton charged track, resulting in much better mass resolution at high luminosity

than for the case of the direct production. In order to suppress the reducible background from QCD jet and $t\bar{t}$ production and from final-state photon radiation, isolation criteria are applied. The irreducible background has been evaluated by considering the $W\gamma\gamma$, $Z\gamma\gamma$, $t\bar{t}\gamma\gamma$ and $b\bar{b}\gamma\gamma$ production. By requiring the lepton-photon mass to be above a given threshold the background has been further suppressed. There are also many sources of reducible backgrounds. Final states containing one, two or three jets in association with a lepton or photon, such as $\gamma\gamma - jet$, $\gamma l - jet$, $\gamma - jet - jet$, $l - jet - jet$ and $jet - jet - jet$, have been considered. The total reducible background is estimated to be at the level of 20-30% of the irreducible one over the mass range considered (80-140 GeV/c^2). The statistical significance in the mass range between 80 to 140 GeV/c^2 is 4 to 3 σ for an integrated luminosity of 100 fb^{-1}.
For low Higgs boson masses (< 140 GeV/c^2) the decay width is of the order of keV. The measured mass resolution will be entirely dominated by the energy resolution of the electromagnetic calorimeter used to detect and measure the photons. The mass resolution will be in the order of 1–1.5 GeV/c^2 at both experiments.

5.2.2 $H \to b\bar{b}$

This channel has about a 10 times larger $\sigma\times$ branching ratio (BR) than the $H \to \gamma\gamma$ mode. Since the direct production, $gg \to H$ with $H \to b\bar{b}$, cannot be efficiently triggered nor extracted as a signal above the huge QCD two-jet background, the associated production with a W or Z boson or a $t\bar{t}$ pair remains the only possible process to observe a signal from $H \to b\bar{b}$ decays. The leptonic decays of the W boson or semi-leptonic decays of one of the top quarks provide an isolated high-p_T lepton for triggering. In addition, requiring this high-p_T lepton provides a large rejection against background from QCD jet production. The Higgs boson signal might thus be reconstructed as a peak in the invariant jet-jet mass spectrum of tagged b-jets.
Contrary to the TeVatron ZH production with $Z \to ll$ is not considered at LHC because it provides a rate about six times lower than the WH channel and the signal-to-background ratio would not be significantly improved with respect to the EH channel because the main background $Zb\bar{b}$ is only a factor 1.8 smaller than the $Wb\bar{b}$ background.
Besides the WH channel the $t\bar{t}H$ is used, for both channels excellent b-tagging capabilities are needed to achieve a high efficiency. Using pixel layers at small radii allows to achieve efficiencies around 60% (50%) at low (high) luminosity, for rejection factors of about 100 versus u-jets. The background to the WH channel can be divided into three classes:

- Irreducible background from $WZ \to l\nu b\bar{b}$ and from $Wb\bar{b}$ production.
- Reducible background with at least two b-quarks in the final state, which arises predominantly from $t\bar{t} \to WWb\bar{b}$, and from single top production through $gq \to t\bar{b}q \to l\nu b\bar{b} + q$.
- Reducible background containing jets misidentified as b-jets, which arises mainly from $W + jet$ production.

It is not clear in all cases how to achieve an accurate knowledge of the various backgrounds from the data. For example the shape and magnitude of the $Wb\bar{b}$ background cannot be obtained directly from the experimental data and one will have to rely on Monte Carlo simulations. If a systematic uncertainty of $\pm 5\%$ on the shape of the $Wb\bar{b}$ background is assumed in the $H \to b\bar{b}$

signal region, the statistical significance is between 3.0 σ (m_H=80 GeV/c^2) and 1.7 σ (m_H=120 GeV/c^2) for an integrated luminosity of 30 fb^{-1} and assuming a systematic uncertainty of $\pm$ 5 %. on the shape of the $Wb\bar{b}$ background in the $H \rightarrow b\bar{b}$ signal region. In conclusion, the extraction of a signal from $H \rightarrow b\bar{b}$ decays in the WH channel will be very difficult at the LHC, even under the most optimistic assumptions for the b-tagging performance and calibration of the shape and magnitude of the various background sources from the data itself.

The cross section for associated $t\bar{t}H$ production [127,128] is about the same as for WH production. The final state is however considerably more complex, since it consists of two W bosons and four b-jets. For trigger purposes, one of the W bosons should decay leptonically, whereas the other one is assumed to decay into a $q\bar{q}$ pair. A signal from $t\bar{t}H$ production can be extracted by a complete reconstruction of both top-quark decays. This solves the large combinatorial problem arising from the presence of four b-quarks in the final state. This channel is observable both at low and high luminosity. The signal should appear as a peak in the $m_{b\bar{b}}$ distribution, above the various background processes. The resonant $t\bar{t}4Z$ and continuum $t\bar{t}b\bar{b}$ production are the irreducible backgrounds. Reducible backgrounds which are containing jets misidentified as b-jets, such as $t\bar{t}jetjet$, $W + 6jets$, $WWb\bar{b}jetjet$, etc. The W bosons are reconstructed from the jets not tagged as b-jets and from the reconstructed lepton and the neutrino. In the case of the leptonic decay, the W mass constraint is used to determine the longitudinal component of the neutrino momentum. Ambiguities arise in the pairing of the two W bosons, with two of the four b-jets. These ambiguities are resolved by selecting from all $l\nu b - jjb$ combinations the one which minimizes $\chi^2 = (m_{jjb} - m_t)^2 + (m_{l\nu b} - m_t)^2$. For events passing all kinematic cuts, the $b\bar{b}$ invariant mass, $m_{b\bar{b}}$, is computed and a final cut is applied to select events in a mass window around the nominal Higgs boson mass. The $m_{b\bar{b}}$ distribution for the summed signal and background events is shown in Figure 40 for a Higgs boson mass of 120 GeV/c^2 and for an integrated luminosity of 100 fb^{-1} (30 fb^{-1} at low luminosity operation and 70 fb^{-1} with high luminosity operation). The summed background is shown by the dashed line, and the points with error bars represent the result of a single experiment.

A similar study has been done for CMS [129]. Here events are triggered and preselected if there is an isolated lepton (p_T >10 GeV, $|\eta| < 2.4$) and at least six jets ($E_T > 20$ GeV, $|\eta|$ <2.5). In the next step, the best jet configuration in the event has been found by defining an event likelihood function which takes into account the probabilities of jets to be b-jets, two reconstructed top masses, one reconstructed W-mass and the order of b-jet energies. After the best configuration is found with the highest value of the event likelihood function, the signal events are enriched cutting on values of the likelihood functions which take into account b-tagging and kinematics of the event. Applying k-factors of 1.9 for $t\bar{t}q\bar{q}$ background and of 1.5 for $t\bar{t}H$ and $t\bar{t}Z$ leads to a signal-to-background ratio S/B=73% with m_H=115 GeV/c^2. In the Standard Model the Higgs boson can be discovered in this channel with 5σ significance for a Higgs mass up to 122 GeV/c^2 for L_{int}=30 fb^{-1}. Figure 41 shows the invariant mass distribution of signal (dark shaded, m_H =115 GeV/c^2) plus background for L_{int}=30 fb^{-1}.

5.2.3 $H \rightarrow ZZ^{(*)} \rightarrow 4l$

The decay channel H$\rightarrow$ $l^+l^-l^+l^-$ provides a very clean signature for a Standard Model Higgs boson in the mass range from $120 < m_H < 600$ GeV/c^2. The signal can be well identified

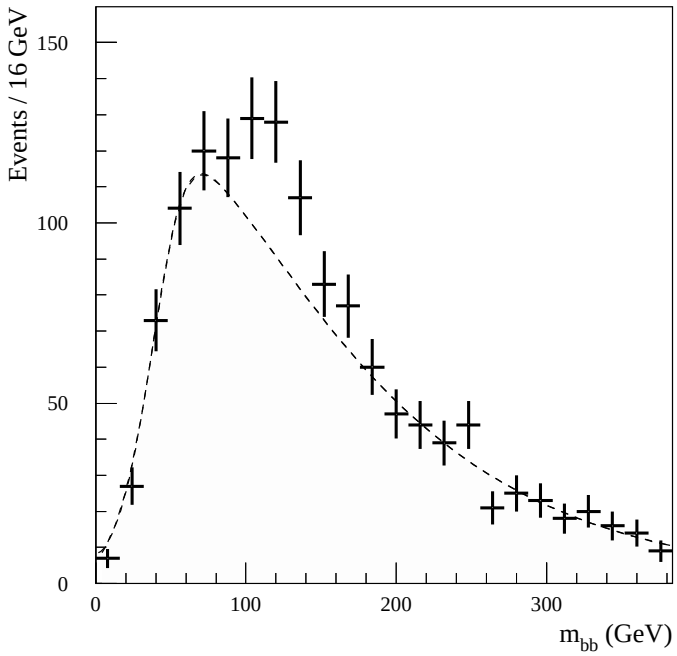

Figure 40: Invariant mass distribution, $m_{b\bar{b}}$, of tagged b-jet pairs in fully reconstructed $t\bar{t}H$ signal events with a Higgs boson of 120 GeV/c^2 above the summed background. Assumed is an integrated luminosity of 100 fb^{-1} (30 fb^{-1} at low luminosity operation and 70 fb^{-1} with high luminosity operation). The points with error bars represent the result of a single experiment (ATLAS) and the dashed line represents the background distribution.

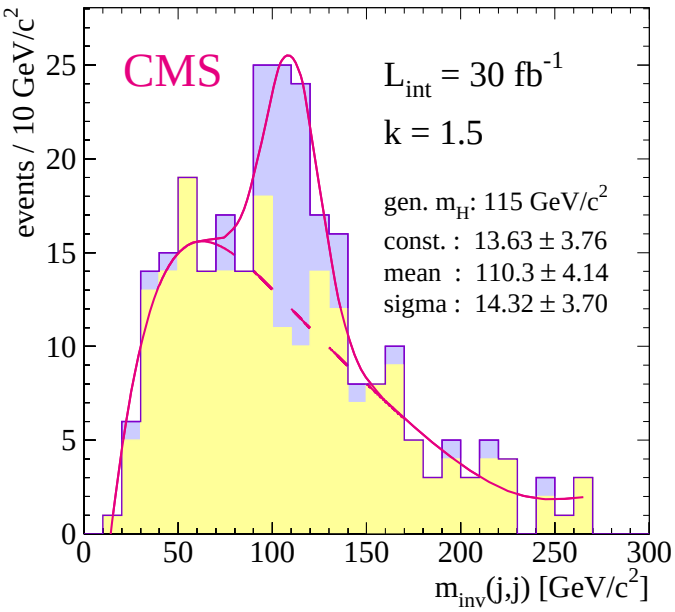

Figure 41: Invariant mass distribution, $m_{b\bar{b}}$, of signal (dark shaded, m_H =115 GeV/c^2) plus background for L_{int}=30 fb^{-1} (CMS experiment) [129].

and reconstructed above rather low backgrounds. The branching ratio is larger than for the $\gamma\gamma$ channel and increases with increasing m_H up to $m_H \sim 150$ GeV/c^2. For $m_H < 2 \cdot m_Z$, i.e. $H \rightarrow ZZ^* \rightarrow 4l$, the Higgs boson is narrow, hence a good mass resolution for electron and muon final states is essential. Both electrons and muons are considered in the final state, thus yielding $eeee$, $ee\mu\mu$ and $\mu\mu\mu\mu$ event topologies.
The background is composed of three components: ZZ^*/γ^* continuum, this process represents an irreducible background; $t\bar{t}$, this is a reducible background with the largest production cross section and $Zb\bar{b}$. The following kinematic selection cuts were designed to match the lepton triggers and to reject the $t\bar{t}$ and $Zb\bar{b}$ background:

a. Pseudo-rapidity cut for each lepton: $|\eta_l| < 2.5$.

b. Transverse momentum, p_T^l, for each lepton should be greater than 7 GeV, and at least two leptons should have p_T^l greater than 20 GeV.

c. The di-lepton invariant mass of one selected pair of leptons should be consistent with the Z^0 mass: $|M_{ll} - M_{Z^0}| < 6$ GeV. This cut rejects most of the non-resonant $t\bar{t}$ background.

d. The other pair of the leptons should have an invariant mass greater than 20 GeV. This cut considerably reduces both the contributions from cascade decays and the $Z\gamma^*$ background.

The detection efficiencies obtained from the full simulations and reconstructions for different Higgs masses ranges from 34% to 54% for masses between 130 GeV/c^2 and 180 GeV/c^2.
For the decay into four electrons inner bremsstrahlung degrades the response, yielding a mass resolution for $m_H = 130$ GeV/c^2 of 1.4 GeV [115] with 20% of the events in tails of the mass

distribution outside $\pm 2\sigma$. For the decay into four muons, the mass resolution using the muon system information alone gives 2 GeV, whereas a combination with the information from the inner tracker will give 1.4 GeV [130, 131].

The $H \rightarrow ZZ^* \rightarrow 4$ lepton channel allows a discovery of a Standard Model Higgs boson in the mass range from 130 to 180 GeV/c^2, already after a running period of 3 years at low luminosity, by combining the electron and muon signatures. The signal-to-background ratios are large and the reducible backgrounds can be kept at the level of 10-20% of the ZZ* continuum.

Figure 42 shows the invariant mass distribution of the four leptons for the process $H \rightarrow ZZ^* \rightarrow$ 4l. The peaks for m_H=130,150 and 170 GeV/c^2 are shown over the Standard Model background assuming an integrated luminosity of 100 fb^{-1} for the CMS experiment.

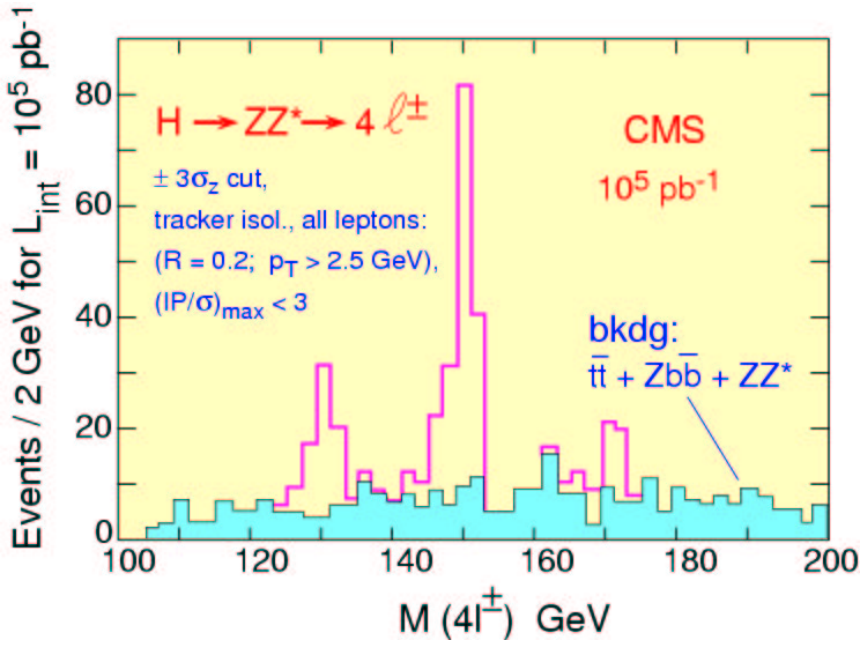

Figure 42: Invariant mass distribution of the four leptons for the process $H \rightarrow ZZ^* \rightarrow$ 4l. The peaks for m_H=130,150 and 170 GeV/c^2 are shown over the Standard Model background assuming an integrated luminosity of 100 fb^{-1} for the CMS experiment.

For Higgs boson masses larger than 180 GeV/c^2 the $H \rightarrow ZZ \rightarrow 4l$ signal would be observed easily above the $ZZ \rightarrow 4l$ continuum background after less than one year of low luminosity operation for $180 < m_H < 600$ GeV/c^2. For larger values of m_H, the Higgs boson signal becomes very broad and the signal rate drops rapidly, but a signal in the $H \rightarrow ZZ \rightarrow 4l$ channel could be observed up to $m_H \sim 800$ GeV/c^2, possibly even through the WW/ZZ fusion process if jet tagging in the forward regions is required.

5.2.4 $H \to WW^{(*)} \to l\nu l\nu$

This channel is extremely interesting near the $2m_W$ mass threshold, where the decay $H \to ZZ \to 4l$ is suppressed. By applying kinematical cuts on the outgoing leptons, based on different kinematics between the Higgs and the WW processes, one can observe a broad excess of events in the spectrum of the transverse dilepton mass, m_T, above the dominant WW background with S/B $\sim$1 [132], [133]. The background consists of the irreducible WW^* continuum

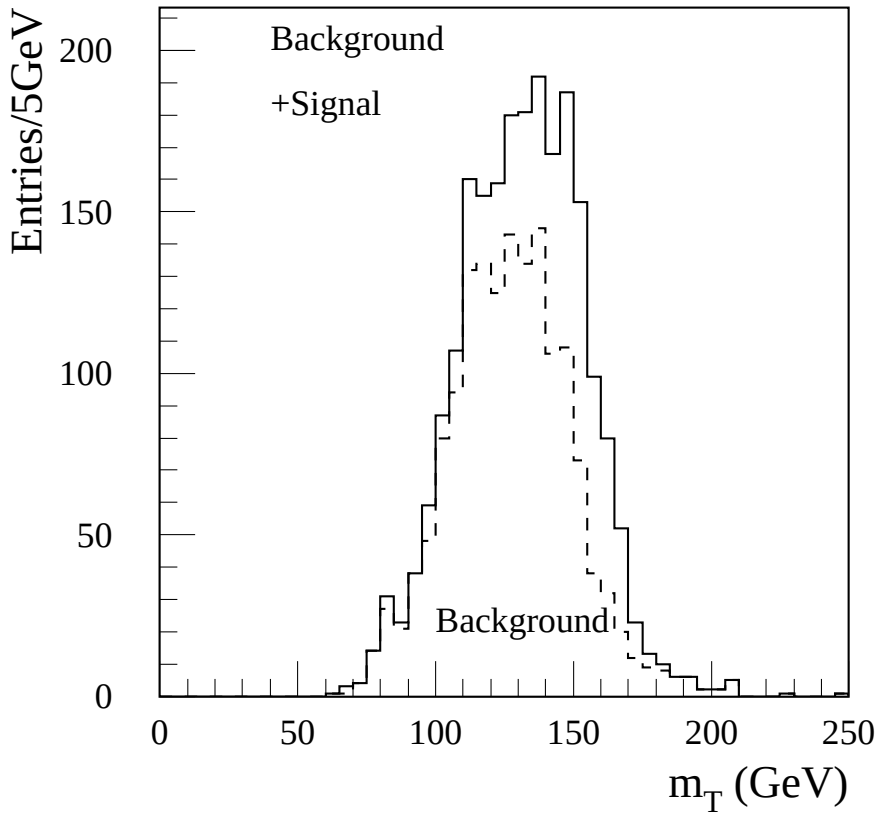

Figure 43: Transverse mass distribution for a Higgs signal ($M_H = 170$ GeV/c^2) in the $H \to WW^* \to l\nu l\nu$ channel (ATLAS experiment) and the total background. The distribution for the background alone is shown separately (dashed line).

production, where both W's decay leptonically, and of the following reducible contributions: (1) $t\bar{t}$ production, (2) Single top production Wt and (3) W+jet(s) production, with a leptonic W decay and a jet faking an electron. The distribution of the transverse mass is shown for all signal and background events passing the selection criteria in Figure 43 for a Higgs mass of 170 GeV/c^2. In order to evaluate the significance, it has been assumed that a normalization between the Monte Carlo prediction and the data can be performed outside the signal region and that the

$t\bar{t}$, the WW and the Wt backgrounds are known with a systematic uncertainty of $\pm 5\%$. Taking this into account the significance for the signal observation in the ATLAS experiment is found to be above 5 standard deviations in the mass region between 155 and 190 GeV/c^2 assuming an integrated luminosity of 30 fb^{-1}. The sensitivity to the Higgs mass is given by the upper falling edge of the distribution. It has been estimated that the Higgs mass can be determined with an accuracy of better than ± 5 GeV from this distribution. The CMS collaboration has done a study applying cuts based on the boost and the spin-correlation of the WW-system which enables the difficult separation from the irreducible continuum background production. A discovery for $155 < m_H < 180$ GeV/c^2 is possible for only 5 fb^{-1} [134].

5.2.5 WH with $H \to WW^{(*)} \to l\nu l\nu$ and $W \to l\nu$

The associated production of a Higgs boson with a W boson, with $W \to l\nu$ and $H \to WW* \to l\nu l\nu$ provides an additional discovery channel at the LHC [135]. The three-lepton final state appears as promising, since low background levels are expected. The two important backgrounds to this channel are: WZ production and $t\bar{t}$ production. The large reducible $t\bar{t}$ background can be suppressed by using high cuts on the lepton p_T in conjunction with jet veto cuts. At high luminosity a 5 σ discovery of a Standard Model Higgs boson in this channel will be possible in the mass range between $\sim 155 < m_H < 175$ GeV/c^2, assuming an integrated luminosity of 100 fb^{-1}. Similar to the $H \to WW^*$ channel the transverse mass spectrum provides some information on the Higgs boson mass.

5.2.6 Higgs Production via Weak Gauge Boson Fusion

The largest Higgs production cross-section is predicted for gluon-gluon fusion, but the second largest cross-section is predicted for weak gauge boson fusion, $q\bar{q} \to q\bar{q}VV \to q\bar{q}H(V = W, Z)$ (see Figure 38). With the Higgs boson decaying to $H \to W^{(*)}W^{(*)} \to e^{\pm}\mu^{\pm}p_T^{miss}$ a significant Higgs boson signal with an integrated luminosity of 5 fb^{-1} or less would be seen in the mass range of 130–200 GeV/c^2. The additional very energetic forward jets in these events can be exploited to significantly reduce the backgrounds. Another feature is the lack of color exchange between the initial-state quark in contrast to most background processes. This channel has been first proposed by Rainwater and Zeppenfeld [136]. This channel is also interesting for a measurement of the $t\bar{t}H/WWH$ coupling ratio. The dominant backgrounds are the production of W pairs, $t\bar{t}$ and $Z \to \tau\tau$ in association with jets. First studies by ATLAS and CMS including a detector simulation have been performed and are promising. Recently this channel has been investigated as discovery mode for a light Higgs boson with a mass of around 115 GeV/c^2 [137]. The signal to background ratio is better than 1:1 and allows a 5σ signal with 35 fb^{-1} of data.
Besides the decay channel described above decays of the Higgs boson to $\tau^+\tau^-$ pairs or $H \to \gamma\gamma$ are investigated. Both decay channels allow a 5 σ discovery in the mass range of 110–150 GeV/c^2 [138–140].

5.2.7 Heavy Higgs Boson

For Higgs masses in the range $180 < m_H < 700$ GeV/c^2, the $H \to ZZ \to l^+l^-l^+l^-$ decay mode is the most reliable channel for the discovery of a Standard Model Higgs at LHC. The mo-

menta of the final state leptons are high and their measurement does not put severe requirements on the detector performance. Therefore, the Higgs discovery potential in this channel is primarily determined by the available luminosity. The $H \rightarrow ZZ \rightarrow 4l$ becomes nevertheless rate limited around $m_H \sim 700$ GeV/c^2. To access Higgs masses up to the TeV mass range one needs also to allow hadronic or neutrino final states. The channels available are $H \rightarrow ZZ \rightarrow llν\nu$, with a rate six times larger than the 4-lepton mode, and with a large missing E_T signature and the $H \rightarrow WW \rightarrow l\nu jj$ mode, with a rate 150 times larger than the the sum of the 4-lepton mode and the $H \rightarrow ZZ \rightarrow llν\nu$ mode. The $WW \rightarrow l\nu jj$ mode provides a discovery potential from 600 to 1000 GeV/c^2, and a sensitivity to masses down to 300 GeV/c^2. This mode is complemented by the $ZZ \rightarrow llν\nu$ mode in the mass range from 500-700 GeV/c^2, thus giving redundancy and robustness to the search in that mass region, and allowing to compare H to WW and H to ZZ couplings.

5.2.8 Overall Sensitivity to the Standard Model Higgs Searches

The overall sensitivity for the discovery of a Standard Model Higgs boson over the relevant mass range from 80 GeV/c^2 to 1 TeV/c^2 is shown in Figure 44. The sensitivity is given in terms of $S/\sqrt{B}$ for the individual channels as well as for the combination of the various channels assuming an integrated luminosity of 30 fb^{-1}. A Standard Model Higgs boson can be discovered in the ATLAS experiment over the full mass range up to ∼1 TeV/c^2 with a high significance. A discovery sensitivity of 5σ can already be reached over the full mass range after a few years of running at low luminosity [115]. No K-factors have been included in the evaluation of the signal significance. This is a conservative assumption, provided the K-factor for the signal process of interest is larger than the square root of the K-factor for the corresponding background process.
Most of the decay channels studied in the mass range below 200 GeV/c^2 are challenging in terms of detector performance. Even though the natural width of the Standard Model Higgs boson in this mass range is narrow, the backgrounds are relatively large and thus, an excellent detector performance in terms of energy resolution and background rejection is required. The $H \rightarrow \gamma\gamma$ decay mode requires high performance of the electromagnetic calorimetry in terms of photon energy resolution, photon direction measurements, and γ/jet separation. Impact parameter measurements in the inner detector are crucial for the discovery of the $b\bar{b}$ decay mode: efficient tagging of b-jets with a high rejection against light quark and gluon jets allows a rather clean and complete reconstruction of $t\bar{t}$ final states together with the $b\bar{b}$ mass peak from Higgs boson decays. Finally, excellent performance in terms of the identification, reconstruction and measurement of isolated leptons with $p_T > 7$ GeV is required to discover the Higgs boson in the $H \rightarrow ZZ^* \rightarrow 4l$ channel. For $m_H > 2m_Z$, the dominant discovery channel is the four-lepton channel. In this case the background is small and dominated by irreducible ZZ continuum production. For $m_H > 300$ GeV/c^2 the requirements on the detector performance are rather modest in this channel, since the Higgs width is larger than the detector resolution. A high-significance discovery of the Higgs boson can be achieved for Higgs boson masses up to 600 GeV/c^2 over less than one year of data-taking at low luminosity.
By combining the two experiments ATLAS and CMS the minimum luminosity required to start seeing a 115 GeV/c^2 Higgs boson at 5 σ is $\sim$ 10 fb^{-1} (see Figure 45), which may be achieved after two years of LHC running. Since at most a few weeks of very low luminosity collisions can

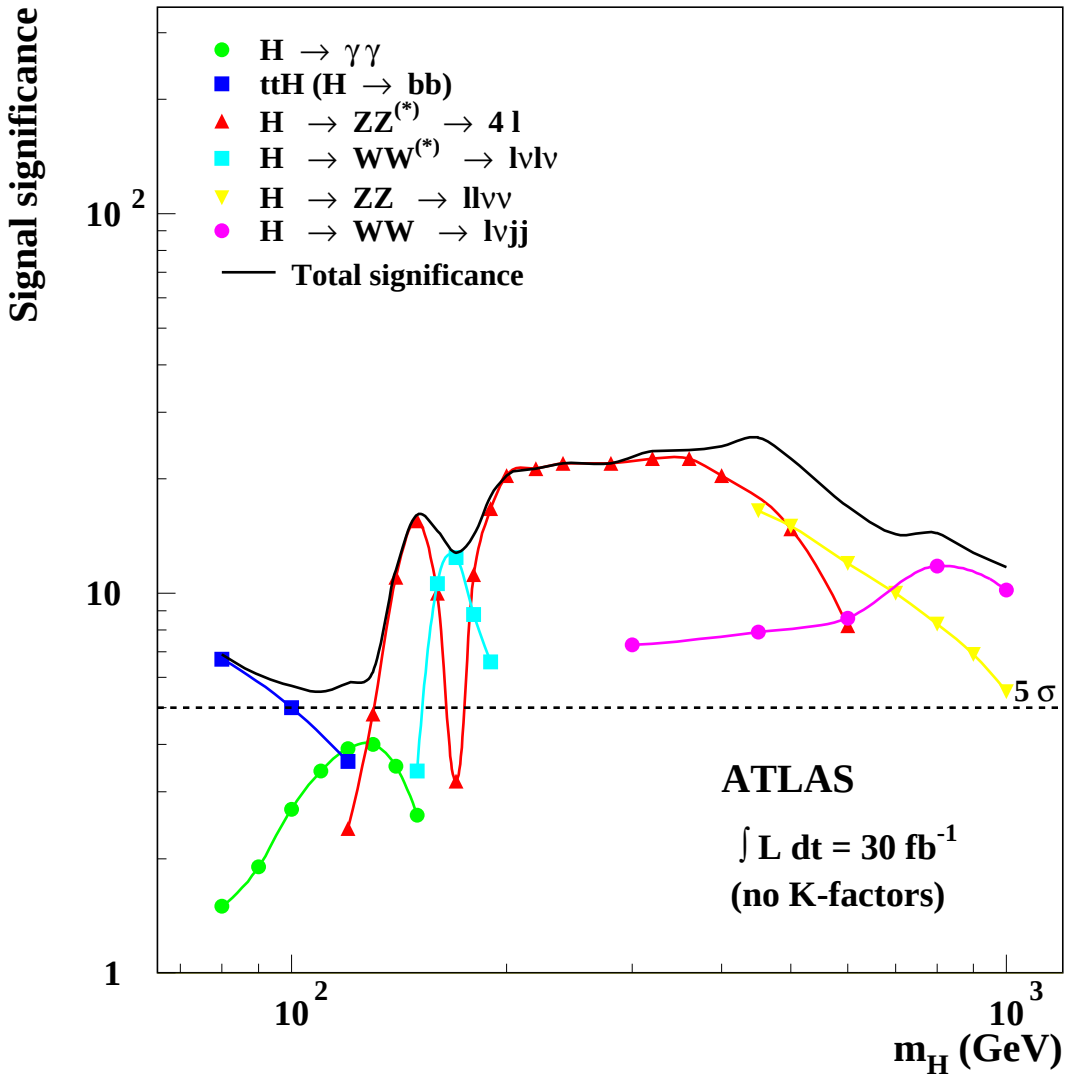

Figure 44: Sensitivity for the discovery of a Standard Model Higgs boson. The sensitivity in terms of $S/\sqrt{B}$ is plotted for individual channels and for a combination as a function of the Higgs mass assuming an integrated luminosity of 30 fb^{-1} at the ATLAS experiment.

be envisaged in 2005, and only 1 or 2 fb^{-1} is anticipated in 2006, this presumably means that the LHC could hope to discover a 115 GeV/c^2 Higgs boson after the 2007 run. For higher masses, i.e. for $130 < m_H < 500$ GeV/c^2, the discovery is expected to be much faster (a few months of data-taking) thanks to the gold-plated and background-free $H \to ZZ^{(*)} \to 4l$ channel.

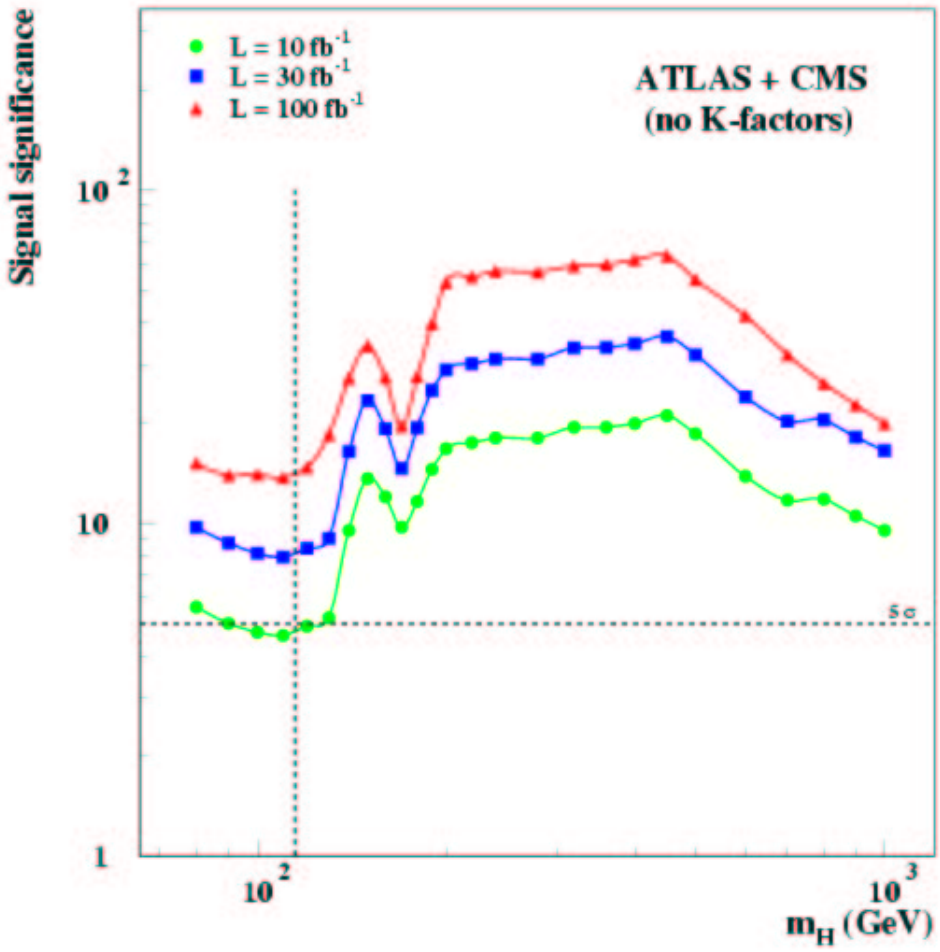

Figure 45: The combined sensitivity of the two LHC experiments ATLAS and CMS to a Standard Model Higgs boson, as a function of its mass, for different accumulated luminosities.

5.3 Determination of the Standard Model Higgs Boson Parameters

The determination of the Higgs boson parameters is a major goal once the Higgs boson will have been discovered. Precision measurements of these parameters allow a deeper understanding of the electroweak symmetry-breaking mechanism. They may also be useful to distinguish a Standard Model Higgs boson from a MSSM Higgs boson. The ATLAS experiment provides excellent tools to measure precisely the Higgs boson parameters like mass, production rates, couplings to bosons and fermions and the total width. A detailed description can be found in Ref. [141].

In most of the channels the Higgs boson appears as a resonant peak above the background ($H \to \gamma\gamma$, $H \to ZZ \to 4l$), thus the background can be subtracted using control regions outside the resonance. The error on the mass reconstruction includes the statistical error due to the limited number of signal events and the error of the subtraction of the background. The uncertainty on the absolute energy scale introduces a systematic error, which is assumed to be 0.1% for photons and leptons and 1% for each jet. This is a conservative estimate since the ATLAS goal is to determine the absolute energy scale for photons and leptons with a precision of 0.02%.

In the channel $H \to \gamma\gamma$ the fractional error is found to be 0.2-0.3% for 300 fb^{-1} - this corresponds to about ten years of operation at the LHC - in the mass range of 110 to 150 GeV/c^2. The channel $H \to ZZ \to 4l$ offers the best possibility of determining the mass of the Higgs boson. An accuracy of 0.1% is achievable over the whole mass range of 120 to 400 GeV/c^2 and an integrated luminosity of $\int \mathcal{L}dt = 300\text{fb}^{-1}$. For larger masses the precision deteriorates because the Higgs width becomes large and therefore the statistical error increases. However, even for masses as large as 700 GeV/c^2 the Higgs mass can be measured with an accuracy of 1%.

Figure 46 shows the fractional errors in the channels considered for an integrated luminosity of $\int \mathcal{L}dt = 300$ fb^{-1}. For the combination of the channels an energy scale uncertainty of $\pm 0.1\%$ is assumed. The goal is to reach an energy scale uncertainty of $\pm 0.02\%$ by determining the scale from $Z \to ll$.

The determination of the rates in the various production and decay channels allows to set constraints on the couplings and the branching ratios. Using the $H \to ZZ \to 4l$ channel a differentiation between Standard Model and MSSM may be feasible, since this channel is suppressed in the MSSM. Furthermore the Higgs width differs from Standard Model to MSSM and thus can also be used for the distinction.

The statistical error on the rate is expected to be smaller than 10% over the mass region 120 to 600 GeV/c^2 using the $\gamma\gamma$, $b\bar{b}$ and 4 lepton final states. The main systematic error comes from the knowledge of the luminosity, a value of 5% has been considered for the luminosity uncertainty. An additional systematic error of 10% for the $H \to b\bar{b}$ and 5% for the $H \to WW$ has been included to take into account the uncertainty on the background subtraction for channels where the background is not completely flat under the peak. Figure 47 shows the expected experimental uncertainty on the Higgs boson rates, for various production and decay channels. The left part displays the results from direct production. Over the mass region 120 to 600 GeV/c^2, the Higgs boson production rate can be measured with a precision of 7%. The right part gives the results from associated production. Over the mass range of 100 to 200 GeV/c^2 the expected precision is between 6 and 30%. An integrated luminosity of $\int \mathcal{L}dt = 300\text{fb}^{-1}$ per experiment (ATLAS+CMS) is assumed.

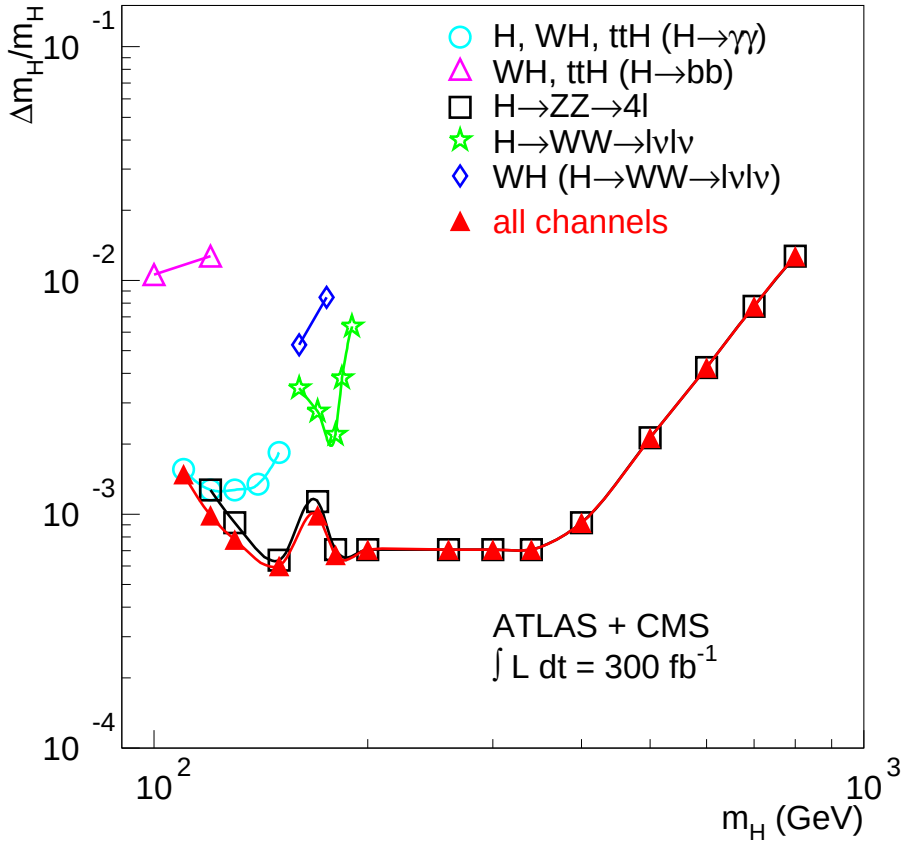

Figure 46: Relative precision $\Delta M_H/M_H$ of the Higgs mass reconstruction assuming an integrated luminosity of $\int \mathcal{L}dt = 300\text{fb}^{-1}$ per experiment (ATLAS+CMS). The open symbols correspond to the different channels. The combination of all channels with an uncertainty of 0.1% on the energy scale is represented by the dark triangles.

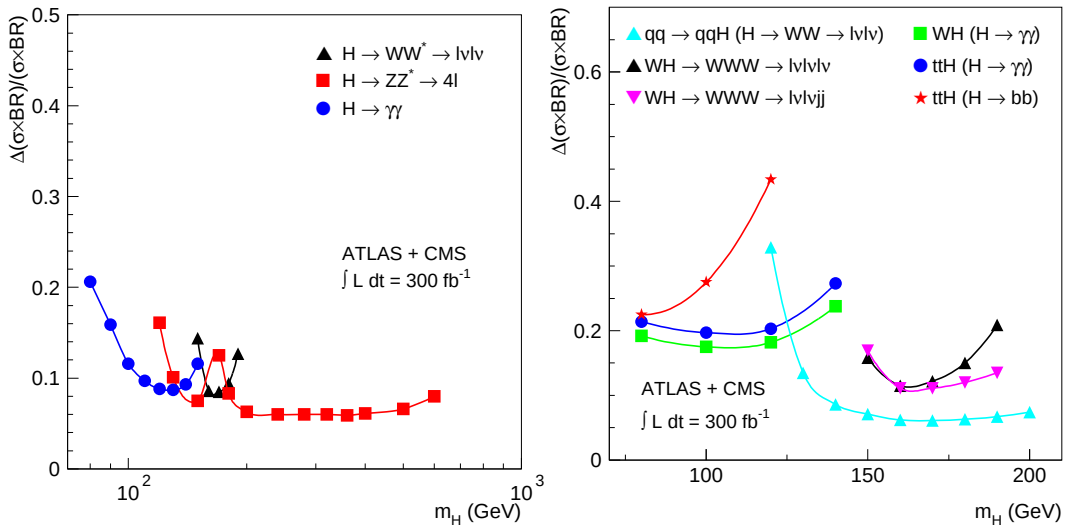

Figure 47: Relative precision on the measurement of the Higgs boson rate ($\sigma \times$BR for various channels, as a function of m_H, assuming an integrated luminosity of 300 fb^{-1}. The left figure shows predictions using direct production, the right figure shows the predictions using associated production.

Without any theoretical input only a measurement of coupling ratios will be possible at LHC. From the direct measurement of $\sigma \times BR(H \rightarrow WW^*)$ and $\sigma \times BR(H \rightarrow ZZ^*)$. The ratio of the HWW coupling to the HZZ coupling, g_{HWW}/g_{HZZ}, can be measured with an accuracy of 10–15%. In both channels the same production processes are involved. As long as exclusive couplings can be considered , the QCD corrections cancel. Besides the direct measurement in the mass range 150$<$ m_H $<$180 GeV/c^2 also an indirect determination is feasible in the mass range m_H $<$150 GeV/c^2 by using the $H \rightarrow \gamma\gamma$ and $H \rightarrow ZZ^* \rightarrow$4l channels. The Higgs boson decay into two photons proceeds via a diagram, where the loop is dominated by a WW pair. The indirect measurement allows to measure g_{HWW}/g_{HZZ} with an accuracy of 10–20% including an theoretical uncertainty of 10% because of higher order corrections. For both measurements an integrated luminosity of 300 fb^{-1} per experiment is assumed. Measurements of the boson/fermion couplings are affected by more theoretical constraints and the measurement is restricted at LHC. $g_{HWW}/g_{Ht\bar{t}}$, $g_{HWW}/g_{H\tau\tau}$, $g_{HWW}/g_{Hb\bar{b}}$ can be measured with an error of 15–30%. At a future e^+e^- collider it will be possible to measure the ratio of fermion/boson couplings with higher precision and to measure the ratio of fermion/fermion couplings [142].

The width of the Higgs, can be measured directly above the ZZ decay threshold where the width grows rapidly. ATLAS and CMS will be able to measure the Higgs width with a precision of 5 to 6% over the mass range 300-700 GeV/c^2. The systematical error is dominated by the uncertainty of radiative decays, assumed to be 1.5%. Below 300 GeV/c^2 the instrumental resolution is larger than the Higgs width Γ_H.

To determine the width of the Higgs boson for masses less than 300 GeV/c^2, an indirect method, which is proposed in [143], can be used. From rates of $qq \rightarrow qqH$ with $H \rightarrow \gamma\gamma, \tau\tau, WW$

decays assuming a branching ratio of less than 10% for $H \to c\bar{c}$ and non-standard decays a measurement of the Higgs width in the mass range of 120 to 150 GeV/c^2 is possible with an expected precision of 6 to 20%. Figure 48 shows the relative precision $\Delta\Gamma_H/\Gamma_H$ of the Higgs

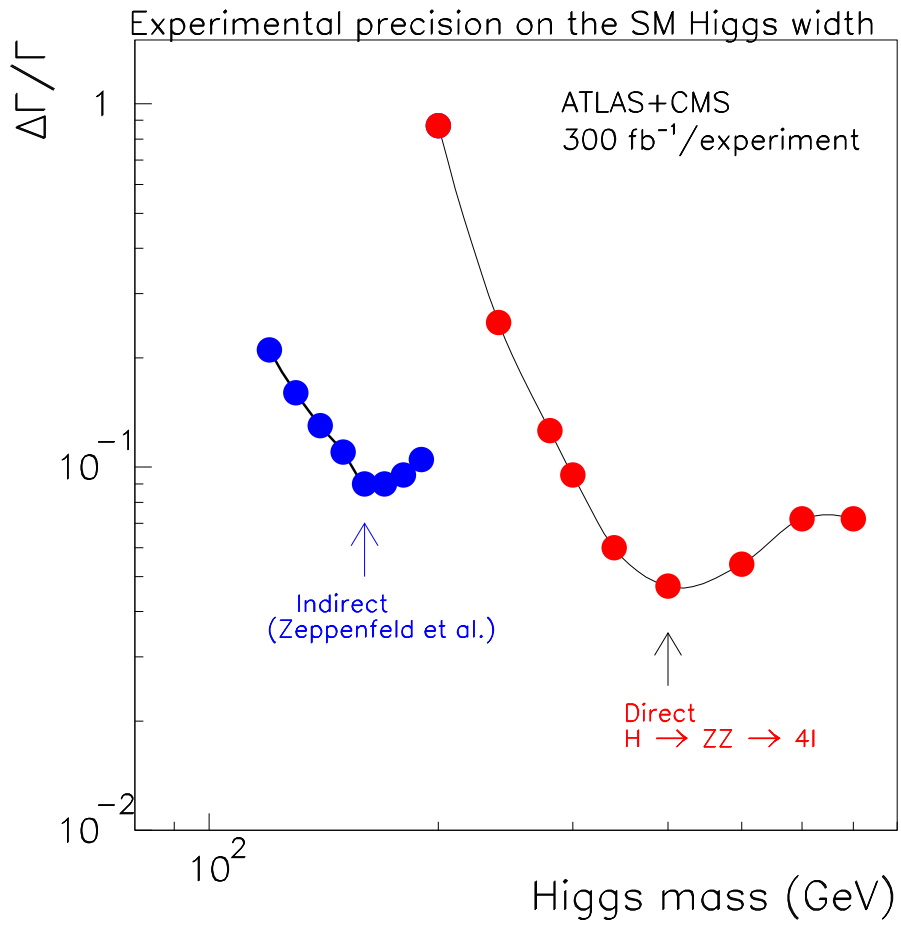

Figure 48: Relative precision $\Delta\Gamma_H/\Gamma_H$ of the Higgs width Γ_H reconstruction assuming an integrated luminosity of $\int \mathcal{L}dt = 300\text{fb}^{-1}$. The open channels correspond to the different channels.

width reconstruction assuming an integrated luminosity of $\int \mathcal{L}dt = 300\text{fb}^{-1}$.

The Higgs production rate can be measured with a precision of 12% (respectively 7%) if the luminosity is known to 10% (respectively 5%). Several couplings and branching ratios can be measured with precisions of the order of 25%

First studies have been performed to determine the spin of the Higgs boson [141]. A direct measurement of the Higgs boson spin through the measurement of the angular distributions between the decay planes of the two Z bosons coming from the $H \to ZZ^* \to 4\text{l}$ channel will be possible [144].

5.4 Minimal Supersymmetric Standard Model Higgs

There are strong theoretical arguments suggesting that the theory of elementary particles should obey supersymmetry. The most interesting choice for the SUSY model is the one with a minimum number of Higgs fields, the Minimal Supersymmetric Standard Model, MSSM [21]. Extensive simulation work has been done to study the possibilities to search for the MSSM Higgs bosons with the ATLAS detector [115]. The Higgs sector in the MSSM contains two CP-even (h,H), one CP-odd (A) neutral states and one charged ($H^{\pm}$) state.
At tree level there are two free parameters determining their masses and couplings. Usually m_A and the ratio of the expectation values of the Higgs doublets, $\tan\beta$, are chosen. The investigation of the Higgs sector of the MSSM is complex and one has to deal with a rich spectrum of possible signals. For the benchmark sets of MSSM parameters [145], where M_{SUSY} is fixed to 1 TeV, an extreme configuration of stop mixing parameters ($A-t, \mu$) has been chosen, the so-called minimal mixing scenario ($A_t, \mu \ll M_{SUSY}$). This scenario corresponds to the most pessimistic discovery scenario at the LHC, since these choices for the additional MSSM parameters give the lowest possible upper limit for m_h. This reduces the LHC potential for h-boson discovery in the $h \to \gamma\gamma$ channel, and also suppresses the $H \to ZZ^{(*)} \to 4l$ channel.
The interest is focussed on the potential of various decay modes accessible also to the Standard Model Higgs: $h \to \gamma\gamma$, $h \to b\bar{b}$, $H \to ZZ \to l^+l^-l^+l^-$, and on modes strongly enhanced at large $\tan\beta$: $H/A \to \tau^+\tau^-$, $H/A \to \mu^+\mu^-$. Much attention is given also to other potentially interesting channels such as $H/A \to t\bar{t}$, $A \to Zh$, $H \to hh$.

5.4.1 Overlap with Standard Model Searches

As an example for an MSSM decay channel we discuss the $h \to b\bar{b}$ channel. In the MSSM case the rates can be enhanced by 10-20% compared to the Standard Model rates [146]. The sensitivity region in the MSSM plane has been determined from the numbers obtained for the Standard Model analysis, after accounting for the different production and decay rates. The 5 σ discovery contours in the ($m_A, \tan\beta$) plane are shown in Figure 49. For an integrated luminosity of 30 fb^{-1}, the h boson could be discovered in this channel for $m_A > 150$ GeV/c^2 and $\tan\beta < 4$. For integrated luminosities above 100 fb^{-1}, the observability of the h boson in this channel extends to 90% of the ($m_A, \tan\beta$) plane. For completeness, Figure 49 shows also the 5 σ discovery contour curve for the Wh, $h \to b\bar{b}$ channel for an integrated luminosity of 30 fb^{-1}.
The expected MSSM rates for $h \to \gamma\gamma$ and $H \to \gamma\gamma$ are generally suppressed with respect to the Standard Model case. In order to evaluate the overall sensitivity to $\gamma\gamma$ decays of the MSSM Higgs bosons, the results of the Standard Model searches have been used. A combined 5 σ discovery is possible for all values of $\tan\beta$ provided m_A is larger than 180 GeV/c^2 (260 GeV/c^2), for an integrated luminosity of 300 fb^{-1} (100 fb^{-1}). The heavy Higgs boson decay, $H \to \gamma\gamma$, would be observable only as narrow strip for low m_A value ($m_A = 70 - 80$ GeV/c^2) corresponding to $m_H = 110 - 120$ GeV/c^2. This range of m_A is already excluded by searches at LEP [49].
As in the $h \to \gamma\gamma$ and $h \to b\bar{b}$ channels, the observability of the $H \to ZZ^{(*)} \to 4l$ channel in the MSSM is estimated by extrapolating the detailed studies performed in the Standard Model case. In the MSSM, the rates of $H \to ZZ^{(*)} \to 4l$ are strongly suppressed with respect to the

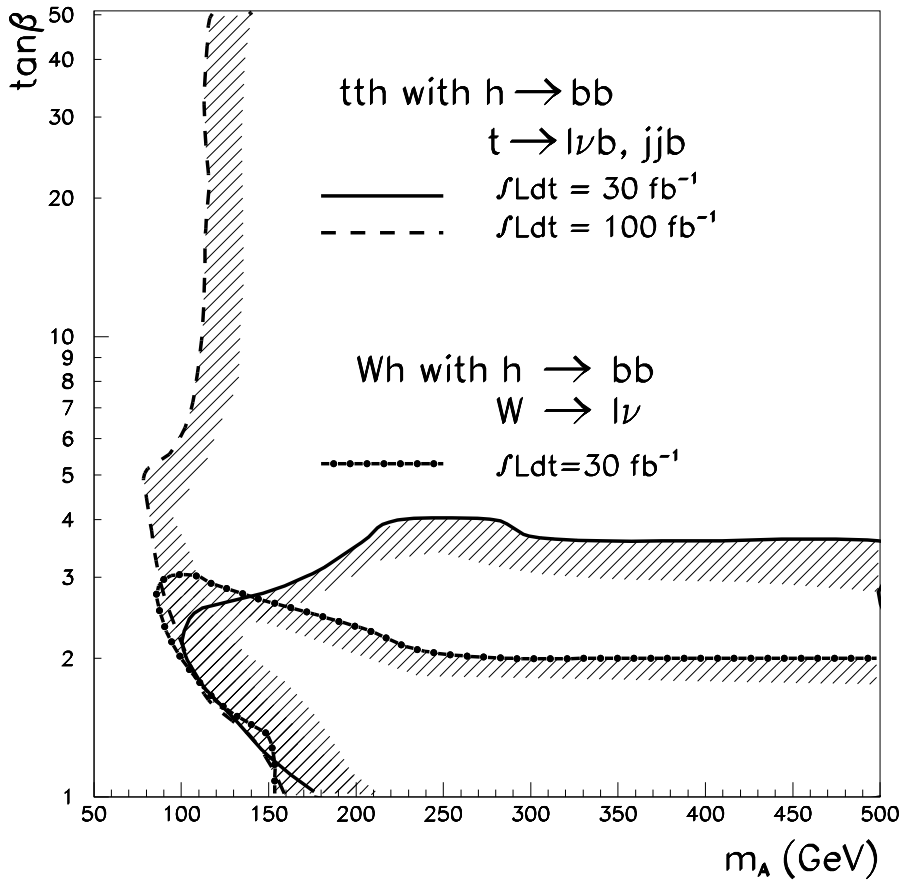

Figure 49: 5 σ discovery contour curves for the $t\bar{t}h$ and Wh with $h \to b\bar{b}$ channel in the $(m_A, \tan\beta)$ plane for integrated luminosities of 30 fb^{-1} and 100 fb^{-1}.

Standard Model case over the full $\tan\beta$ range, except for values of $\tan\beta$ smaller than one. This is due to the suppression of the HZZ coupling, to the opening of the $H \to hh$ decay channel, and to the enhancement of the $H \to t\bar{t}$ channel. These characteristics of the Higgs boson in the MSSM case limit the observability in this channel to the range $2m_H < m_H < 2m_t$ and to low values of $\tan\beta$.

5.4.2 New Decay Channels

Despite rather optimistic recent theoretical estimates [138], the $H \to \tau\tau$ decay mode is not expected to be observable at the LHC in the Standard Model case, because the expected signal rates are too low compared to the large backgrounds from various Standard Model processes. However, in the MSSM case, the $H \to \tau\tau$ and $A \to \tau\tau$ rates are strongly enhanced over a large region of the parameter space. For low values of $\tan\beta$, the $gg \to A$, $A \to \tau\tau$ rates are dominant and significantly larger than in the Standard Model case for a Higgs boson of the same mass. For large values of $\tan\beta$, the production is dominated by the strongly enhanced associated $b\bar{b}H$ and $b\bar{b}A$ production and the $H/A \to \tau\tau$ ratio is about 10% in the mass range 200–500 GeV/c^2. The relative contribution from the associated production is roughly 50% for $\tan\beta = 5$ and about 90% for $\tan\beta = 20$. The backgrounds are a mixture of irreducible $Z \to \tau\tau$ background and of $t\bar{t}$, $b\bar{b}$ and $W + jet$ production, where a jet is misidentified as a τ lepton. The signal significances combined for the direct and the associated production for an integrated luminosity of 30 fb^{-1} and for $\tan\beta = 10$ are 5.7 σ for m_A=150 GeV/c^2 and 1.2 σ for m_A=300 GeV/c^2. The inclusion of the direct production increases the signal significance by 10%.

The $H/A \to \mu\mu$ decay channel cannot be observed for a Standard Model Higgs boson because of both the very small signal rate and the large backgrounds from several Standard Model processes. However, because of the large enhancement of rates through $b\bar{b}H$ and $b\bar{b}A$ production and of some enhancement of the branching ratio, which both present at large $\tan\beta$, it can be observed in the MSSM case. The rates for this channel are governed by the same couplings as for the $\tau\tau$ channel, but the branching ratio scales as $(m_\mu/m_\tau)^2$. This huge reduction in signal rates with respect to the $\tau\tau$ channel is compensated to some extent by the much better identification efficiency and experimental resolution, which can be achieved in the $\mu\mu$ channel. The background in this channel is dominated by irreducible $Z/\gamma^* \to \mu\mu$ Drell-Yan production and reducible $t\bar{t}$ production with both top-quarks decaying into muons, $t \to \mu\nu b$. The signal will be observed above the background as a narrow peak in the invariant di-muon mass distribution, $M_{\mu\mu}$ [147].

Due to the strong coupling of the Standard Model Higgs boson to gauge boson pairs, the $H \to t\bar{t}$ branching ratio is too small for this channel to be observable in the Standard Model case. In the MSSM case, however, the $H \to t\bar{t}$ and $A \to t\bar{t}$ branching ratios are close to 100% for $m_H, m_A > 2m_t$ and for $\tan\beta \sim 1$. As discussed in [148, 149], a signal from $H/A \to t\bar{t}$ would appear as a peak in the $t\bar{t}$ invariant mass spectrum above the $t\bar{t}$ continuum background for values of m_H smaller than 500 GeV/c^2. For $m_H \geq$500 GeV/c^2 the total cross section differs very little from the cross section with no Higgs boson present. The signal is extracted by searching for $WWb\bar{b}$ final states, with one $W \to l\nu$ and one $W \to jj$ decay. The signal significance varies between 8.2 and 4.3 over the mass range from 370 to 450 GeV/c^2 for an integrated luminosity of 30 fb^{-1} and $\tan\beta = 1.5$.

The charged Higgs bosons have masses which are almost degenerate with the masses of the H and A bosons. Several mechanisms can be potential sources for production:

- If the charged Higgs boson is lighter than the top quark decays represent a copious source of charged Higgs boson production, via the channel $t \rightarrow H^+b$. Since top quarks are produced with very large rates at LHC, $\sigma_{t\bar{t}} \sim 600$ pb a charged Higgs boson can be searched for in this channel for masses up to the kinematic limit imposed by the top quark mass.

- If the charged Higgs boson is heavier than the top quark, it can be produced via the gb and gg fusion processes, $pp \rightarrow tH^{\pm}$ and $pp \rightarrow tbH^{\pm}$ respectively, in which the Higgs boson is emitted from the heavy quark.

The main decay channels of the charged Higgs bosons are the fermionic decays $H^{\pm} \rightarrow \tau\nu$ below the tb threshold and $H^{\pm} \rightarrow tb$ above.

5.4.3 Overall Sensitivity

The 5σ discovery contour as determined for the various channels in the (m_A,$\tan\beta$) plane are superimposed in Figure 50 for an integrated luminosity of 10 fb^{-1} and in Figure 51 for an integrated luminosity of 30 fb^{-1} per experiment (ATLAS+CMS). From Figure 50 it can be seen that a large part of the (m_A,$\tan\beta$) plane can be explored in the year 2007. The region between $3 \lesssim \tan\beta \lesssim 10$ and $100 \lesssim m_A \lesssim 250$ GeV/c^2 can not be covered with 10 fb^{-1} integrated luminosity. For a region $3 \lesssim \tan\beta \lesssim 15$ and $m_A \gtrsim 100$ GeV/c^2 only the lightest Higgs boson h is accessible. The figure also displays the LEP limit [49] which excludes the region below $\tan\beta < 2.4$ and $m_A \approx 93 GeV/c^2$. The details of the contour curves can be affected by changes in some of the parameters in the MSSM model. These studies have selected sets of parameters, for which SUSY particle masses are large, so that Higgs-boson decay to SUSY particles are kinematically forbidden.
With a modest integrated luminosity of 30 fb^{-1}, the ATLAS discovery potential covers a large fraction of the parameter space. In most of the parameter space more than one Higgs boson would be discovered thus allowing a clean distinction between the Standard Model and the MSSM case. At the very high integrated luminosity of 300 fb^{-1}, the ATLAS discovery potential covers the whole parameter space. The overall discovery potential in the ($m_A, \tan\beta$) plane relies heavily on the $H/A \rightarrow \tau\tau$ channel and on the $t\bar{t}h$ with $h \rightarrow b\bar{b}$ and on the $h \rightarrow \gamma\gamma$ channels. From Figure 52 it can be seen that over a large range of the parameter space more than one Higgs boson is observable and the experiment would be able to distinguish between Standard Model and MSSM. In this Figure an integrated luminosity of 300 fb^{-1} for the ATLAS experiment is assumed. At small $\tan\beta$ a large number of channels are accessible allowing a measurement of many couplings including Hhh and AZh. For almost all cases, the experiment would be able to distinguish between the Standard Model and the MSSM case. The region with $m_A > 250$ GeV/c^2 and $4 < \tan\beta < 5 - 10$ is only covered by the $h \rightarrow \gamma\gamma$ and $h \rightarrow b\bar{b}$ channels thus making the distinction very difficult. Over large regions for $m_A > 160$ GeV/c^2, all three neutral Higgs bosons, and in some cases also the charged Higgs boson would be discovered with ATLAS. Over most of this region, the H and A bosons are degenerate in mass and would

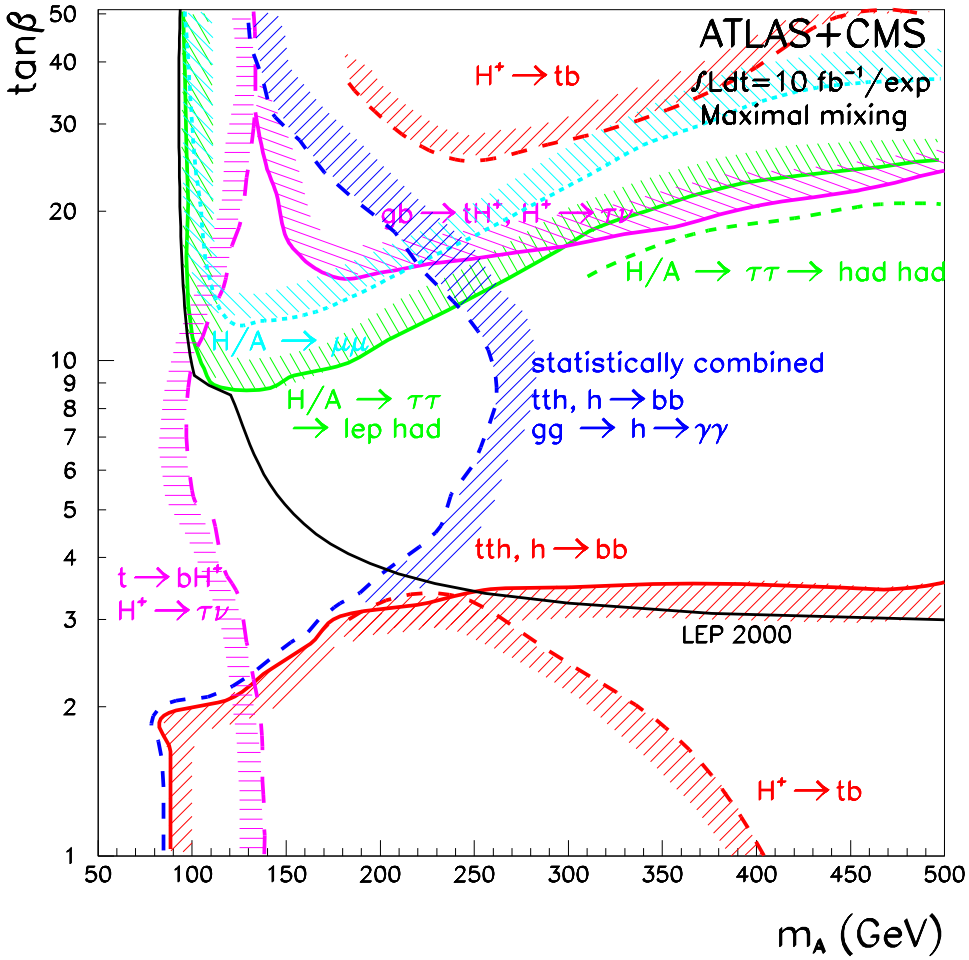

Figure 50: For an integrated luminosity of 10 fb^{-1} per experiment (ATLAS+CMS), 5σ discovery contour curves in the (m_A, $\tan\beta$) plane for all Higgs boson signals are shown.

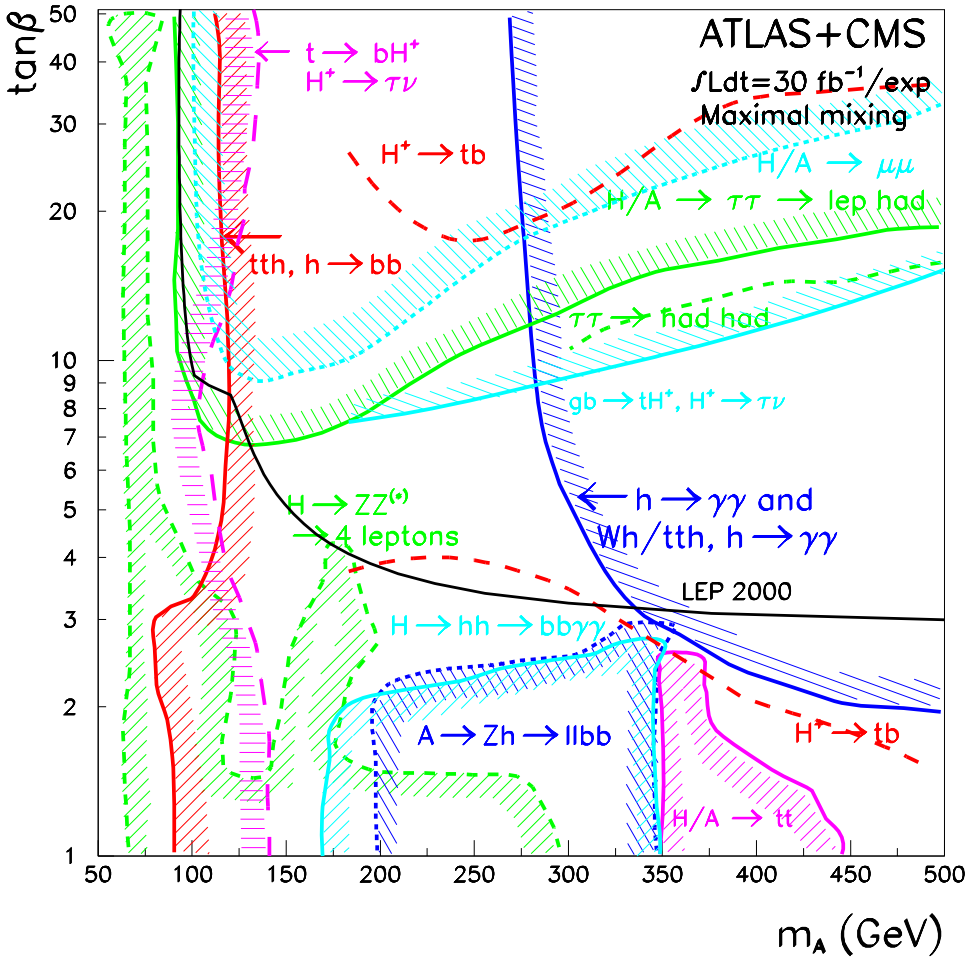

Figure 51: For an integrated luminosity of 30 fb^{-1} per experiment (ATLAS+CMS), 5σ discovery contour curves in the $(m_A, \tan\beta)$ plane for all Higgs boson signals are shown.

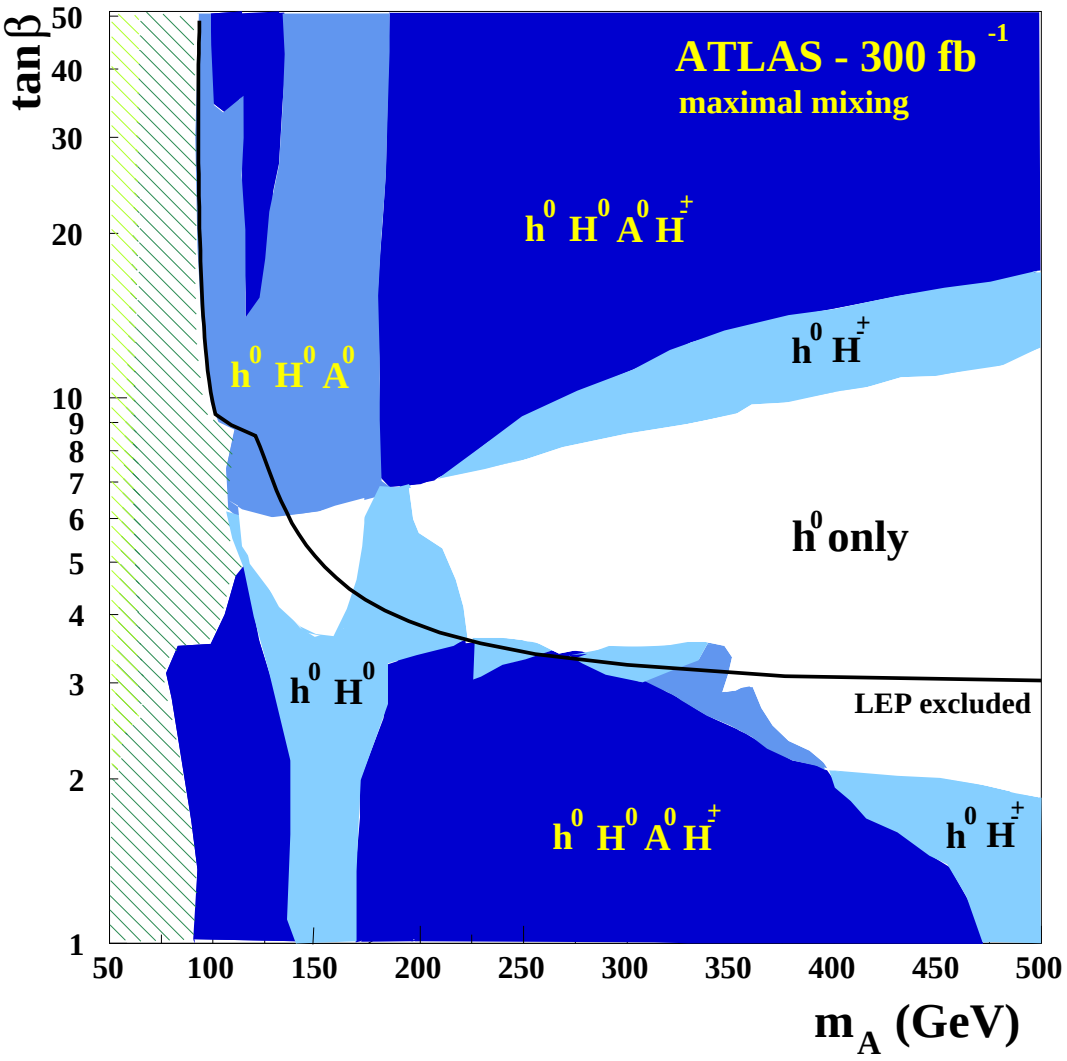

Figure 52: Number of Higgs bosons of the MSSM in the plane of $\tan\beta$ versus m_A (maximal scalar top mixing) observable at the LHC with 300 fb^{-1} of integrated luminosity with ATLAS.

be very difficult to distinguish. For $\sim$ 10% of the parameter space, i.e. for $\tan\beta$ >2 and 90 GeV/c^2 < m_A < 130 GeV/c^2, the two neutral Higgs bosons and the charged Higgs boson would be discovered with ATLAS.
The interplay between SUSY particles and the Higgs sector has also been addressed in the ATLAS studies. SUSY scenarios have an impact on the discovery potential through the opening of Higgs boson decays to SUSY particles (mostly for H and A) and through the presence of SUSY particles in loops.

5.5 Determination of the MSSM Higgs Parameters

The theoretical motivation for precision measurements in the MSSM is even stronger than in the Standard Model. In the MSSM, the Higgs sector constrains strongly the predicted relations between Higgs boson masses, $\tan\beta$ and other parameters of SUSY models. If no SUSY particles are found, measurements of the Higgs boson parameters should allow in some cases to distinguish between the Standard Model and the MSSM models and to check the consistency with the relations between Higgs boson masses predicted by the model. If, for example, the signal were to be observed in the $H \rightarrow ZZ^{(*)} \rightarrow 4l$ channel, the measured signal rate would provide the best tool to understand its origin, since the MSSM rates are suppressed by an order of magnitude with respect to the Standard Model case over most of the parameter space. The Higgs boson couplings will be measured, but most likely with an accuracy not better than 10-20%, since in most cases these measurements will be based on signal rates.
The expected precisions on the masses of the MSSM Higgs bosons over the complete set of possible discovery channels and over the full parameter space for an integrated luminosity of 300 fb^{-1} are in the range of 0.1 to 3%. The h Boson mass can be measured with an accuracy of 0.1 to 0.5% if the $h \rightarrow \gamma\gamma$ channel is accessible. Over the region where only the $h \rightarrow b\bar{b}$ is observable the expected precision is 1 to 3%. For the inclusive H or A to $\gamma\gamma$ channel a measurement with a precision of 0.1 to 0.5% is possible. For other H or A decay channels like the $\mu^+\mu^-$ or 4 lepton decay the precision is 0.1 to 2%.
The strong $\tan\beta$ dependence of the $gg \rightarrow H, A$ discovery modes will provide an opportunity to determine the $\tan\beta$ parameter. The method proposed in [150] was followed for the evaluation of $\sigma \times$BR. The systematic error is dominated by the luminosity and is taken conservatively to be 10%. The expected precision depends on the decay channel and ranges from 10 to 25% in the $H \rightarrow ZZ^{(*)} \rightarrow 4$ lepton channel to 10 to 15% in the $\mu^+\mu^-$ and $\tau^+\tau^-$ channels.

5.6 Comparison: TeVatron and LHC

In comparing TeVatron and LHC a particular interesting situation is the existence of a Higgs boson in the mass range about 115–120 GeV/c^2.
The TeVatron sensitivity arises mainly from the associated production: $WH \rightarrow l\nu b\bar{b}$, $ZH \rightarrow \nu\nu b\bar{b}$ and $ZH \rightarrow llb\bar{b}$. At LHC the region $M_H \sim 115$ GeV/c^2 is mainly covered by two different and complementary channels: $H \rightarrow \gamma\gamma$ and $t\bar{t}H$ with $H \rightarrow b\bar{b}$, $t \rightarrow bl\nu$ and $t \rightarrow bjj$. The availability of two channels should give robustness to the discovery and should allow the interpretation of the observed signal as indeed coming from a Higgs boson. Both channels cannot be used at the TeVatron because of the much smaller expected signal rate.

The signal cross-sections are ∼10 times larger at LHC for $q\bar{q} \rightarrow W/Z + H$ and ∼70 times larger for $gg \rightarrow H$ production, because there is a large gluon contribution to the parton density functions at LHC. In Table 5 the cross-sections for different processes at LHC and TeVatron are summarized.

Process	$\sigma \times$BR (fb) $p\bar{p}$ 2 TeV	$\sigma \times$BR (fb) pp 14 TeV	LHC/TeVatron
$q\bar{q} \rightarrow WH \rightarrow l\nu b\bar{b}$ m_H=120 GeV/c^2	20	210	10
$gg \rightarrow H \rightarrow \gamma\gamma$ m_H=120 GeV/c^2	0.6	35	58
$gg \rightarrow H \rightarrow WW^* \rightarrow l\nu l\nu$ m_H=150 GeV/c^2	15	1150	77
$gg \rightarrow H \rightarrow ZZ \rightarrow$ 4l m_H=150 GeV/c^2	0.07	5.5	78

Table 5: Cross-sections for different Higgs production and decay processes at LHC and TeVatron. Cross sections are calculated using the PYTHIA [125] event generator.

The cross-sections for the most important backgrounds are given in Table 6. At LHC the electroweak cross-sections are ∼10 times larger and the QCD cross sections more than 100 times larger compared to TeVatron because the gg and qg contributions are strongly enhanced.

Process	$\sigma \times$BR (fb) $p\bar{p}$ 2 TeV	$\sigma \times$BR (fb) pp 14 TeV	LHC/TeVatron
WZ	2.5	26	10
W^+W^-	8.5	71	8.5
$q\bar{q} \rightarrow W^* \rightarrow t\bar{b}$	0.5	5	10
$t\bar{t}$	6.4	600	95
QCD jets (p_T^{hard} >30 GeV)	10^6	10^8	100

Table 6: Cross-sections for different background processes at LHC and TeVatron. Cross sections are calculated using the PYTHIA [125] event generator.

The channel $WH \rightarrow l\nu b\bar{b}$ has not been included in the LHC results because the expected background is higher by a factor of ∼25 at LHC, the signal-to-background ratio is in the order of a few percent and the uncertainty on the background is larger than 10% [151, 152]. The ZH channels have a smaller sensitivity and/or even higher backgrounds then the WH channels and are also not included in the LHC results.
Figure 53 and 54 [152] show the $m_{b\bar{b}}$ distribution for signal and background assuming an integrated luminosity of 30 fb^{-1} in the WH channel with $W \rightarrow l\nu$ and $H \rightarrow b\bar{b}$. For both figures the parameters of the ATLAS detector have been used. By comparing the two figures the differences in the expected signal and background rates and compositions of the backgrounds are clearly visible.

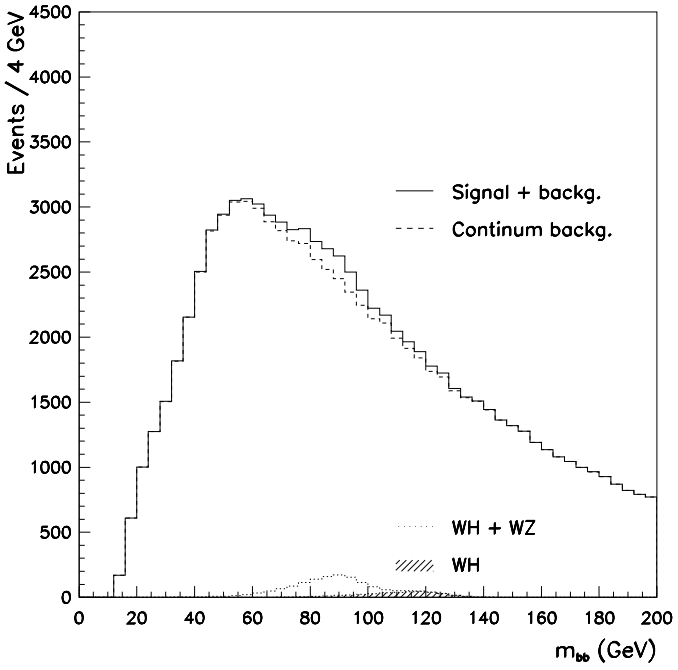

Figure 53: The expected $m_{b\bar{b}}$ distributions for signal and background for a Higgs boson mass of 120 GeV/c^2 at LHC. The plots are normalized to the expected number of events for an integrated luminosity of 30 fb^{-1}. The continuum background (dashed), the resonant signal+background (dotted) and the signal alone (hatched) are also shown.

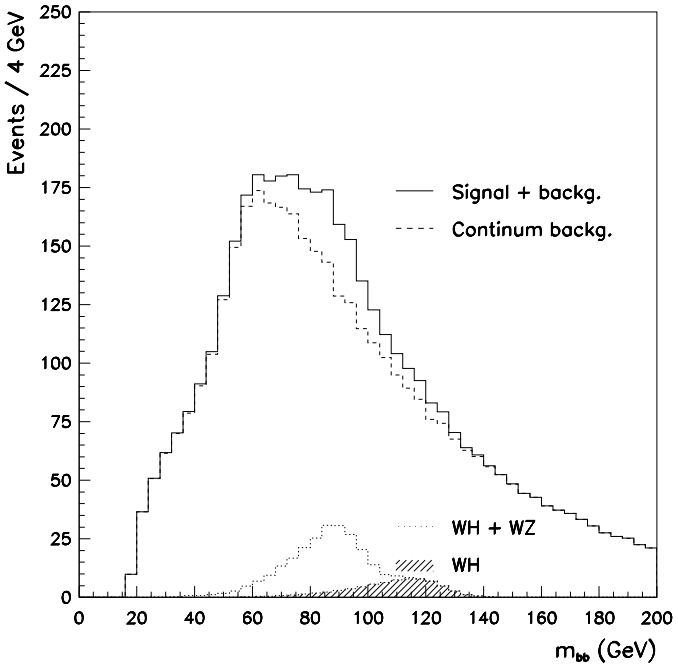

Figure 54: The expected $m_{b\bar{b}}$ distributions for signal and background for a Higgs boson mass of 120 GeV/c^2 at TeVatron. The plots are normalized to the expected number of events for an integrated luminosity of 30 fb^{-1}. The continuum background (dashed), the resonant signal+background (dotted) and the signal alone (hatched) are also shown.

A direct comparison of studies performed at LHC [151, 152] with studies performed at TeVatron [104] show different results. The LHC studies are on the conservative side, the TeVatron studies are more optimistic. TeVatron has used K-factors to determine the cross-section for the Higgs signal. On the other hand, leading order cross-sections were used for some of the backgrounds (WZ, Wjj), which leads to an overestimate of the signal significance. The efficiency for reconstructing and tagging both b-jets in the final state in the TeVatron study is larger by almost a factor of two than in the ATLAS study. But this can in part be attributed to the use of a three-dimensional b-tagging algorithm in the TeVatron study. The pseudorapidity coverage is smaller and a softer jet veto is used. Finally the TeVatron studies are based on fast (parametrized) simulations of the detector performance, in contrast to the full GEANT-based simulation used by ATLAS.

The acceptance of cuts assuming the same detector and the same analysis is two times larger at TeVatron because the physics is more central, i.e. the efficiency of $|\eta|$ cuts is higher. At TeVatron the initial state radiation is less because of the smaller centre-of-mass energy, i.e. a jet veto is less harmful [153]. For the same integrated luminosity, same detector and the same analysis [151, 152] after kinematic cuts both experiments have a similar potential for the WH and ZH channel. The signal rate is five times larger at LHC. The background is about a factor 25 larger compared to TeVatron, but the resulting $S/\sqrt{B}$ is similar.

For the $H \rightarrow WW^*$ the potential at $\sqrt{s}$=14 TeV is larger because the production is dominated by $gg \rightarrow H$. The signal rate is about a factor 30 larger at $\sqrt{s} = 14$ TeV whereas the background rate is only a factor six higher at $\sqrt{s} = 14$ TeV.

Assuming an integrated luminosity of 10 fb^{-1} and a Higgs boson mass of ~ 115 GeV, a total signal significance of $\sim$ 3–4 (Figure 32) is expected at TeVatron [104] combining the ZH and WH channels. This has to be compared to a total signal significance of $\sim$ 4–5 (Figure 45) at the LHC combining the $H \rightarrow \gamma\gamma$ and the $t\bar{t}H$ with $H \rightarrow b\bar{b}$ channels. By using the weak gauge boson fusion channels [137, 140] the significance at LHC might be increased.

It is possible that the TeVatron experiments discover a Higgs boson signal in the mass region around 115 GeV before the LHC experiments start assuming TeVatron is collecting 15 fb^{-1} of data per experiment.

Because at TeVatron the sensitivity relies on the $\phi \rightarrow b\bar{b}(\phi = h, H, A)$ channel the experiments are only sensitive to MSSM Higgs bosons with a similar $\phi \rightarrow b\bar{b}$ branching ratio as in the Standard Model and a similar production cross section ($\sin^2(\alpha - \beta) \approx \mathcal{O}(1)$) [154]. The LHC experiments are using the $h \rightarrow \gamma\gamma$ channel in addition. The studies done by the ATLAS collaboration [115] show that this channel together with the $t\bar{t}h$ channel cover wide regions of the ($m_A, \tan\beta$) plane of the MSSM, with the small m_A region (m_A <250 GeV/c^2) being the most difficult (Figure 50). In conclusion the LHC experiments are most sensitive to large m_A, where m_h approaches its upper bound. As m_A decreases, the $\phi b\bar{b}(\phi = h, H, A)$ coupling increases, so that BR($\phi \rightarrow \gamma\gamma$) decreases. At the TeVatron, the region of large m_A and large $\tan\beta$ (Figure 34 and 35) is harder to cover, because the $\phi b\bar{b}$ coupling decreases towards the Standard Model value. Simultaneously, the lightest Higgs boson (h) approaches its upper bound ($m_h \approx 135$ GeV/c^2), so that more luminosity would be needed to probe this region.

If there is a Higgs boson around 115 GeV/c^2 TeVatron has very good chances to discover the only missing particle in the Standard Model before LHC starts in the year 2006. For LHC such a discovery has to wait for the year 2007 but will then be based on a more robust analysis using

two different channels. The discrimination between a Standard Model Higgs boson or a MSSM Higgs boson will only be possible at LHC.

6 Summary and Conclusions

The increase of the centre-of-mass energy at LEP2 up to $\sqrt{s} = 209$ GeV and the very successful running of the accelerator allowed a search for Higgs bosons up to masses of 115 GeV/c^2. The last year of data-taking at LEP has given us first exciting evidence for a Higgs boson with a mass of 115 GeV/c^2. In the summer 2000 the ALEPH collaboration reported an excess of Higgs boson like events with a mass around 115 GeV/c^2. It was decided to continue the LEP running for an other period of 4 weeks. Finally all four experiments saw signal-like events with a signal-to-background ratio larger than 0.3 in two different channels, in the four-jet and in the missing energy channel. Unfortunately the amount of data was not sufficient for a 5 σ discovery. The upper bound for the Higgs boson mass has been set to

$$113.5 \text{ GeV/c}^2$$

at the 95% confidence level with an expected limit of 115.3 GeV/c^2. The excess of events observed can be interpreted as an indication for the production of a Standard Model Higgs boson with a mass of 115 GeV/c^2.
The cross section is compatible with a Standard Model Higgs boson at a mass of

$$m_H = 115.0^{+1.3}_{-0.9} \text{GeV/c}^2.$$

This excess is concentrated mainly in the data sets with centre-of-mass energies higher than 206 GeV. It has a probability of 4.2$\times$ 10^{-3} to be due to a local statistical fluctuation of the Standard Model background, corresponding to a significance of 2.9 σ.
The sensitivity to electroweak radiative corrections at LEP, SLC and TeVatron predicted the Higgs boson mass to be

$$m_H = 98^{+58}_{-38} \text{ GeV/c}^2.$$

Translated into an upper limit at the 95% confidence level that yields to $m_H < 212$ GeV/c^2. The possible existence of a light Higgs boson at around 115 GeV/c^2 implies that the Standard Model remains valid at most up to scales limited by about 10^6 GeV.
LEP has extended the Standard Model searches into the framework of the Minimal Supersymmetric Standard Model and Two Higgs Doublet Models in general. In a scenario which is designed to yield the maximal value of the lightest Higgs boson h values of $\tan\beta$ between

$$0.48 < \tan\beta < 2.38$$

are excluded. The observed Higgs mass limits are

$$m_h \geq 91.0 \text{ GeV/c}^2$$

and

$$m_A \geq 92.9 \text{ GeV/c}^2.$$

The combined lower 95% confidence level bound for charged Higgs bosons decaying only into $H^+ \to c\bar{s}$ and $\tau^+\nu$ is

$$m_{H^\pm} \geq 78.5 \text{ GeV/c}^2.$$

An excess of events at L3 around $m_{H^\pm}$=68 GeV/c^2 is compatible with a 4.4 σ fluctuation in the background. For many other extensions of the Standard Model limits have been set using the LEP data.

Both - the direct search and the prediction from indirect measurements at LEP - prefer a low Higgs boson mass. At TeVatron the search for the Higgs boson continues. With an integrated luminosity of 2 fb^{-1} per experiment in the next two years the experiments CDF and DØ can exclude Higgs boson masses up to 115 GeV/c^2.

After an upgrade of the detectors TeVatron can collect 15 fb^{-1} integrated luminosity per experiment until the year 2006. With this data TeVatron has the unique chance to detect a Higgs boson with a mass up to 120 GeV/c^2 or exclude a Higgs boson with a mass up to 180 GeV/c^2. The amount of data will not allow to measure the properties of the Higgs bosons with high precision or to distinguish between a Standard Model or a MSSM Higgs boson.

This will be done at the next generation of hadron colliders. The LHC will most probably allow to solve one of the most interesting remaining questions in particle physics: whether one or more Higgs bosons exist or not. By combining the two experiments ATLAS and CMS the minimum luminosity required to observe a 115 GeV/c^2 Higgs boson with 5 σ significance is $\sim$ 10 fb^{-1}, which may be achieved after two years of LHC running. The availability of two channels, $H \to \gamma\gamma$ and $H \to b\bar{b}$, should give robustness to the discovery and should allow the interpretation of the observed signal as indeed coming from a Higgs boson. For higher masses, i.e. for 130 $< m_H <$ 500 GeV/c^2, the discovery is expected to be much faster (a few months of data-taking) thanks to the gold-plated and background-free $H \to ZZ^{(*)} \to$ 4l channel.

With a modest integrated luminosity of 30 fb^{-1}, the ATLAS discovery potential covers a large fraction of the MSSM parameter space in the (m_A,tan β) plane. In most of the MSSM parameter space more than one Higgs boson would be discovered thus allowing a clean distinction between the Standard Model and the MSSM case. If only one Higgs boson can be detected LHC has to measure the properties of the Higgs boson to disentangle Standard Model and MSSM.

The experimental precision with which the Higgs boson mass will be measured assuming 300 fb^{-1} integrated luminosity for the ATLAS and CMS detector will be 0.1% up to masses of 400 GeV/c^2. The Higgs boson width can be obtained from a measurement of the width of the reconstructed Higgs peak, over the mass range 300$< m_H <$700 GeV the precision of the measurement is of the order of 6%. The statistical error on the measurement of the cross section times the branching ratio is expected to be smaller than 10% over the mass region 120–600 GeV/c^2. By combining these measurements for several channels, one can obtain constraints on the Higgs boson couplings.

Note added: September 2001

Since the time of submitting this review article the LEP collaborations have released a new preliminary LEP combined result [155]. The results are based on the recent publications published by the LEP collaborations [50, 54, 58, 156]. Only the L3 publication [156] is final. The ALEPH

and L3 excesses have decreased since the beginning of November 2000. Combining the data from the four LEP experiments, a new lower bound for the mass of the Standard Model Higgs boson of 114.1 GeV/c^2 at the 95% confidence level has been derived. The current combined result corresponds to an excess over the background at the 2 σ level. The excess still can be interpreted as production of a Standard Model Higgs boson with a mass higher than the quoted limit. The maximum consistency with an eventual signal occurs at m_H=115.6 GeV/c^2 as the preferred mass.
The main differences in the inputs with respect to the combined result presented in this review article are due to improvements to the four-jet search and a revision of the missing energy search by the L3 collaboration which reduced the overall significance of the L3 observation with respect to the Standard Model background processes from 1.7 σ to 1 σ. The ALEPH collaboration updated its inputs to include a 2D correlation correction in the four-jet channel. The overall significance of the ALEPH observation with respect to the Standard Model background processes was reduced from 3.4 σ to 3.2 σ. Finally all four experiments have included the data collected during the last days of LEP running at $\sqrt{s} > 206$ GeV and which had not been included in the November 2000 result. The data added amounts to ≈ 55 pb^{-1}.
Towards the end of the year 2001 the final combination from LEP is expected, after the final results of ALEPH, DELPHI and OPAL will be published.

Acknowledgements

Such a review is clearly not possible without the support from many people. I am grateful to the members of the LEP Higgs Working Group, the Tevatron Higgs Working Group and the ATLAS Higgs Working Group, and particularly to my colleagues from the OPAL, DØ and ATLAS experiments, for helpful discussions and advice in preparing this review. On the academic side I want to express my gratitude towards Dorothee Schaile, for giving me the freedom to work in the area of Higgs physics and to write this review.

References

[1] M. Veltman, Nucl. Phys. **B7** (1968) 637.

[2] G. 't Hooft, Nucl. Phys. **B33** (1971) 173 and Nucl. Phys. **B35** (1971) 167.

[3] S. L. Glashow, Nucl. Phys. **20** (1961) 579.

[4] S. Weinberg, Phys. Rev. Lett **19** (1967) 1264.

[5] A. Salam, in Elementary Particle Theory, ed. N. Svartholm (Almqvist and Wiksells, Stockholm, 1968).

[6] P. W. Higgs, Phys. Rev. Lett. **12** (1964) 132 and Phys. Rev. **145** (1966) 1156.

[7] F. Englert and R. Brout. Phys. Rev. Lett. **13** (1964) 321.

[8] G. S. Guralnik, C. R. Hagen and T. W. Kibble, Phys. Rev. Lett. **13** (1964) 585.

[9] J. Gunion, H. Haber, G. Kane and S. Dawson, *The Higgs Hunter's Guide*, Perseus Publishing, Cambridge, Massachusetts (2000).

[10] B. W. Lee, C. Quigg, and H. B. Thacker, Phys.Rev.Lett **38** (1977) 883.

[11] N. Cabbibo, L. Maiani, G. Parisi and R. Petronzio, Nucl. Phys **B158** (1979) 295.

[12] R. A. Flores and M. Sher, Phys. Rev. **D27** (1983) 1679.

[13] M. Lindner, Z. Phys. **C31** (1986) 295.

[14] M. Sher, Phys. Rep. **179** (1989) 273.

[15] J. Casas, J. Espinosa and M. Quiros, Phys. Lett. **B353** (1995) 171.

[16] G. Altarelli and G. Isidori, Phys. Lett. **B337** (1994) 141.

[17] J. Espinosa and M. Quiros, Phys. Lett **B353** (1995) 257.

[18] T. Hambye and K. Riesselmann, *SM Higgs mass bounds from theory*, hep-ph/9708416 (1997).

[19] M. Spira and P. M. Zerwas, hep-ph/9803257 (2000).

[20] E. Witten, Phys. Lett **B105** (1981) 267.

[21] For reviews see: H. P. Nilles, Phys. Rep. **1** (1984) 111;
H. E. Haber and G. L. Kane, Phys. Rep. **117** (1985) 75.

[22] J. F. Gunion and H. E. Haber, Nucl. Phys. **B272** (1986) 1 and **B278** (1986) 449.

[23] Y. Okada, M. Yamaguchi and T. Yanagida, Prog. Theor. Phys. **85** (1991) 1.

[24] H. E. Haber and R. Hempfling, Phys. Rev. Lett. **66** (1991) 1815.

[25] J. Ellis, G. Ridolfi and F. Zwirner, Phys. Lett. **B257** (1991) 83.

[26] J. Ellis, G. Ridolfi and F. Zwirner, Phys. Lett. **B262** (1991) 477.

[27] A. Brignole, J. Ellis, G. Ridolfi and F. Zwirner, Phys. Lett. **B271** (1991) 123.

[28] R. Hempfling and A. Hoang, Phys. Lett. **B331** (1994) 99.

[29] J. Kodeira, Y. Yasui and K. Sasaki, Phys. Rev. **D50** (1994) 7035.

[30] H. E. Haber and R. Hemplfing, Phys. Lett. **D48** (1993) 4280.

[31] M. Carena, J. R. Espinosa, M. Quiros, C. E. M. Wagner, Phys. Lett. B355 (1995) 209.

[32] S. Heinemeyer, W. Hollik, G. Weiglein, Phyd. Rev. **D58** (1998) 091701.

[33] R.-J. Zhang, Phys. Lett. **B447** (1999) 89.

[34] A. G. Akeroyd, Nucl. Phys. **B544** (1999) 311.

[35] P. Igo-Kemenes, for the LEP Working Group on Higgs boson searches, talk at the LEPC open session on Nov.3rd, 2000, http://lephiggs.web.cern.ch/LEPHIGGS/talks/index.html.

[36] D. Decamp *et al.*, ALEPH Collaboration, Nucl. Instr. and Meth. **A360** (1995) 481.

[37] P. Aarnio *et al.*, DELPHI Collaboration, Nucl. Instr. and Meth. **A303** (1991) 233.

[38] B. Adeva *et al.*, L3 Collaboration, Nucl. Instr. and Meth. **A289** (1990) 35.

[39] H. Ahmet *et al.* OPAL Collaboration, Nucl. Instr. and Meth. **A305** (1991) 275.

[40] The LEP Collaborations, ALEPH, DELPHI, L3, OPAL, the LEP Electroweak Working Group and the SLD Heavy Flavour and Electroweak Group, *A Combination of PReliminary Electroweak Measurements and Constraints on the Standard Model*, CERN-EP/2001-021, hep-ex/0103048 (2001).

[41] W. Hollik, G. Duckeck, *Electroweak precision tests at LEP*, Berlin, Germany: Springer (2000) 161 p.

[42] The LEP collaborations ALEPH, DELPHI, L3 and OPAL and the Lineshape subgroup

[43] T. Kawamoto, *Standard Model Fit Results*, Proceedings of XXXVIth Recontres de Moriond QCD and High Energy Interactions, Moriond, France (2001).

[44] H. Burkhardt and B. Pietrzyk, *Update of the hadronic contribution to the QED vacuum polarization*, LAPP-EXP-2001-03 (2001).

[45] J. Z. Bai *et al.* BES Collaboration, *Measurements of the cross section for e+ e $\rightarrow$ hadrons at center-of-mass energies from 2-GeV to 5-GeV*, hep-ex/0102003 (2001).

[46] A. D. Martin, J. Outhwaite and M. G. Ryskin, Phys. Lett. B **492** (2000) 69. of the LEP electroweak working group, CERN-EP-2000-153 (2000).

[47] G. Degrassi, *Where is the Higgs?*, hep-ph/0102137 (2001).

[48] J. Erler, Phys. Rev. **D63** (2001) 071301.

[49] ALEPH, DELPHI, L3 and OPAL Collaboration, The LEP working group for Higgs boson searches, *Searches for Higgs bosons: Preliminary combined results using LEP data collected at energies up to 202 GeV*, CERN-EP/2000-055

[50] OPAL Collaboration, Phys. Lett. **B499** (2001) 38.

[51] OPAL Collaboration, G. Abbiendi *et al.* Phys. Lett **B493** (2000) 249.

[52] A. L. Read *Optimal Statistical Analysis of Search Results based on the Likelihood Ratio and its Apllication to the Search for the MSM Higgs boson at 161 and 172 GeV*, DELPHI note 97-158 PHYS 737 (1997).

[53] T. Junk, Nucl. Instr. and Meth. **A434** (1999) 435.

[54] ALEPH Collaboration, R. Barate *et al.* Phys. Lett. **B495** (2000) 1.

[55] ALEPH Collaboration, *Searches for neutral Higgs bosons in e^+e^- collisions at centre-of-mass energies from 192 to 202 GeV*, CERN-EP/2000/131 (2000), submitted to Phys.Lett.B.

[56] ALEPH Collaboration, Phys. Lett. **B412** (1997) 173.

[57] S. Jin and P. McNamara, hep-ph/9812030 (1998), to be published in Nucl. Instr. and Meth. A.

[58] DELPHI Collaboration, P. Abreu *et al.*, Phys. Lett. **B499** (2001) 23.

[59] DELPHI Collaboration, P. Abreu *et al.* Eur. Phys. J **C17** (2000) 187.

[60] L3 Collaboration, M. Acciarri *et al* Phys. Lett **B495** (2000) 18.

[61] OPAL Collaboration, G. Abbiendi *et al.* Eur. Phys. J. **C12** (2000) 567.

[62] T. Junk, for the LEP Working Group on Higgs boson searches, talk at the LEP Fest 10.10.2000, http://lephiggs.web.cern.ch/LEPHIGGS/talks/index.html.

[63] J. Ellis, G. Ganis, D. V. Nanopoulos and K. A. Olive, hep-ph/0009355 (2000).

[64] E. Fari and L. Susskind, Phys. Rep. **74** (1981) 277.

[65] J. Ellis, M. K. Gaillard, D. V. Nanopoulos and P. Sikive, Nucl. Phys. **B182** (1981) 529.

[66] H. Goldberg, Phys. Rev. Lett. **50** (1983) 1419.

[67] M. Carena, S. Heinemeyer, C. E. M. Wagner and G. Weiglein, CERN-TH/99-374, DESY 99-186 (1999).

[68] ALEPH, DELPHI, L3 and OPAL Collaboration, The LEP working group for Higgs boson searches, *Searches for the Neutral Higgs bosons of the MSSM: Preliminary combined results using LEP data collected at energies up to 209 GeV*, LHWG Internal Note 2001-2.

[69] S. Heinemeyer, W. Hollik and G. Weiglein, *Constraints on $\tan\beta$ in the MSSM from the upper bound on the mass of the lightest Higgs boson*, `hep-ph/9909540` (1999).

[70] M. Carena, M. Quirós and C.E.M. Wagner, Nucl. Phys. **B461** (1996) 407, hep-ph/9508343.

[71] M. Carena, H. E. Haber, S. Heinemeyer, W. Hollik, C. E. M. Wagner and G. Weiglein, *Reconciling the Two-Loop Diagrammatic and Effective Field Theory Computations of the Mass of the lightest CP-even Higgs Boson in the MSSM*, hep-ph/0001002 (2000).

[72] OPAL Collaboration, *Search for Neutral Higgs Bosons in e^+e^- Collisions at $\sqrt{s} \approx$ 192–202 GeV*, OPAL Physics Note PN426 (2000).

[73] ALEPH Collaboration, *Searches for Neutral Higgs Bosons of the MSSM at Centre-of-mass Energies up to 209 GeV with the ALEPH detector at LEP*, ALEPH 2001-022 CONF 2001-019 (2001).

[74] DELPHI Collaboration, *Searches for Neutral Supersymmetric Higgs Bosons in e^+e^- Collisions up to $\sqrt{s}$ =209 GeV*, DELPHI 2001-017 CONF 458 (2001).

[75] S. Wynhoff, Presentation at the 27th February, 2001 LEP Seminar, for the L3 Collaboration.

[76] OPAL Collaboration, *Searches for Higgs Bosons in Extensions to the Standard Model in e^+e^- Collisions at the Highest LEP Energies*, OPAL Physics Note PN472 (2001).

[77] OPAL Collaboration, *Two Higgs Doublet Model and model independent interpretation of neutral Higgs boson searches*, CERN-EP/2000/092 (2000), submitted to Eur.Phys.J.C.

[78] ALEPH Collaboration, ALEPH 2001-021 CONF 2001-018 (2001).

[79] L3 Collaboration, L3 Note 2576 (2000).

[80] X. Calmet, H. Fritzsch, Phys. Lett. **B496** (2000) 190.

[81] ALEPH Collaboration, Phys. Lett. **B487** (2000) 241;
ALEPH Collaboration, ALEPH 2001-015 CONF 2001-012 (2001).

[82] DELPHI Collaboration, CERN-EP/2001-013 (2001), submitted to Phys. Lett. B.

[83] L3 Collaboration, L3 note 2652 (2001).

[84] L3 Collaboration, L3 note 2649 (2001).

[85] A. Djouadi, J. Kalinowski and P. M. Zerwas, Z. Phys **C57** (1993) 569.

[86] P. Janot, Physics at LEP2, Volume 2, CERN 96-01 (1996).

[87] ALEPH Collaboration, ALEPH 2001-016 CONF 2001-013 (2001).

[88] DELPHI Collaboration, DELPHI 2001-071 CONF 499 (2001).

[89] L3 Collaboration, L3 note 2643 (2001).

[90] P. Garcia-Abia, *Search for charged Higgs bosons in L3*, hep-ex/0105057 (2001).

[91] F. Abe *et al.*, NUcl. Instr. and Meth., **A271** (1988) 387.

[92] S. Abachi *et al.*, Nucl. Instr. and Meth., **A338** (1994) 185.

[93] CDF Collaboration, Phys. Rev. Lett. bf 74 (1995) 2626.

[94] DØ Collaboration, Phys. Rev. Lett. bf 74 (1995) 2632.

[95] CDF II, Technical Design Report, FERMILAB-PUB-96/390-E (1996).

[96] M. Roco, FERMILAB-CONF-98-268-E (1998).

[97] CDF Collaboration, T. Affolder *et al.*, hep-ex/0010052 (2000), submitted to Phys. Rev. Lett.

[98] The LEP2 working group for Higgs boson searches, CERN-EP/2000-055; ALEPH 2000-028 CONF 2000-023; DELPHI 2000-050 CONF 365; L3 note 2525; OPAL TN646 (2000).

[99] CDF Collaboration, F. Abe *et al.*, Phys. Rev. Lett. **79** (1997) 3819.

[100] CDF Collaboration, F. Abe *et al.*, Phys. Rev. Lett. **81** (1998) 5748.

[101] J. Guimaraes da Costa, FERMILAB-CONF-01/002 (2001).

[102] DØ Collaboration, B. Abbott *et al*, Phys. Rev. Lett. **82** (1999) 4975.

[103] CDF Collaboration, T. Affolder *et al*, Phys. Rev. **D62** (2000) 12004.

[104] M. Carena *et al.*, Report of the Higgs working group, FERMILAB-CONF-00-279-T (2000).

[105] M. Spira, *Higgs boson production and decay at the TeVatron*, hep-ph/9810289.

[106] P. Bhat, R. Gilmartin and H. Prosper, Phys. Rev. **D62** (2000) 074022.

[107] J. Conway, SHW 2.0, available at http://www.physics.rutgers.edu/∼conway/-soft/shw/shw.html (unpublished).

[108] J. Goldstein, C. S. Hill, J. Incandela, S. Parke, D. Rainwater and D. Stuart, Phys. Rev. Lett. **86** (2001) 1694.

[109] T. Han, A. S. Turcot and R. Zhang, Phys. Rev. **D59** (1999) 093001.

[110] T. Han and R. Zhang, Phys. Rev. Lett **82** (1999) 25.

[111] G. D'Agostini, *Bayesian reasoning in high-energy physics: Principles and applications*, CERN-99-03 (1999).

[112] J. S. Conway, *Higgs searches in Run 2 at the Tevatron*, FERMILAB-Conf-99/156-E (2000).

[113] The ATLAS Technical Proposal for a general purpose pp experiment at the Large Hadron Collider at CERN, CERN/LHCC 94-43 (1994).

[114] CMS Collaboration, Technical Proposal, CERN/LHCC 94-38 (1994).

[115] ATLAS Detector and Physics Performance Technical Design Report, CERN/LHCC/99-15 (1999).

[116] Proceedings of the Large Hadron Collider Workshop, Aachen, 1990, CERN 90-10/ECFA 90-133.

[117] Proceedings of the Workshop on Physics at Future Accelerators, La Thuile, 1987.

[118] T. Trefzger, Proceedings of the 7th Inernational conference on Instrumentation for Colliding Beam Physics, Hamamatsu, Japan, Nucl. Instr. and Meth. **A453** (2000) 188.

[119] M. Spira, A. Djouadi, D. Graudenz and P. M. Zerwas, Nucl. Phys. **B453** (1995) 17.

[120] R. Cahn and S. Dawson, Phys. Lett **B136** (1984) 196.

[121] K. Hikasa, Phys. Lett. **B164** (1985) 341.

[122] G. Altarelli *et al.*, Nucl. Phys. **B287** (1987) 205.

[123] T. Han *et al.*, Phys. Rev. Lett **69** (1992) 3274.

[124] T. Han *et al.*, Phys. Lett. **B273** (1991) 167.

[125] T. Sjöstrand, Comp. Phys. Comm. **82** (1994) 74;
T. Sjöstrand, LU TP 95-20.

[126] M. Spira, Fortschr. Phys. **46** (1998) 203.

[127] D. Froidevaux and E. Richter-Was, Z. Phys. **C67** (1995) 213.

[128] E. Richter-Was and M. Sapinski, Acta Phys. Polon. **B30** (1999) 1001.

[129] V. Drollinger, *Finding H0 $\rightarrow$ b anti-b at the LHC*, hep-ex/0105017 (2001).

[130] T. Trefzger et al, ATLAS-PHYS-98-116 (1998).

[131] T. Trefzger, Proceedings of the 13th Topical Conference on Hadron Collider Physics, Bombay, India (1999) 455.

[132] M. Dittmar and H. Dreiner, Phys. Rev. **D55** (1997) 167.

[133] K. Jakobs and T. Trefzger, ATL-PHYS-2000-015 (2000).

[134] M. Dittmar and H. Dreiner, hep-ph/9703401 (1997).

[135] H. Baer and J. D. Wells, Phys. Rev. **D57** (1998) 4446.

[136] D. Rainwater and D. Zeppenfeld, Phys. Rev. D **60** (1999) 113004.

[137] N. Kauer, T. Plehn, D. Rainwater and D. Zeppenfeld, Phys. Lett. **B503** (2001) 113.

[138] D. Rainwater, D. Zeppenfeld, K. Hagiwara, Phys. Rev. **D59** (1999) 14037.

[139] D. Rainwater and D. Zeppenfeld, JHEP**9712** (1997) 005.

[140] T. Plehn, D. Rainwater and D. Zeppenfeld, Phys. Rev. D **61** (2000) 093005.

[141] M. Hohlfeld, *On the determination of Higgs parameters in the ATLAS experiment at the LHC*, ATLAS-COM-PHYS-2000-021 (2000).

[142] R. D. Heuer, D. . Miller, F. . Richard and P. . Zerwas, DESY-01-011C (2001).

[143] D. Zeppenfeld, R. Kinnunen, A. Nikitenko and E. Richter-Was, Phys. Rev. D **62** (2000) 013009.

[144] C. A. Nelson, Phys. Rev. **D37** (1988) 1220.

[145] M. Carena, P. M. Zerwas *et al.*, *Higgs Physics at LEP2*, Proceedings of the LEP2 workshop, CERN (1995).

[146] E. Richter-Was, D. Froidevaux, F. Gianotti, L. Poggioli, D. Cavalli and S. Resconi, Int. J. Mod. Phys. **A13** (1998) 1371.

[147] T. Trefzger et al, ATLAS-PHYS-98-117 (1998).

[148] K. J. F. Gaemers and G. Hoogeveen, Phys. Lett. **B146** (1984).

[149] D. Dicus, A. Stange and S. Willenbrock, Phys. Lett. **B333** (1994) 126.

[150] J. F. Gunion, L. Poggioli, R. Van Kooten, C. Kao and P. Rowson, *Higgs boson discovery and properties*, Snowmass 96, hep-ph/9703330 (1997).

[151] E. Richter-Was, Acta Phys. Polon. B **31** (2000) 1973.

[152] E. Richter-Was, Acta Phys. Polon. B **31** (2000) 1931.

[153] F. Gianotti, *Higgs prospects at LHC*, talk given at Higgs and Supersymmetry, Orsay (2001).

[154] M. Carena, S. Mrenna, C. E. M. Wagner, Phys. Rev. **D62** (2000) 055008.

[155] The LEP Higgs Working Group, *Standard Model Higgs Boson at LEP*, CERN-EP/2001-055 (2001).

[156] L3 Collaboration, *Standard Model Higgs Boson with the L3 Experiment at LEP*, CERN-EP/2001-049 (2001).